

The Custodial Randall-Sundrum Model: From Precision Tests to Higgs Physics

S. CASAGRANDE^a, F. GOERTZ^b, U. HAISCH^b, M. NEUBERT^{b,c} AND T. PFOH^b

^a *Excellence Cluster Universe, Technische Universität München
D-85748 Garching, Germany*

^b *Institut für Physik (THEP), Johannes Gutenberg-Universität
D-55099 Mainz, Germany*

^c *Institut für Theoretische Physik, Ruprecht-Karls-Universität Heidelberg
Philosophenweg 16, D-69120 Heidelberg, Germany*

Abstract

We reexamine the Randall-Sundrum (RS) model with enlarged gauge symmetry $SU(2)_L \times SU(2)_R \times U(1)_X \times P_{LR}$ in the presence of a brane-localized Higgs sector. In contrast to the existing literature, we perform the Kaluza-Klein (KK) decomposition within the mass basis, which avoids the truncation of the KK towers. Expanding the low-energy spectrum as well as the gauge couplings in powers of the Higgs vacuum expectation value, we obtain analytic formulas which allow for a deep understanding of the model-specific protection mechanisms of the T parameter and the left-handed Z -boson couplings. In particular, in the latter case we explain which contributions escape protection and identify them with the irreducible sources of P_{LR} symmetry breaking. We furthermore show explicitly that no protection mechanism is present in the charged-current sector confirming existing model-independent findings. The main focus of the phenomenological part of our work is a detailed discussion of Higgs-boson couplings and their impact on physics at the CERN Large Hadron Collider. For the first time, a complete one-loop calculation of all relevant Higgs-boson production and decay channels is presented, incorporating the effects stemming from the extended electroweak gauge-boson and fermion sectors.

Contents

1	Introduction	2
2	Preliminaries	4
3	Bulk Gauge Fields in the Custodial RS Model	4
3.1	Action of the 5D Theory	5
3.2	KK Decomposition	9
3.3	Bulk Profiles	11
3.4	Zero-Mode Masses and Oblique Corrections	12
3.5	Summing over KK Modes	14
4	Bulk Fermions	16
4.1	Fermionic Action and Yukawa Couplings	17
4.2	KK Decomposition	19
4.3	Bulk Profiles	24
5	Gauge Interactions with Fermions	25
5.1	Custodial Protection: Gauge-Boson Contributions	26
5.2	Fermion Couplings to the \mathbf{Z} Boson	27
5.3	Custodial Protection: Fermionic Contributions	29
5.4	Four-Fermion Charged-Current Interactions	32
6	Fermion Couplings to the Higgs Boson	34
7	Phenomenological Applications	38
7.1	Bottom-Quark Pseudo Observables	39
7.2	Rare Decay $t \rightarrow c\mathbf{Z}$	44
7.3	Rare Decay $t \rightarrow ch$	46
7.4	Higgs-Boson Production	47
7.5	Higgs-Boson Decay	55
8	Conclusions	64
A	IR BCs and Higgs-Boson FCNCs	67
B	Reference Values for the SM Parameters	68
C	Form Factors for Higgs-Boson Production and Decay	69

1 Introduction

Precision experiments in the last two decades have elevated the Standard Model (SM) of particle physics from a promising description to a provisional law of nature, tested as a quantum field theory at the level of one percent or better. Despite its triumphs the SM is not an entirely satisfactory theory, however, because it has various theoretical shortcomings. In particular, the gauge hierarchy problem, *i.e.*, the instability of the electroweak scale Λ_W under radiative corrections, has spurred the imagination of many theorists and led to the development of a plethora of models of physics beyond the SM that envision new phenomena at or not far above the TeV scale. A particularly appealing proposal for stabilizing the electroweak scale, featuring one compact extra dimension with a non-factorizable anti-de Sitter (AdS₅) metric, is the Randall-Sundrum (RS) model [1], which by virtue of the AdS/CFT correspondence [2, 3, 4] can be thought of as dual to a strongly coupled four-dimensional (4D) CFT. With two three-branes acting as the boundaries of the warped extra dimension, the AdS₅ background generates an exponential hierarchy of energy scales, so that the natural scale at one orbifold fixed point (the ultra-violet (UV) brane) is much larger than at the other (the infra-red (IR) brane), $\Lambda_{UV} \gg \Lambda_{IR}$. In the RS framework the gauge hierarchy problem is thus solved by gravitational red-shifting.

There are numerous possibilities for building models of electroweak symmetry breaking in AdS₅. The basic building blocks for the construction of a viable theory include, among others, the choice of the bulk gauge group, the zero-mode fermion localization, and the dynamical mechanism for localizing the Higgs field on (or near) the IR brane. While in the original RS proposal all SM fields were constrained to reside on the IR boundary and the gauge group was taken to be $SU(2)_L \times U(1)_Y$, it was soon realized that allowing gauge [5, 6, 7] and matter fields [8, 9] to spread in the AdS₅ bulk not only avoids dangerous higher-dimensional operators suppressed only by powers of Λ_{IR} , but also admits a natural explanation of the flavor structure of the SM [10, 11] via geometrical sequestering [12]. This way of generating fermion hierarchies also implies a certain amount of suppression of dangerous flavor-changing neutral currents (FCNCs) [9], a scheme referred to as the RS-GIM mechanism [13, 14]. Harmful contributions to the T parameter can be cured in an elegant way by extending the bulk hypercharge group to $SU(2)_R \times U(1)_X$ and breaking it to $U(1)_Y$ on the UV brane [15]. An appropriate embedding of the down-type SM quarks into the custodial RS model further furnishes the possibility to reduce the tree-level corrections to the $Zb_L\bar{b}_L$ vertex [16] and its flavor-changing counterparts [17]. As a result, all existing electroweak precision and CP-conserving FCNC constraints are typically satisfied for the mass of the lightest Kaluza-Klein (KK) gauge boson below a few TeV. However, in spite of the RS-GIM mechanism, CP-violating effects in the neutral kaon system [18, 19] and corrections to the neutron electric dipole moment [13, 14] tend to be too large in models with flavor anarchy, pushing the new-physics scale to at least 10 TeV and thus beyond the reach of the CERN Large Hadron Collider (LHC). Relaxing the latter bounds seems to require an additional flavor alignment in warped models and has triggered a lot of model-building activity.¹

The purpose of this article is to perform a thorough analysis of the structure of the RS

¹A list of relevant references can be found in [20].

variant with extended gauge symmetry $SU(2)_L \times SU(2)_R \times U(1)_X \times P_{LR}$ in the bulk, where P_{LR} interchanges the two $SU(2)$ groups and is responsible for the protection of the $Zb_L\bar{b}_L$ vertex. While in the existing literature on the custodial RS model the couplings of the bulk fields to the Higgs sector are treated as a perturbation, we instead construct the exact solutions to the bulk equations of motion (EOMs) subject to appropriate boundary conditions (BCs). In that way we obtain exact results for the profiles and masses of the various SM particles and their KK excitations. This approach is not only more elegant but also offers several advantages over the perturbative approach. In particular, it facilitates the analytic calculation of all terms of order $\Lambda_W^2/\Lambda_{\text{IR}}^2$, including those arising from the breaking of the P_{LR} symmetry by the BCs and possibly the bulk masses. The physical interpretation of the obtained results in terms of (ir)reducible sources of symmetry breaking is thus evident in our approach, while it remains somewhat hidden if the couplings of the bulk fields to the Higgs sector are treated as a perturbation from the very beginning. The exact approach also permits to include the mixing of fermions between different generations in a completely general way, making the dependence on the exact realization of the matter sector explicit. In turn, it is straightforward to address questions about the model-dependence of the resulting gauge- and Higgs-boson interactions with the SM fermions. In summary, our work puts the theory of custodial warped extra dimensions on a more sound basis, both at the field theoretical and phenomenological level. In a forthcoming paper we will apply the derived results to tree-level flavor-violating $\Delta F = 1$ and $\Delta F = 2$ processes in the quark sector.

This article is organized as follows. After recalling important definitions and notations, we discuss in Section 3 the KK decomposition of the bulk gauge fields in the presence of the brane-localized Higgs sector, working in a covariant R_ξ gauge. We also show how to compute sums over KK towers of gauge bosons in closed form. The analogous discussion for bulk fermions is presented in Section 4. Special attention is devoted to the correct implementation of Yukawa couplings containing Z_2 -odd fermion profiles. In Sections 5 and 6 we present the main results of our work. We first analyze the structure of gauge-boson interactions with SM fermions and then study the couplings of the Higgs boson to matter. In the first case, we give analytic formulas that expose, on one hand, the prerequisites for achieving a custodial protection of the left-handed Z -boson couplings and, on the other, which are the terms that necessarily escape protection. In addition, we show explicitly that no protection mechanism is present in the charged-current sector. In the second case, the exact dependence on the realization of the fermion sector of the Higgs-fermion couplings is worked out. In our article we concentrate on the leading contributions to the observables of interest, ignoring possible effects of brane-localized kinetic terms [21, 22, 23]. Although the UV dynamics is not specified, it is natural to assume that these terms are loop suppressed, so that they can be neglected to first order. The most important phenomenological implications of our findings are discussed in Section 7. We begin by studying the constraints imposed by the precision measurements of the bottom-quark pseudo observables, including all tree-level corrections that avoid protection. We further discuss the phenomenology of rare top decays in the extended RS model and compare it to the one of the minimal formulation. Finally, we explore the possible changes of the Higgs production cross section and branching fractions at the LHC, including all leading-order quantum corrections stemming from the extended electroweak gauge-boson and fermion sectors. In a series of appendices we collect details on the derivation of the IR

BCs and Higgs-boson FCNCs in the presence of both Z_2 -even and -odd Yukawa couplings, our input values for the SM parameters, and the explicit expressions for the form factors needed to calculate the production cross section and the branching ratios of the Higgs boson in the RS model.

2 Preliminaries

We work with the non-factorizable RS geometry

$$ds^2 = e^{-2\sigma(\phi)} \eta_{\mu\nu} dx^\mu dx^\nu - r^2 d\phi^2, \quad \sigma(\phi) = kr|\phi|, \quad (1)$$

where x^μ denote the coordinates on the 4D hyper-surfaces of constant ϕ with metric $\eta_{\mu\nu} = \text{diag}(1, -1, -1, -1)$. The fifth dimension is an S^1/Z_2 orbifold of size r labeled by $\phi \in [-\pi, \pi]$. The extra dimension has orbifold fixed points at $\phi = 0$ (the UV brane) and $\phi = \pi$ (the IR brane). Since the ratio of the warp factor and the curvature, $e^{\sigma(\phi)}/k$, corresponds to an inverse energy scale in the 4D theory, the gauge hierarchy problem can be tamed by an appropriate choice of the product $kr\pi$. In order to address the hierarchy between the electroweak scale, $\Lambda_W \approx M_W$, and the fundamental Planck scale, $\Lambda_{UV} \approx M_{\text{Pl}}$, one has to choose

$$L \equiv kr\pi \approx \ln\left(\frac{M_{\text{Pl}}}{M_W}\right) \approx \ln(10^{16}) \approx 37. \quad (2)$$

Below we will sometimes refer to L as the ‘‘volume’’ of the extra dimension. The quantity $\epsilon \equiv e^{-kr\pi}$ also sets the mass scale for the low-lying KK excitations of the SM fields to be of order of the ‘‘KK scale’’

$$M_{\text{KK}} \equiv k\epsilon \approx \Lambda_{\text{IR}} = \mathcal{O}(\text{few TeV}). \quad (3)$$

For instance, the masses of the first KK photon and gluon are approximately $2.5M_{\text{KK}}$.

It will often be convenient to introduce a coordinate $t \equiv \epsilon e^{\sigma(\phi)}$, which equals ϵ on the UV brane and 1 on the IR brane [8]. Integrals over the orbifold are then obtained using the following replacements

$$\int_{-\pi}^{\pi} d\phi \rightarrow \frac{2\pi}{L} \int_{\epsilon}^1 \frac{dt}{t}, \quad \int_{-\pi}^{\pi} d\phi e^{\sigma(\phi)} \rightarrow \frac{2\pi}{L\epsilon} \int_{\epsilon}^1 dt. \quad (4)$$

We now have enough definitions and notations in place to start our discussion.

3 Bulk Gauge Fields in the Custodial RS Model

In this section we construct the KK decomposition in the gauge sector and derive exact solutions for the bulk fields, including the effects of an IR brane-localized Higgs sector. In all previous works on the RS model with custodial protection, the couplings of the Higgs sector to bulk fields were treated as a perturbation, expanding the theory in powers of v^2/M_{KK}^2 . This leads to the necessity of diagonalizing infinite-dimensional matrices which have to be truncated, including only one (or a few) KK excitations. While such an approach should in

general lead to sensible results [25], it is worthwhile to study the set-up within the basis of mass eigenstates, thereby obtaining exact results [9, 24]. Indeed, we will see that the summation over the entire KK tower receives additional contributions, which are lost through truncation [26]. As the sum can be evaluated in closed form, it is convenient to work with the complete sum and afterwards expand the obtained expressions in powers of v^2/M_{KK}^2 . Proceeding in this way one can clearly distinguish between leading and subleading terms. Alternatively one could use five-dimensional (5D) propagators [27], which would be equivalent to our method. An exhaustive treatment of the perturbative approach featuring truncation after the first mode can be found in [28].

3.1 Action of the 5D Theory

We consider the RS model with custodial protection as proposed in [15], with the bulk gauge symmetry $SU(2)_L \times SU(2)_R \times U(1)_X \times P_{LR}$. On the IR brane, the symmetry-breaking pattern $SU(2)_L \times SU(2)_R \rightarrow SU(2)_V$ provides a custodial symmetry, which protects the T parameter. The additional P_{LR} symmetry prevents the left-handed $Zb\bar{b}$ coupling from receiving excessively large corrections [16]. On the UV brane, the symmetry breaking $SU(2)_R \times U(1)_X \rightarrow U(1)_Y$ generates the SM gauge group. The symmetry breaking down to $U(1)_{\text{EM}}$ is related to the interplay of UV and IR BCs and will become clear later on. The 5D action of the gauge sector takes the form

$$S_{\text{gauge}} = \int d^4x r \int_{-\pi}^{\pi} d\phi \left(\mathcal{L}_{\text{L,R,X}} + \mathcal{L}_{\text{Higgs}} + \mathcal{L}_{\text{GF}} \right), \quad (5)$$

with the gauge-kinetic terms

$$\mathcal{L}_{\text{L,R,X}} = \frac{\sqrt{G}}{r} G^{KM} G^{LN} \left(-\frac{1}{4} L_{KL}^a L_{MN}^a - \frac{1}{4} R_{KL}^a R_{MN}^a - \frac{1}{4} X_{KL} X_{MN} \right), \quad (6)$$

where G^{MN} denotes the 5D metric. As it is not needed for our analysis, we ignore the Faddeev-Popov Lagrangian. The Higgs Lagrangian

$$\mathcal{L}_{\text{Higgs}} = \frac{\delta(|\phi| - \pi)}{r} \left(\frac{1}{2} \text{Tr} |(D_\mu \Phi)|^2 - V(\Phi) \right) \quad (7)$$

is localized on the IR brane. A simple prescription of how to deal with $\delta(|\phi| - \pi)$ has already been presented in [24] and we postpone a refined treatment to Section 4.2. The gauge-fixing Lagrangian, \mathcal{L}_{GF} , will be given in the next section. We choose the four-vector components of the gauge fields to be even under the Z_2 parity, while the scalar fifth components are odd, in order to arrive at a low-energy spectrum that is consistent with observation. The Higgs bi-doublet, responsible for breaking $SU(2)_L \times SU(2)_R$ to the diagonal subgroup $SU(2)_V$ on the IR brane, transforms as $(\mathbf{2}, \mathbf{2})_0$ and explicitly reads²

$$\Phi(x) = \frac{1}{\sqrt{2}} \begin{pmatrix} v + h(x) - i\varphi^3(x) & -i\sqrt{2}\varphi^+(x) \\ -i\sqrt{2}\varphi^-(x) & v + h(x) + i\varphi^3(x) \end{pmatrix}, \quad (8)$$

²Notice that compared to [29] the sign of the would-be Goldstone boson fields is switched.

where φ^i are real scalar fields, $\varphi^\pm = (\varphi^1 \mp i\varphi^2)/\sqrt{2}$, and $v \approx 246$ GeV is the vacuum expectation value (VEV) of the Higgs field. $SU(2)_L$ transformations act from the left on the bi-doublet, while the $SU(2)_R$ transformations act from the right. The covariant derivative in the Higgs sector reads

$$D_\mu \Phi = \partial_\mu \Phi - ig_{L5} L_\mu^a T_L^a \Phi + ig_{R5} \Phi R_\mu^a T_R^a, \quad (9)$$

with $T_{L,R}^a = \sigma^a/2$. An explicit calculation leads to

$$D_\mu \Phi = \frac{1}{\sqrt{2}} \begin{pmatrix} \partial_\mu (h - i\varphi^3) - i\frac{v}{2} (g_{L5} L_\mu^3 - g_{R5} R_\mu^3) & -\partial_\mu i\sqrt{2}\varphi^+ - i\frac{v}{2} (g_{L5} L_\mu^+ - g_{R5} R_\mu^+) \\ -\partial_\mu i\sqrt{2}\varphi^- - i\frac{v}{2} (g_{L5} L_\mu^- - g_{R5} R_\mu^-) & \partial_\mu (h + i\varphi^3) + i\frac{v}{2} (g_{L5} L_\mu^3 - g_{R5} R_\mu^3) \end{pmatrix} \quad (10)$$

+ terms bi-linear in fields,

where we have introduced

$$L_\mu^\pm = \frac{1}{\sqrt{2}} (L_\mu^1 \mp iL_\mu^2), \quad R_\mu^\pm = \frac{1}{\sqrt{2}} (R_\mu^1 \mp iR_\mu^2). \quad (11)$$

The structure of (10) motivates us to define the new fields [29]

$$\begin{pmatrix} \tilde{A}_M \\ V_M \end{pmatrix} = \frac{1}{\sqrt{g_L^2 + g_R^2}} \begin{pmatrix} g_L & -g_R \\ g_R & g_L \end{pmatrix} \begin{pmatrix} L_M \\ R_M \end{pmatrix}, \quad (12)$$

which lead to a diagonal mass matrix. We have introduced the 4D gauge couplings $g_a = g_{a5}/\sqrt{2\pi r}$. The rotations are analogous to the usual definitions of the Z boson and photon fields in the SM, which are themselves postponed to (18). Finally, the mass term adopts the form

$$\mathcal{L}_{\text{mass}} = \frac{\delta(|\phi| - \pi)}{r} \frac{(g_{L5}^2 + g_{R5}^2) v^2}{8} \tilde{A}_\mu^a \tilde{A}^{\mu a} \equiv \frac{\delta(|\phi| - \pi)}{r} \frac{1}{2} M_{\tilde{A}}^2 \tilde{A}_\mu^a \tilde{A}^{\mu a}, \quad (13)$$

and reveals the breaking pattern

$$SU(2)_L \times SU(2)_R \xrightarrow{\text{IR}} SU(2)_V, \quad (14)$$

induced by the Higgs VEV $\langle \Phi \rangle = v/\sqrt{2} \mathbf{1}$. Appropriate BCs break the extended electroweak gauge group down to the SM gauge group on the UV boundary

$$SU(2)_R \times U(1)_X \xrightarrow{\text{UV}} U(1)_Y. \quad (15)$$

Explicitly, this is done by introducing the new fields

$$\begin{pmatrix} Z'_M \\ B^Y_M \end{pmatrix} = \frac{1}{\sqrt{g_R^2 + g_X^2}} \begin{pmatrix} g_R & -g_X \\ g_X & g_R \end{pmatrix} \begin{pmatrix} R^3_M \\ X_M \end{pmatrix}, \quad (16)$$

$\partial_\phi L_\mu^\pm(x, 0) = 0$	$L_5^\pm(x, 0) = 0$	$\partial_\phi \tilde{A}_\mu^\pm(x, \pi^-) = -\frac{r}{2\epsilon^2} M_{\tilde{A}}^2 \tilde{A}_\mu^\pm(x, \pi)$	$\tilde{A}_5^\pm(x, \pi) = 0$
$R_\mu^\pm(x, 0) = 0$	$R_5^\pm(x, 0) = 0$	$\partial_\phi V_\mu^\pm(x, \pi) = 0$	$V_5^\pm(x, \pi) = 0$
$\partial_\phi Z_\mu(x, 0) = 0$	$Z_5(x, 0) = 0$	$\partial_\phi \tilde{Z}_\mu(x, \pi^-) = -\frac{r}{2\epsilon^2} M_{\tilde{A}}^2 \tilde{Z}_\mu(x, \pi)$	$\tilde{Z}_5(x, \pi) = 0$
$Z'_\mu(x, 0) = 0$	$Z'_5(x, 0) = 0$	$\partial_\phi Z_\mu^H(x, \pi) = 0$	$Z_5^H(x, \pi) = 0$
$\partial_\phi A_\mu(x, 0) = 0$	$A_5(x, 0) = 0$	$\partial_\phi A_\mu(x, \pi) = 0$	$A_5(x, \pi) = 0$

Table 1: UV (left) and IR (right) BCs.

and giving Dirichlet BCs to Z'_μ and $R_\mu^{1,2}$ on the UV brane. The $U(1)_Y$ hypercharge coupling is related to the $SU(2)_R \times U(1)_X$ couplings by

$$g_Y = \frac{g_R g_X}{\sqrt{g_R^2 + g_X^2}}. \quad (17)$$

The SM-like neutral electroweak gauge bosons are defined in the standard way through

$$\begin{pmatrix} Z_M \\ A_M \end{pmatrix} = \frac{1}{\sqrt{g_L^2 + g_Y^2}} \begin{pmatrix} g_L & -g_Y \\ g_Y & g_L \end{pmatrix} \begin{pmatrix} L_M^3 \\ B_M^Y \end{pmatrix}. \quad (18)$$

It follows that the definitions of the sine and cosine of the weak-mixing angle,

$$\sin \theta_w = \frac{g_Y}{\sqrt{g_L^2 + g_Y^2}}, \quad \cos \theta_w = \frac{g_L}{\sqrt{g_L^2 + g_Y^2}}, \quad (19)$$

agree with the ones in the SM. Furthermore, the fields V_M^3 and X_M can be rotated to the photon field A_M and a state Z_M^H via

$$\begin{pmatrix} Z_M^H \\ A_M \end{pmatrix} = \frac{1}{g_{LRX}^2} \begin{pmatrix} g_L g_R & -g_X \sqrt{g_L^2 + g_R^2} \\ g_X \sqrt{g_L^2 + g_R^2} & g_L g_R \end{pmatrix} \begin{pmatrix} V_M^3 \\ X_M \end{pmatrix}, \quad (20)$$

where

$$g_{LRX}^2 = \sqrt{g_L^2 g_R^2 + g_L^2 g_X^2 + g_R^2 g_X^2}, \quad (21)$$

and we write $\tilde{Z}_M \equiv \tilde{A}_M^3$, as it is a linear combination of Z_M and Z'_M , which is orthogonal to Z_M^H as we will see below.

In Table 1 we summarize the BCs that we choose for the fields in order to obtain the correct mass spectrum for the SM gauge bosons. They are given in terms of fields with individual BCs at the two different branes. In the following we will refer to these sets of fields as the UV and IR basis, respectively. The situation is summarized in Figure 3.1, where we also recall the symmetry-breaking patterns on the different branes. The BCs can easily be transformed to another basis at the expense of obtaining expressions that mix different fields. The photon A_μ has individual and source-free Neumann BCs at both branes, and therefore its zero mode remains massless. Note that there is just one mass parameter $M_{\tilde{A}}$ entering the IR BCs, in

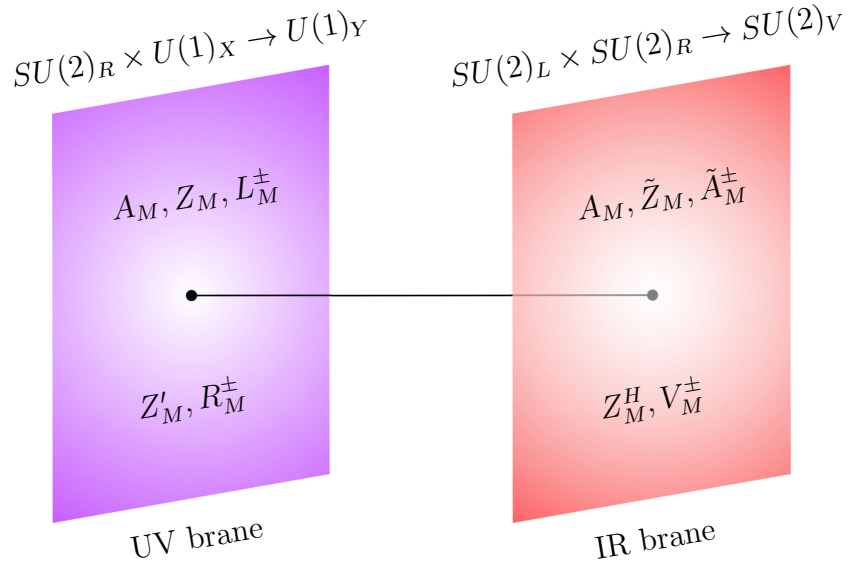


Figure 1: UV and IR basis, *i.e.*, gauge fields with individual BCs on the corresponding branes. The fields in the first (second) row on the UV brane do (do not) possess a zero mode. The symmetry-breaking pattern on the UV and IR brane is also indicated. See text for details.

contrast to the two parameters M_Z and M_W appearing in the minimal model. In the custodial model, the different masses for the lightest electroweak gauge bosons are accomplished through the mixed UV BCs of the gauge fields in the IR basis (see (22) below). The fact that there is just one fundamental mass parameter is crucial for the custodial protection of the T parameter. We will elaborate on this in Section 3.4.

The action of the theory still contains mixing terms between gauge fields and scalars, which can be removed by an appropriate gauge-fixing Lagrangian. As the Higgs sector is localized on the IR brane, it is natural to work in the IR basis for that purpose. For this reason, we define the 5D theory in the IR basis. The concrete form of the gauge fixing will be given below in (30).

Before discussing the KK decomposition, we summarize the relations between the UV (right) and IR basis (left). They read

$$\begin{aligned}
 \begin{pmatrix} \tilde{Z}_M \\ Z_M^H \end{pmatrix} &= \begin{pmatrix} \cos \theta_Z & -\sin \theta_Z \\ \sin \theta_Z & \cos \theta_Z \end{pmatrix} \begin{pmatrix} Z_M \\ Z'_M \end{pmatrix} \equiv \mathbf{R}_Z \begin{pmatrix} Z_M \\ Z'_M \end{pmatrix}, \\
 \begin{pmatrix} \tilde{A}_M^\pm \\ V_M^\pm \end{pmatrix} &= \begin{pmatrix} \cos \theta_W & -\sin \theta_W \\ \sin \theta_W & \cos \theta_W \end{pmatrix} \begin{pmatrix} L_M^\pm \\ R_M^\pm \end{pmatrix} \equiv \mathbf{R}_W \begin{pmatrix} L_M^\pm \\ R_M^\pm \end{pmatrix},
 \end{aligned} \tag{22}$$

where

$$\sin \theta_Z = \frac{g_R^2}{\sqrt{(g_L^2 + g_R^2)(g_R^2 + g_X^2)}}, \quad \cos \theta_Z = \frac{g_{LRX}^2}{\sqrt{(g_L^2 + g_R^2)(g_R^2 + g_X^2)}},$$

$$\sin \theta_W = \frac{g_R}{\sqrt{g_L^2 + g_R^2}}, \quad \cos \theta_W = \frac{g_L}{\sqrt{g_L^2 + g_R^2}}, \quad (23)$$

and g_{LRX}^2 has been defined in (21). In order to shorten the notation we will hereafter employ the abbreviations $s_a \equiv \sin \theta_a$ and $c_a \equiv \cos \theta_a$ for $a = w, Z, W$.

3.2 KK Decomposition

We now perform the KK decomposition of the 5D fields. It is convenient to work with profiles that obey definite Neumann (+) or Dirichlet (−) BCs at the UV brane. Therefore we include a rotation to the UV basis, *i.e.*, the basis in which the UV BCs decouple, in our decomposition. Furthermore, as different UV fields get mixed by the IR BCs, these fields should be expressed through the same 4D basis. We consequently introduce the vectors $\vec{Z}_M = (\tilde{Z}_M, Z_M^H)^T$ and $\vec{W}_M^\pm = (\tilde{A}_M^\pm, V_M^\pm)^T$ and write

$$\begin{aligned} A_\mu(x, \phi) &= \frac{1}{\sqrt{r}} \sum_n \chi_n^{(+)}(\phi) A_\mu^{(n)}(x), & A_\phi(x, \phi) &= \frac{1}{\sqrt{r}} \sum_n \partial_\phi \chi_n^{(+)}(\phi) a_n^A \varphi_A^{(n)}(x), \\ \vec{Z}_\mu(x, \phi) &= \frac{\mathbf{R}_Z}{\sqrt{r}} \sum_n \chi_n^+(\phi) \vec{A}_n^Z Z_\mu^{(n)}(x), & \vec{Z}_\phi(x, \phi) &= \frac{\mathbf{R}_Z}{\sqrt{r}} \sum_n \partial_\phi \chi_n^+(\phi) \vec{A}_n^Z a_n^Z \varphi_Z^{(n)}(x), \\ \vec{W}_\mu^\pm(x, \phi) &= \frac{\mathbf{R}_W}{\sqrt{r}} \sum_n \chi_n^+(\phi) \vec{A}_n^W W_\mu^{\pm(n)}(x), & \vec{W}_\phi^\pm(x, \phi) &= \frac{\mathbf{R}_W}{\sqrt{r}} \sum_n \partial_\phi \chi_n^+(\phi) \vec{A}_n^W a_n^W \varphi_W^{\pm(n)}(x), \end{aligned} \quad (24)$$

where the sums run over $n = 0, \dots, \infty$. Note that $A_\mu^{(n)}(x)$ *etc.* are 4D mass eigenstates and the lightest modes are identified with the SM gauge bosons. The matrices $\mathbf{R}_{Z,W}$ are defined in (22) and we have introduced the diagonal matrix

$$\chi_n^+(\phi) = \begin{pmatrix} \chi_n^{(+)}(\phi) & 0 \\ 0 & \chi_n^{(-)}(\phi) \end{pmatrix}, \quad (25)$$

as well as two-component vectors \vec{A}_n^a , with $a = Z, W$, representing the mixings between the different gauge fields and their KK excitations. These vectors are normalized according to

$$(\vec{A}_n^a)^T \vec{A}_n^a = 1. \quad (26)$$

Notice that the matrix $\chi_n^+(\phi)$ should in principle also carry a superscript a , indicating the field to which it belongs, but we will not show it, as the correct index should be always clear from the context. The superscripts (+) and (−) label the type of BC we impose on the profiles at the UV brane, *i.e.*, they indicate untwisted and twisted even functions³ on the orbifold. Remember from Table 1 that both profiles satisfy a Neumann BC at the IR boundary, which

³We use the term twisted even functions for profiles with even Z_2 -parity, which obey Dirichlet BC on the UV brane and are thus not smooth at this orbifold fix point. These fields are sometimes called odd, as they look like an odd function if one just considers half of the orbifold. Untwisted even functions correspond to ordinary profiles with Neumann UV BCs.

we do not indicate explicitly by a superscript (+) to avoid unnecessary clutter of notation. Let us also introduce the shorthand notations

$$\vec{\chi}_n^Z(\phi) = \begin{pmatrix} \chi_n^Z(\phi) \\ \chi_n^{Z'}(\phi) \end{pmatrix} = \boldsymbol{\chi}_n^+(\phi) \vec{A}_n^Z, \quad \vec{\chi}_n^W(\phi) = \begin{pmatrix} \chi_n^L(\phi) \\ \chi_n^R(\phi) \end{pmatrix} = \boldsymbol{\chi}_n^+(\phi) \vec{A}_n^W, \quad (27)$$

for the profiles of the UV fields. In analogy to the fermion decomposition in [24], the profiles $\boldsymbol{\chi}_n^+(\phi)$ do not obey exact orthonormality conditions. This fact is related to the decomposition of fields with Neumann and Dirichlet BCs into the same 4D gauge-boson basis. The complete vectors $\vec{\chi}_n^a(\phi)$ with $a = Z, W$ are however orthonormal on each other,

$$\int_{-\pi}^{\pi} d\phi \vec{\chi}_m^a(\phi) \vec{\chi}_n^a(\phi) = \delta_{mn}. \quad (28)$$

Note also that the photon obeys a standard orthonormality condition. We also expand the 4D Goldstone bosons in the basis of mass eigenstates $\varphi_Z^{(n)}(x)$ and $\varphi_W^{\pm(n)}(x)$ by writing [24]

$$\vec{\varphi}^3(x) = \sum_n \vec{b}_n^Z \varphi_Z^{(n)}(x), \quad \vec{\varphi}^{\pm}(x) = \sum_n \vec{b}_n^W \varphi_W^{\pm(n)}(x). \quad (29)$$

Employing the notation introduced in this section, the gauge-fixing Lagrangian takes the form

$$\begin{aligned} \mathcal{L}_{\text{GF}} = & -\frac{1}{2\xi} \left(\partial^\mu A_\mu - \xi \left[\frac{\partial_\phi e^{-2\sigma(\phi)}}{r^2} A_\phi \right] \right)^2 \\ & - \frac{1}{2\xi} \left(\partial^\mu \vec{Z}_\mu - \xi \left[\frac{\delta(|\phi| - \pi)}{r} M_{\vec{A}} \vec{\varphi}^3 + \frac{\partial_\phi e^{-2\sigma(\phi)}}{r^2} \vec{Z}_\phi \right] \right)^2 \\ & - \frac{1}{\xi} \left(\partial^\mu \vec{W}_\mu^+ - \xi \left[\frac{\delta(|\phi| - \pi)}{r} M_{\vec{A}} \vec{\varphi}^+ + \frac{\partial_\phi e^{-2\sigma(\phi)}}{r^2} \vec{W}_\phi^+ \right] \right)^T \\ & \times \left(\partial^\mu \vec{W}_\mu^- - \xi \left[\frac{\delta(|\phi| - \pi)}{r} M_{\vec{A}} \vec{\varphi}^- + \frac{\partial_\phi e^{-2\sigma(\phi)}}{r^2} \vec{W}_\phi^- \right] \right). \end{aligned} \quad (30)$$

Inserting the decomposition (24) into the action and defining the projectors $\mathbf{P}_{(+)} = \text{diag}(1, 0)$ and $\mathbf{P}_{(-)} = \text{diag}(0, 1)$, we derive the EOMs [24, 5, 6]

$$-\frac{1}{r^2} \partial_\phi e^{-2\sigma(\phi)} \partial_\phi \mathbf{R}_a \boldsymbol{\chi}_n^+(\phi) \vec{A}_n^a = (m_n^a)^2 \mathbf{R}_a \boldsymbol{\chi}_n^+(\phi) \vec{A}_n^a - \frac{\delta(|\phi| - \pi)}{r} M_a^2 \mathbf{P}_{(+)} \mathbf{R}_a \boldsymbol{\chi}_n^+(\phi) \vec{A}_n^a, \quad (31)$$

where $a = Z, W, A$ with $M_Z = M_W = M_{\vec{A}}$ and $M_A = 0$, as well as $\mathbf{R}_A = \mathbf{1}$ and $\vec{A}_n^A = (1, 0)^T$. In order to avoid boundary terms due to integration by parts, we move the δ -distribution by an infinitesimal amount into the bulk [24]. We will indicate this limiting procedure by a superscript in the argument of the profiles, *e.g.*, by writing $\boldsymbol{\chi}_n^+(\pi^-)$. The appropriate IR BCs for the profiles can be obtained by integrating the EOMs (31) over an infinitesimal interval around $|\phi| = \pi$. At the 5D level they have already been given in Table 1. However, since the

profiles of the scalar components are taken to be proportional to the ϕ -derivative of the vector profiles, they develop discontinuities at the IR brane [24]. We arrive at

$$\frac{m_n^a}{M_{\text{KK}}} \mathbf{R}_a \chi_n^-(\pi^-) \vec{A}_n^a = -X^2 L \mathbf{P}_{(+)} \mathbf{R}_a \chi_n^+(\pi) \vec{A}_n^a, \quad (32)$$

where

$$\chi_n^-(\phi) \equiv \frac{1}{m_n^a r} e^{-\sigma(\phi)} \partial_\phi \chi_n^+(\phi), \quad X^2 \equiv \frac{(g_L^2 + g_R^2) v^2}{4M_{\text{KK}}^2}. \quad (33)$$

Notice that for the photon the right-hand side in (32) is equal to zero.

After applying the EOMs and the orthonormality condition (28), we observe that the 4D action takes the desired canonical form, if

$$a_n^a = -\frac{1}{m_n^a}, \quad \vec{b}_n^a = \frac{M_a}{\sqrt{r} m_n^a} \mathbf{P}_{(+)} \mathbf{R}_a \chi_n^+(\pi^-) \vec{A}_n^a. \quad (34)$$

The spectrum of the theory is determined by the IR BCs (32). The eigenvalues $x_n^a \equiv m_n^a/M_{\text{KK}}$ are thus solutions of

$$\det [x_n^a \chi_n^-(\pi^-) + L X^2 \mathbf{D}_a \chi_n^+(\pi)] = 0, \quad (35)$$

with

$$\mathbf{D}_a = \mathbf{R}_a^{-1} \mathbf{P}_{(+)} \mathbf{R}_a = \begin{pmatrix} c_a^2 & -s_a c_a \\ -s_a c_a & s_a^2 \end{pmatrix}. \quad (36)$$

Once the eigenvalues are known, the eigenvectors \vec{A}_n^a are determined by (32).

3.3 Bulk Profiles

We now derive expressions for the profiles $\chi_n^{(\pm)}(\phi)$. In order to get the EOMs for the UV basis we multiply (31) by \mathbf{R}_a^T from the left. Introducing the coordinate $t = \epsilon e^{\sigma(\phi)}$, we then write the solutions as [24]

$$\chi_n^{(+)}(t) = N_n^{(+)} \sqrt{\frac{L}{\pi}} t c_n^{(+)+}(t), \quad \chi_n^{(-)}(t) = N_n^{(-)} \sqrt{\frac{L}{\pi}} t c_n^{(-)+}(t), \quad (37)$$

with

$$\begin{aligned} c_n^{(+)+}(t) &= Y_0(x_n \epsilon) J_1(x_n t) - J_0(x_n \epsilon) Y_1(x_n t), \\ c_n^{(-)+}(t) &= Y_1(x_n \epsilon) J_1(x_n t) - J_1(x_n \epsilon) Y_1(x_n t), \\ c_n^{(+)-}(t) &= \frac{1}{x_n t} \frac{d}{dt} (t c_n^{(+)+}(t)) = Y_0(x_n \epsilon) J_0(x_n t) - J_0(x_n \epsilon) Y_0(x_n t), \\ c_n^{(-)-}(t) &= \frac{1}{x_n t} \frac{d}{dt} (t c_n^{(-)+}(t)) = Y_1(x_n \epsilon) J_0(x_n t) - J_1(x_n \epsilon) Y_0(x_n t). \end{aligned} \quad (38)$$

The masses of the KK states normalized to the KK scale, x_n , are determined by the IR BCs as explained above. From the latter expressions, it is obvious that the profiles fulfill the UV

BCs, since $c_n^{(+)-}(\epsilon) = c_n^{(-)+}(\epsilon) = 0$. The normalization constants $N_n^{(\pm)}$ are determined from the orthonormality condition (28). With respect to the formula given in [24], they contain additional terms due to the different UV BCs. We obtain

$$\begin{aligned} (N_n^{(\pm)})^{-2} &= [c_n^{(\pm)+}(1)]^2 + [c_n^{(\pm)-}(1^-)]^2 - \frac{2}{x_n} \left(c_n^{(\pm)+}(1) c_n^{(\pm)-}(1^-) - \epsilon c_n^{(\pm)+}(\epsilon) c_n^{(\pm)-}(\epsilon^+) \right) \\ &\quad - \epsilon^2 \left([c_n^{(\pm)+}(\epsilon)]^2 + [c_n^{(\pm)-}(\epsilon^+)]^2 \right). \end{aligned} \quad (39)$$

Note that, depending on the type of the UV BCs, some of the terms in (39) vanish identically.

3.4 Zero-Mode Masses and Oblique Corrections

It will turn out to be useful to have simple analytical expressions for the masses and profiles of the lightest modes. Expanding (35) in powers of v^2/M_{KK}^2 and inserting the definitions of the mixing angles (23), which connect the UV and IR bases, we arrive at analytic expressions for the masses of the W and Z bosons. They read

$$\begin{aligned} m_W^2 &= \frac{g_L^2 v^2}{4} \left[1 - \frac{g_L^2 v^2}{8M_{\text{KK}}^2} \left(L - 1 + \frac{1}{2L} \right) - \frac{g_R^2 v^2}{8M_{\text{KK}}^2} L + \mathcal{O} \left(\frac{v^4}{M_{\text{KK}}^4} \right) \right], \\ m_Z^2 &= \frac{(g_L^2 + g_Y^2) v^2}{4} \left[1 - \frac{(g_L^2 + g_Y^2) v^2}{8M_{\text{KK}}^2} \left(L - 1 + \frac{1}{2L} \right) - \frac{(g_R^2 - g_Y^2) v^2}{8M_{\text{KK}}^2} L + \mathcal{O} \left(\frac{v^4}{M_{\text{KK}}^4} \right) \right], \end{aligned} \quad (40)$$

where the last terms inside the square brackets are new compared to the minimal model studied in [24].

Interestingly, the latter terms are responsible for the custodial protection of the Peskin-Takeuchi [30, 31] parameter T , which is sensitive to the difference between the corrections to the W - and Z -boson vacuum-polarization functions and thus measures isospin violation. The set of oblique corrections, which are defined as

$$\begin{aligned} S &= \frac{16\pi s_w^2 c_w^2}{e^2} \left[\Pi'_{ZZ}(0) + \frac{s_w^2 - c_w^2}{s_w c_w} \Pi'_{ZA}(0) - \Pi'_{AA}(0) \right], \\ T &= \frac{4\pi}{e^2 c_w^2 m_Z^2} \left[\Pi_{WW}(0) - c_w^2 \Pi_{ZZ}(0) - 2 s_w c_w \Pi_{ZA}(0) - s_w^2 \Pi_{AA}(0) \right], \\ U &= \frac{16\pi s_w^2}{e^2} \left[\Pi'_{WW}(0) - c_w^2 \Pi'_{ZZ}(0) - 2 s_w c_w \Pi'_{ZA}(0) - s_w^2 \Pi'_{AA}(0) \right], \end{aligned} \quad (41)$$

can be computed in an effective Lagrangian approach [32]. Gauge invariance guarantees that $\Pi_{AA}(0) = 0$ to all orders in perturbation theory, and one further has $\Pi_{ZA}(0) = \Pi'_{ZA}(0) = 0$ as long as one works at tree level.

The non-zero tree-level correlators $\Pi_{aa}(0)$ with $a = W, Z$ are calculated from the corrections to the zero-mode masses (40) and profiles (44), where the latter also give rise to non-zero

derivatives $\Pi'_{aa}(0)$ of the correlators at zero momentum. We find

$$\begin{aligned}
\Pi_{WW}(0) &= -\frac{g_L^2 v^4}{32M_{\text{KK}}^2} \left[g_L^2 \left(L - \frac{1}{2L} \right) + g_R^2 L \right], \\
\Pi'_{WW}(0) &= \frac{g_L^2 v^2}{8M_{\text{KK}}^2} \left(1 - \frac{1}{L} \right), \\
\Pi_{ZZ}(0) &= -\frac{(g_L^2 + g_Y^2) v^4}{32M_{\text{KK}}^2} \left[(g_L^2 + g_Y^2) \left(L - \frac{1}{2L} \right) + (g_R^2 - g_Y^2) L \right], \\
\Pi'_{ZZ}(0) &= \frac{(g_L^2 + g_Y^2) v^2}{8M_{\text{KK}}^2} \left(1 - \frac{1}{L} \right).
\end{aligned} \tag{42}$$

Inserting these expressions into (41) yields

$$S = \frac{2\pi v^2}{M_{\text{KK}}^2} \left(1 - \frac{1}{L} \right), \quad T = -\frac{\pi v^2}{4c_w^2 M_{\text{KK}}^2} \frac{1}{L}, \quad U = 0, \tag{43}$$

in agreement with [15, 33]. In contrast to the minimal model [22, 24, 33] there is no L -enhanced term in the T parameter. It has been cancelled by the additional corrections appearing in the contributions to the mass formula (40), which introduces extra terms in the correlators $\Pi_{WW}(0)$ and $\Pi_{ZZ}(0)$. A related discussion including estimates of loop effects on the T parameter has been given in [34, 35]. The one-loop corrections to the S parameter in the custodial RS model arising from Higgs loops have been calculated in [29] and found to be logarithmically UV divergent. This could result in a large and positive S parameter, which is rather problematic [24] in view of the consistency of the global fit of the oblique electroweak precision observables.

The zero-mode profiles, which were used for the above derivations, read

$$\begin{aligned}
\chi_0^{(+)}(t) &= \frac{1}{\sqrt{2\pi}} \left[1 + \frac{x_a^2}{4} \left(1 - \frac{1}{L} + t^2 (1 - 2L - 2 \ln t) \right) + \mathcal{O}(x_a^4) \right], \\
\chi_0^{(-)}(t) &= \sqrt{\frac{L}{2\pi}} t^2 \left[-2 + \frac{x_a^2}{4} \left(t^2 - \frac{2}{3} \right) + \mathcal{O}(x_a^4) \right],
\end{aligned} \tag{44}$$

for $a = W, Z$. Here $x_a^2 \equiv (m_0^a)^2/M_{\text{KK}}^2$ denotes the relevant zero-mode solution in (40). The profiles $\chi_0^{(+)}(t)$ with Neumann IR BC are identical to those appearing in the minimal model, while the profiles $\chi_0^{(-)}(t)$ satisfying Dirichlet IR BC scale like \sqrt{L} , reflecting the localization of KK modes close to the IR boundary. Notice that (44) contains, besides the t -independent terms that are included in (43), also t -dependent contributions that will in general lead to non-universal vertex corrections. While these corrections modify the interactions of the SM fermions with the W and Z bosons, they turn out to be negligibly small for light fermions localized near the UV brane. This is the case for the first two generations of SM fermions, and it helps to avoid excessive contributions to FCNCs. In such a case the oblique corrections are adequately parametrized by the S, T, U parameters as given in (43).

Finally, we can also expand \vec{A}_0^a . Including corrections up to v^2/M_{KK}^2 , we find

$$\vec{A}_0^a = \begin{pmatrix} 1 \\ -s_a c_a \frac{X^2}{4} \sqrt{L} \end{pmatrix}, \quad (45)$$

where the second component parametrizes the admixture of $\chi_0^{(-)}(t)$ in the zero mode. As we will see below in Section 5, the results (44) and (45) play a crucial role in the custodial protection mechanism of the $Zb_L\bar{b}_L$ vertex and its flavor-changing counterparts.

3.5 Summing over KK Modes

In this section we will show how to compute the following sum over gauge-boson profiles $\vec{\chi}_n^a(t)$ weighted by inverse powers of the normalized KK mode masses $(x_n^a)^2$,

$$\Sigma_a(t, t') \equiv \sum_n \frac{\vec{\chi}_n^a(t) \vec{\chi}_n^{aT}(t')}{(x_n^a)^2}, \quad (46)$$

which arises when one attempts to calculate the tree-level exchange of a SM electroweak gauge boson accompanied by its KK excitations in the limit of zero (or negligibly small) momentum transfer. The infinite sum in (46) can be calculated by employing the methods developed in [24, 36]. We first integrate the EOMs (31) twice, accounting for the BCs on both the UV and IR brane. After switching to t coordinates this yields

$$\frac{\vec{\chi}_n^a(t)}{(x_n^a)^2} = \vec{\mathcal{I}}_n^a(t) - (t^2 - \epsilon^2) \mathbf{X}_a \vec{\mathcal{I}}_n^a(1) + [\mathbf{1} - (t^2 - \epsilon^2) \mathbf{X}_a] \mathbf{P}_{(+)} \frac{\vec{\chi}_n^a(\epsilon)}{(x_n^a)^2}, \quad (47)$$

where we have defined

$$\vec{\mathcal{I}}_n^a(t) \equiv \int_\epsilon^t dt' t' \int_{t'}^{1^-} \frac{dt''}{t''} \vec{\chi}_n^a(t''), \quad \mathbf{X}_a \equiv \tilde{X}^2 \mathbf{D}_a \equiv \frac{LX^2}{2 + LX^2(1 - \epsilon^2)} \mathbf{D}_a. \quad (48)$$

Using the completeness relation

$$\sum_n \frac{1}{t} \vec{\chi}_n^a(t) \vec{\chi}_n^{aT}(t') = \frac{L}{2\pi} \delta(t - t') \mathbf{1} \quad (49)$$

for the gauge-boson profiles, it is then easy to prove that

$$\sum_n \vec{\mathcal{I}}_n^a(t) \vec{\chi}_n^{aT}(\phi') = \frac{L}{4\pi} (t_{<}^2 - \epsilon^2) \mathbf{1}, \quad (50)$$

where $t_{<} \equiv \min(t, t')$. With these results at hand it is now a matter of simple algebraic manipulations to arrive at

$$\begin{aligned} \Sigma_a(t, t') &= \frac{L}{4\pi} \left[(t_{<}^2 - \epsilon^2) \mathbf{1} + (t^2 - \epsilon^2) (t'^2 - \epsilon^2) \mathbf{X}_a \right] \\ &\quad + [\mathbf{1} - (t^2 - \epsilon^2) \mathbf{X}_a] \mathbf{P}_{(+)} \Sigma_a(\epsilon, \epsilon) \mathbf{P}_{(+)} [\mathbf{1} - (t'^2 - \epsilon^2) \mathbf{X}_a]^T, \end{aligned} \quad (51)$$

which is exact to all orders in v^2/M_{KK}^2 .

With the help of the orthonormality relation (28), the remaining sum over gauge profiles evaluated at the UV brane can be brought into the form

$$\begin{aligned} \mathbf{P}_{(+)} \boldsymbol{\Sigma}_a(\epsilon, \epsilon) \mathbf{P}_{(+)} &= \frac{L}{2\pi x_a^2} (\vec{\chi}_0^a(\epsilon))_1 \left[\int_{\epsilon}^1 \frac{dt}{t} \left[\left(1 - c_a^2 \tilde{X}^2 (t^2 - \epsilon^2)\right) (\vec{\chi}_0^a(t))_1 \right. \right. \\ &\quad \left. \left. + s_a c_a \tilde{X}^2 (t^2 - \epsilon^2) (\vec{\chi}_0^a(t))_2 \right] \right]^{-1} \mathbf{P}_{(+)}, \end{aligned} \quad (52)$$

where $(\vec{\chi}_0^a(t))_i$ denotes the i^{th} component of the corresponding zero-mode vector. This formula has the advantage that it can be easily expanded in powers of v^2/M_{KK}^2 using (44) and (45). Retaining the first two terms in the expansion leads to

$$\mathbf{P}_{(+)} \boldsymbol{\Sigma}_a(\epsilon, \epsilon) \mathbf{P}_{(+)} = \left(\frac{1}{2\pi x_a^2} + \frac{1}{4\pi} \left[1 - \frac{1}{2L} - \epsilon^2 \left(L - \frac{1}{2L} \right) \right] + \mathcal{O}(x_a^2) \right) \mathbf{P}_{(+)}. \quad (53)$$

Keeping in mind that $X^2 = x_a^2/c_a^2 + \mathcal{O}(x_a^4)$ and dropping phenomenologically irrelevant terms of second order in $\epsilon \approx 10^{-16}$, we finally arrive at

$$\boldsymbol{\Sigma}_a(t, t') = \frac{L}{4\pi} \left[t_{<}^2 \mathbf{1} - \mathbf{P}_a t^2 - \mathbf{P}_a^T t'^2 \right] + \left[\frac{1}{2\pi x_a^2} + \frac{1}{4\pi} \left(1 - \frac{1}{2L} \right) \right] \mathbf{P}_{(+)} + \mathcal{O}(x_a^2), \quad (54)$$

where

$$\mathbf{P}_a = \begin{pmatrix} 1 & 0 \\ -\frac{s_a}{c_a} & 0 \end{pmatrix}. \quad (55)$$

Having at hand an analytic expression for the zero-mode contribution to (46) alone,

$$\boldsymbol{\Pi}_a(t, t') \equiv \frac{\vec{\chi}_0^a(t) \vec{\chi}_0^{aT}(t')}{x_a^2}, \quad (56)$$

will also prove useful later in our discussion. Employing the results (44) and (45), a straightforward calculation leads to

$$\begin{aligned} \boldsymbol{\Pi}_a(t, t') &= -\frac{L}{4\pi} \left[\mathbf{P}_a t^2 + \mathbf{P}_a^T t'^2 \right] \\ &\quad + \left[\frac{1}{2\pi x_a^2} + \frac{1}{4\pi} \left(1 - \frac{1}{L} + t^2 \left(\frac{1}{2} - \ln t \right) + t'^2 \left(\frac{1}{2} - \ln t' \right) \right) \right] \mathbf{P}_{(+)} + \mathcal{O}(x_a^2). \end{aligned} \quad (57)$$

Comparing (54) to (57) we see that all L -enhanced terms in $\boldsymbol{\Sigma}_a(t, t')$ besides the one proportional to the non-factorizable term $t_{<}^2$ arise from the zero-mode contribution $\boldsymbol{\Pi}_a(t, t')$. Factorizable contributions due to the ground-state W and Z bosons are thus enhanced by the logarithm of the warp factor with respect to the contributions from the tower of KK excitations [24]. We also recall that the term $t_{<}^2$ reflects the full 5D structure of the RS model, which is lost when one considers only a few low-lying KK modes [26].

Our analytic results for $\Sigma_a(t, t')$ and $\Pi_a(t, t')$ will turn out to be phenomenologically quite important, as they allow for a clear understanding of the cancellation of certain terms in $\Delta F = 1$ and $\Delta F = 2$ FCNC interactions. In particular, the exact form of the matrix \mathbf{P}_a and its interplay with the terms proportional to the 2×2 unit matrix $\mathbf{1}$ are key ingredients for the custodial protection of the flavor-conserving $Zb_L\bar{b}_L$ coupling as well as of the flavor-violating $Zd_L^i\bar{d}_L^j$ vertices. We will for the moment no further dwell on this issue, but will return to it in detail in Section 5. Before moving on, let us remark that the KK sums involving photon and gluon excitations do not depend on whether the electroweak gauge group is minimal or extended, so that the results for the corresponding sums (excluding the zero modes) can be taken over from [24].

4 Bulk Fermions

We will now present the explicit realization of the quark sector in the model under consideration. Then we will turn to the KK decomposition and derive the bulk profiles for the corresponding fields. As we want to have a custodial protection of the $Zb_L\bar{b}_L$ vertex [16], we impose a discrete P_{LR} symmetry that interchanges the two $SU(2)$ groups. As a consequence, the left-handed bottom quark has to be part of a $SU(2)_L \times SU(2)_R$ bi-doublet with isospin quantum numbers $T_L^3 = -T_R^3 = -1/2$ (see Section 5). This fixes the quantum numbers of the other fields uniquely and implies the following multiplet structure for the quark fields with even Z_2 parity:

$$\begin{aligned}
Q_L &\equiv \begin{pmatrix} u_L^{(+)} \frac{2}{3} & \lambda_L^{(-)} \frac{5}{3} \\ d_L^{(+)} -\frac{1}{3} & u_L'^{(-)} \frac{2}{3} \end{pmatrix}_{\frac{2}{3}}, & u_R^c &\equiv \left(u_R^{c(+)} \frac{2}{3} \right)_{\frac{2}{3}}, \\
\mathcal{T}_R &\equiv \mathcal{T}_{1R} \oplus \mathcal{T}_{2R} \equiv \begin{pmatrix} \Lambda_R'^{(-)} \frac{5}{3} \\ U_R'^{(-)} \frac{2}{3} \\ D_R'^{(-)} -\frac{1}{3} \end{pmatrix}_{\frac{2}{3}} \oplus \left(D_R^{(+)} -\frac{1}{3} \ U_R^{(-)} \frac{2}{3} \ \Lambda_R^{(-)} \frac{5}{3} \right)_{\frac{2}{3}}.
\end{aligned} \tag{58}$$

Here the superscripts (+) and (−) of the chiral fields specify the type of BC on the UV boundary, and as before we have not explicitly shown the BCs at the IR brane, which are understood to be of Neumann type in all cases. The choice of the parities is motivated by the constraint to arrive at a low-energy spectrum of the theory that is consistent with observations. The subscripts correspond to the $U(1)_{EM}$ and $U(1)_X$ charges, respectively, which are connected through the relations $Y = -T_R^3 + Q_X$ and $Q = T_L^3 + Y$. For completeness and future reference, we summarize the quantum numbers of the quark fields in Table 2. The right-handed down-type quarks have to be embedded in a $SU(2)_R$ triplet in order to arrive at an $U(1)_X$ -invariant Yukawa coupling. Note that we have chosen the same $SU(2)_L \times SU(2)_R$ representations for all three generations, which is necessary if one wants to consistently incorporate quark mixing in the fully anarchic approach to flavor in warped extra dimensions. The chosen representations also play a crucial role in the suppression of flavor-changing left-handed Z -boson couplings [17]. Altogether they feature 15 different quark fields in the up-type and nine in the down-type sector. Due to the BCs, there will be three light modes in each sector to be identified

	Q	Q_X	Y	T_L^3	T_R^3
$u_L^{(+)}$	2/3	2/3	1/6	1/2	1/2
$d_L^{(+)}$	-1/3	2/3	1/6	-1/2	1/2
$\lambda_L^{(-)}$	5/3	2/3	7/6	1/2	-1/2
$u_L'^{(-)}$	2/3	2/3	7/6	-1/2	-1/2

	Q	Q_X	Y	T_L^3	T_R^3
$u_R^{c(+)}$	2/3	2/3	2/3	0	0
$\Lambda_R'^{(-)}$	5/3	2/3	2/3	1	0
$U_R'^{(-)}$	2/3	2/3	2/3	0	0
$D_R'^{(-)}$	-1/3	2/3	2/3	-1	0

	Q	Q_X	Y	T_L^3	T_R^3
$D_R^{(+)}$	-1/3	2/3	-1/3	0	1
$U_R^{(-)}$	2/3	2/3	2/3	0	0
$\Lambda_R^{(-)}$	5/3	2/3	5/3	0	-1

Table 2: Charge assignments of the different quark fields in the extended RS model.

with the SM quarks. These are accompanied by KK towers which consist of groups of 15 and nine modes of similar masses in the up- and down-type quark sector, respectively. Moreover one also faces a KK tower of exotic fermion fields of electric charge 5/3, which exhibits nine excitations with small mass splitting in each level. In addition to (58) we have a second set of multiplets, belonging to the components of opposite chirality. The corresponding states have opposite BCs. In particular, they all obey Dirichlet BCs at the IR brane. Remember that the $SU(2)_L$ transformations act vertically, while the $SU(2)_R$ transformations act horizontally on the multiplets.

4.1 Fermionic Action and Yukawa Couplings

The structure of the 5D action of the quark fields has already been given in [24]. It is straightforward to generalize the action to the custodial model [28]. The only non-trivial part are the Yukawa couplings, where the possible gauge-invariant terms take the form

$$\begin{aligned}
S_{\text{Yukawa}} = & - \int d^4x r \int_{-\pi}^{\pi} d\phi \delta(|\phi| - \pi) \frac{e^{-3\sigma(\phi)}}{r} \left[(Y_u^{(5D)})_{ij} \left\{ (\bar{Q}_L^i)_{a\alpha} u_R^{cj} + (\bar{Q}_R^i)_{a\alpha} u_L^{cj} \right\} \Phi_{a\alpha} \right. \\
& + \frac{(Y_d^{(5D)})_{ij}}{\sqrt{2}} \left\{ [(\bar{Q}_L^i)_{a\alpha} (\mathcal{T}_{1R}^j)^c + (\bar{Q}_R^i)_{a\alpha} (\mathcal{T}_{1L}^j)^c] (\sigma^c)_{ab} \Phi_{b\alpha} \right. \\
& \left. \left. + [(\bar{Q}_L^i)_{a\alpha} (\mathcal{T}_{2R}^j)^\gamma + (\bar{Q}_R^i)_{a\alpha} (\mathcal{T}_{2L}^j)^\gamma] (\sigma^\gamma)_{\alpha\beta} \Phi_{a\beta} \right\} + \text{h.c.} \right]. \tag{59}
\end{aligned}$$

Here Φ is the Higgs bi-doublet introduced in (8), and repeated indices are understood to be summed over. Notice that (59) contains operators like $(Y_u^{(5D)})_{ij} (\bar{Q}_R^i)_{a\alpha} u_L^{cj} \Phi_{a\alpha}$ not included in [24]. Furthermore, we will choose the same Yukawa matrix for the coupling of both chirality structures, *i.e.*, LR and RL . The action (59) can thus be regarded as the limit of a set-up

with a bulk Higgs approaching the IR brane. The generalization of our results to the case of different Yukawa matrices, which would in general be allowed for a perfectly brane-localized Higgs, is straightforward. Since the 5D Lorentz group is irreducible, a splitting of different chiralities is not possible in the case of a bulk Higgs.

In (59) the Latin (Greek) letters from the beginning of the alphabet refer to $SU(2)$ indices, while superscripts i, j label the quark generations. Moreover, the components of the triplets in the expression above refer to the representations

$$\mathcal{T}_{1R} = \begin{pmatrix} \frac{1}{\sqrt{2}} \begin{pmatrix} D_R^{(-)} - \frac{1}{3} + \Lambda_R^{(-)} \frac{5}{3} \\ D_R^{(-)} - \frac{1}{3} - \Lambda_R^{(-)} \frac{5}{3} \\ U_R^{(-)} \frac{2}{3} \end{pmatrix} \\ \frac{i}{\sqrt{2}} \begin{pmatrix} D_R^{(+)} - \frac{1}{3} + \Lambda_R^{(+)} \frac{5}{3} \\ -D_R^{(+)} - \frac{1}{3} + \Lambda_R^{(+)} \frac{5}{3} \\ U_R^{(+)} \frac{2}{3} \end{pmatrix} \end{pmatrix}, \quad \mathcal{T}_{2R} = \begin{pmatrix} \frac{1}{\sqrt{2}} \begin{pmatrix} D_R^{(+)} - \frac{1}{3} + \Lambda_R^{(+)} \frac{5}{3} \\ -D_R^{(+)} - \frac{1}{3} + \Lambda_R^{(+)} \frac{5}{3} \\ U_R^{(+)} \frac{2}{3} \end{pmatrix} \\ \frac{i}{\sqrt{2}} \begin{pmatrix} D_R^{(-)} - \frac{1}{3} + \Lambda_R^{(-)} \frac{5}{3} \\ D_R^{(-)} - \frac{1}{3} - \Lambda_R^{(-)} \frac{5}{3} \\ U_R^{(-)} \frac{2}{3} \end{pmatrix} \end{pmatrix}^T, \quad (60)$$

which ensures that one ends up in the desired mass basis, and $\sigma^{c,\gamma}$ are the Pauli matrices. After electroweak symmetry breaking, the Yukawa couplings (59) give rise to mass terms which mix different 5D fields with the same $U(1)_{\text{EM}}$ charge.

In analogy to the KK decomposition for the gauge bosons in (24), we will later work in the basis of 4D mass eigenstates for the quark fields. Therefore it is convenient to introduce the vectors

$$\vec{U} \equiv \begin{pmatrix} u \\ u' \end{pmatrix}, \quad \vec{u} \equiv \begin{pmatrix} u^c \\ U' \\ U \end{pmatrix}, \quad \vec{D} \equiv d, \quad \vec{d} \equiv \begin{pmatrix} D \\ D' \end{pmatrix}, \quad \vec{\Lambda} \equiv \lambda, \quad \vec{\lambda} \equiv \begin{pmatrix} \Lambda' \\ \Lambda \end{pmatrix}, \quad (61)$$

which leads to a one-to-one correspondence between the analysis of [24] and the one presented here. The action can now be expressed in the simple form

$$\begin{aligned} S_{\text{ferm},2} = \int d^4x r \int_{-\pi}^{\pi} d\phi \left\{ \sum_{q=U,u,D,d,\Lambda,\lambda} \left(e^{-3\sigma(\phi)} \bar{q} i \not{\partial} q - e^{-4\sigma(\phi)} \text{sgn}(\phi) \bar{q} \mathbf{M}_q q \right. \right. \\ \left. \left. - \frac{1}{2r} \left[\bar{q}_L e^{-2\sigma(\phi)} \overleftrightarrow{\partial}_\phi e^{-2\sigma(\phi)} q_R + \text{h.c.} \right] \right) \\ \left. - \delta(|\phi| - \pi) e^{-3\sigma(\phi)} \frac{v}{\sqrt{2}r} \left[\vec{U}_L \mathbf{Y}_{\vec{u}}^{(5D)} \vec{u}_R + \vec{D}_L \mathbf{Y}_{\vec{d}}^{(5D)} \vec{d}_R + \vec{\Lambda}_L \mathbf{Y}_{\vec{\lambda}}^{(5D)} \vec{\lambda}_R \right. \right. \\ \left. \left. + \vec{U}_R \mathbf{Y}_{\vec{u}}^{(5D)} \vec{u}_L + \vec{D}_R \mathbf{Y}_{\vec{d}}^{(5D)} \vec{d}_L + \vec{\Lambda}_R \mathbf{Y}_{\vec{\lambda}}^{(5D)} \vec{\lambda}_L + \text{h.c.} \right] \right\}, \quad (62) \end{aligned}$$

with the Yukawa matrices

$$\mathbf{Y}_{\vec{u}}^{(5D)} \equiv \begin{pmatrix} \mathbf{Y}_u^{(5D)} & \frac{1}{\sqrt{2}} \mathbf{Y}_d^{(5D)} & \frac{1}{\sqrt{2}} \mathbf{Y}_d^{(5D)} \\ \mathbf{Y}_u^{(5D)} & -\frac{1}{\sqrt{2}} \mathbf{Y}_d^{(5D)} & -\frac{1}{\sqrt{2}} \mathbf{Y}_d^{(5D)} \end{pmatrix}, \quad \mathbf{Y}_{\vec{d}}^{(5D)} \equiv \mathbf{Y}_{\vec{\lambda}}^{(5D)} \equiv \begin{pmatrix} \mathbf{Y}_d^{(5D)} & \mathbf{Y}_d^{(5D)} \end{pmatrix}. \quad (63)$$

The symmetric derivative $\overleftrightarrow{\partial}_\phi \equiv \overrightarrow{\partial}_\phi - \overleftarrow{\partial}_\phi$ ensures hermicity of the action in the presence of boundary terms. In the case of the SM with three generations each entry of (63) corresponds

to a 3×3 matrix. We define dimensionless 4D Yukawa couplings via

$$\mathbf{Y}_q^{(5D)} \equiv \frac{2\mathbf{Y}_q}{k}, \quad (64)$$

where k denotes the AdS₅ curvature and $q = u, d$. The generalized bulk mass matrices $\mathbf{M}_{\vec{q}}$ take the form

$$\begin{aligned} \mathbf{M}_{\vec{U}} &\equiv \begin{pmatrix} \mathbf{M}_Q & 0 \\ 0 & \mathbf{M}_Q \end{pmatrix}, & \mathbf{M}_{\vec{D}} &\equiv \mathbf{M}_Q, & \mathbf{M}_{\vec{\Lambda}} &\equiv \mathbf{M}_Q, \\ \mathbf{M}_{\vec{u}} &\equiv \begin{pmatrix} \mathbf{M}_{u^c} & 0 & 0 \\ 0 & \mathbf{M}_{\mathcal{T}_1} & 0 \\ 0 & 0 & \mathbf{M}_{\mathcal{T}_2} \end{pmatrix}, & \mathbf{M}_{\vec{d}} &\equiv \begin{pmatrix} \mathbf{M}_{\mathcal{T}_2} & 0 \\ 0 & \mathbf{M}_{\mathcal{T}_1} \end{pmatrix}, & \mathbf{M}_{\vec{\lambda}} &\equiv \begin{pmatrix} \mathbf{M}_{\mathcal{T}_1} & 0 \\ 0 & \mathbf{M}_{\mathcal{T}_2} \end{pmatrix}, \end{aligned} \quad (65)$$

where \mathbf{M}_A are the 3×3 bulk mass matrices of the corresponding multiplets $A = Q, u^c, \mathcal{T}_1, \mathcal{T}_2$.

4.2 KK Decomposition

As motivated above, we decompose different 5D spinors that get mixed by the IR BCs (*i.e.*, by the Yukawa couplings) into the same basis of 4D spinors⁴

$$\begin{aligned} \vec{Q}_L(x, \phi) &= \frac{e^{2\sigma(\phi)}}{\sqrt{r}} \sum_n \mathbf{C}_n^Q(\phi) \vec{a}_n^Q q_L^{(n)}(x), & \vec{Q}_R(x, \phi) &= \frac{e^{2\sigma(\phi)}}{\sqrt{r}} \sum_n \mathbf{S}_n^Q(\phi) \vec{a}_n^Q q_R^{(n)}(x), \\ \vec{q}_L(x, \phi) &= \frac{e^{2\sigma(\phi)}}{\sqrt{r}} \sum_n \mathbf{S}_n^q(\phi) \vec{a}_n^q q_L^{(n)}(x), & \vec{q}_R(x, \phi) &= \frac{e^{2\sigma(\phi)}}{\sqrt{r}} \sum_n \mathbf{C}_n^q(\phi) \vec{a}_n^q q_R^{(n)}(x), \end{aligned} \quad (66)$$

where $Q = U, D, \Lambda$ and $q = u, d, \lambda$. Furthermore

$$\begin{aligned} \mathbf{C}_n^U &\equiv \text{diag}(\mathbf{C}_n^{Q(+)}, \mathbf{C}_n^{Q(-)}), & \mathbf{C}_n^u &\equiv \text{diag}(\mathbf{C}_n^{u^c(+)}, \mathbf{C}_n^{\mathcal{T}_1(-)}, \mathbf{C}_n^{\mathcal{T}_2(-)}), \\ \mathbf{S}_n^U &\equiv \text{diag}(\mathbf{S}_n^{Q(+)}, \mathbf{S}_n^{Q(-)}), & \mathbf{S}_n^u &\equiv \text{diag}(\mathbf{S}_n^{u^c(+)}, \mathbf{S}_n^{\mathcal{T}_1(-)}, \mathbf{S}_n^{\mathcal{T}_2(-)}), \\ \mathbf{C}_n^D &\equiv \mathbf{C}_n^{Q(+)}, & \mathbf{C}_n^d &\equiv \text{diag}(\mathbf{C}_n^{\mathcal{T}_2(+)}, \mathbf{C}_n^{\mathcal{T}_1(-)}), \\ \mathbf{S}_n^D &\equiv \mathbf{S}_n^{Q(+)}, & \mathbf{S}_n^d &\equiv \text{diag}(\mathbf{S}_n^{\mathcal{T}_2(+)}, \mathbf{S}_n^{\mathcal{T}_1(-)}), \\ \mathbf{C}_n^\Lambda &\equiv \mathbf{C}_n^{Q(-)}, & \mathbf{C}_n^\lambda &\equiv \text{diag}(\mathbf{C}_n^{\mathcal{T}_1(-)}, \mathbf{C}_n^{\mathcal{T}_2(-)}), \\ \mathbf{S}_n^\Lambda &\equiv \mathbf{S}_n^{Q(-)}, & \mathbf{S}_n^\lambda &\equiv \text{diag}(\mathbf{S}_n^{\mathcal{T}_1(-)}, \mathbf{S}_n^{\mathcal{T}_2(-)}), \end{aligned} \quad (67)$$

⁴Here we have already made use of the fact that $\vec{Q}_{L,R}(x, \phi)$ ($\vec{q}_{L,R}(x, \phi)$) can be expanded in terms of the same vector \vec{a}_n^Q (\vec{a}_n^q). With this choice, the profiles $\mathbf{C}_n^Q(\phi)$ and $\mathbf{S}_n^Q(\phi)$ ($\mathbf{C}_n^q(\phi)$ and $\mathbf{S}_n^q(\phi)$) are normalized in the same way.

and

$$\vec{a}_n^U \equiv \begin{pmatrix} a_n^u \\ a_n^{u'} \end{pmatrix}, \quad \vec{a}_n^u \equiv \begin{pmatrix} a_n^{u^c} \\ a_n^{U'} \\ a_n^U \end{pmatrix}, \quad \vec{a}_n^D \equiv a_n^d, \quad \vec{a}_n^d \equiv \begin{pmatrix} a_n^D \\ a_n^{D'} \end{pmatrix}, \quad \vec{a}_n^\Lambda \equiv a_n^\lambda, \quad \vec{a}_n^\lambda \equiv \begin{pmatrix} a_n^{\Lambda'} \\ a_n^\Lambda \end{pmatrix}, \quad (68)$$

where in order to simplify the notation we have dropped the argument ϕ in the profile functions. Each component of the vector of spinors on the left-hand side of (66) contains three entries belonging to the three quark generations. The 3×3 matrices $\mathbf{C}_n^{A(\pm)}(\phi)$ ($\mathbf{S}_n^{A(\pm)}(\phi)$) with $A = Q, u^c, \mathcal{T}_1, \mathcal{T}_2$ correspond to even (odd) profiles on the orbifold, and the superscript (\pm) indicates the type of BC on the UV brane. With some abuse of notation, the superscripts of the odd profiles refer to the UV BC of the associated even profiles. The quarks present already in the minimal RS model hence all carry a (+) superscript. Labels for the IR BCs are again omitted to simplify the notation. The flavor structure is encoded in the three-component vectors a_n^A with $A = u, u', u^c, U', U, d, D', D, \lambda, \Lambda', \Lambda$, which are then combined into larger flavor vectors $\vec{a}_n^{Q,q}$ with Q and q defined as above. Finally, $q_L^{(n)}(x)$ and $q_R^{(n)}(x)$ are 4D spinors, and the index n labels the different mass eigenstates with masses m_n , *i.e.*, $m_1 = m_u$, $m_2 = m_c$, $m_3 = m_t$, *etc.* in the case of up-type quarks, and similarly for down-type quarks.

By virtue of the vector notation (61), we have reached complete analogy to the decomposition of bulk quark fields in the minimal model [24]. The further analysis in this section thus follows almost entirely the corresponding part in that article. An exception is the inclusion of the Yukawa couplings involving Z_2 -odd fermion profiles, which, as pointed out in [37], have not been considered in our previous work. In the following we will close this gap, confirming the $\mathcal{O}(v^2/M_{\text{KK}}^2)$ results for a brane-localized Higgs presented in [37] and extending them to all orders in the ratio of the weak over the KK scale. A detailed discussion of the impact of the inclusion of the Z_2 -odd fermion couplings on the flavor misalignment between the SM fermion masses and the Yukawa couplings is deferred to Section 6.

The 5D variational principle requires all the variations of the action (62) to vanish for arbitrary infinitesimal changes of the fermionic fields. After KK decomposition (66), this leads to the following EOMs

$$\begin{aligned} \left(-\frac{1}{r} \partial_\phi - \mathbf{M}_{\bar{q}} \text{sgn}(\phi) \right) \mathbf{S}_n^Q(\phi) \vec{a}_n^Q &= -m_n e^{\sigma(\phi)} \mathbf{C}_n^Q(\phi) \vec{a}_n^Q \\ &+ \delta(|\phi| - \pi) e^{\sigma(\phi)} \frac{\sqrt{2}v}{kr} \mathbf{Y}_{\bar{q}} \mathbf{C}_n^q(\phi) \vec{a}_n^q, \\ \left(\frac{1}{r} \partial_\phi - \mathbf{M}_{\bar{q}} \text{sgn}(\phi) \right) \mathbf{S}_n^q(\phi) \vec{a}_n^q &= -m_n e^{\sigma(\phi)} \mathbf{C}_n^q(\phi) \vec{a}_n^q \\ &+ \delta(|\phi| - \pi) e^{\sigma(\phi)} \frac{\sqrt{2}v}{kr} \mathbf{Y}_{\bar{q}}^\dagger \mathbf{C}_n^Q(\phi) \vec{a}_n^Q, \end{aligned}$$

$$\begin{aligned}
\left(\frac{1}{r}\partial_\phi - \mathbf{M}_{\bar{q}}\text{sgn}(\phi)\right)\mathbf{C}_n^Q(\phi)\vec{a}_n^Q &= -m_n e^{\sigma(\phi)}\mathbf{S}_n^Q(\phi)\vec{a}_n^Q \\
&\quad + \delta(|\phi| - \pi)e^{\sigma(\phi)}\frac{\sqrt{2}v}{kr}\mathbf{Y}_{\bar{q}}\mathbf{S}_n^q(\phi)\vec{a}_n^q, \\
\left(-\frac{1}{r}\partial_\phi - \mathbf{M}_{\bar{q}}\text{sgn}(\phi)\right)\mathbf{C}_n^q(\phi)\vec{a}_n^q &= -m_n e^{\sigma(\phi)}\mathbf{S}_n^q(\phi)\vec{a}_n^q \\
&\quad + \delta(|\phi| - \pi)e^{\sigma(\phi)}\frac{\sqrt{2}v}{kr}\mathbf{Y}_{\bar{q}}^\dagger\mathbf{S}_n^Q(\phi)\vec{a}_n^Q. \tag{69}
\end{aligned}$$

Within the bulk, *i.e.*, for $\phi \neq 0, \pm\pi$, where no brane-localized terms are present, the general solutions [9, 8] to the above equations can be written as linear combinations of Bessel functions (see Section 4.3). The presence of the source terms on the IR brane dictates the boundary behavior of the fields and causes both the Z_2 -even and -odd profiles to become discontinuous at the IR brane with $\mathbf{C}_n^{Q,q}(\pm\pi) \neq \mathbf{C}_n^{Q,q}(\pm\pi^-)$ and $\mathbf{S}_n^{Q,q}(\pm\pi) = 0$ but $\mathbf{S}_n^{Q,q}(\pm\pi^-) \neq 0$ [38]. Finding the correct IR BCs requires a proper regularization of the δ -functions appearing in (69). In the following, we will view the δ -function as the limit of a sequence of regularized functions δ^η with support on the interval $x \in [-\eta, 0]$. This limit is understood in the weak sense so that

$$\lim_{\eta \rightarrow 0^+} \int_{-\infty}^{+\infty} dx \delta^\eta(x) f(x) = f(0), \tag{70}$$

for all test functions $f(x)$, *i.e.*, smooth functions having compact support.

In an infinitesimal interval around $|\phi| = \pi$, the source terms in (69) are formally singular and as a result the behavior of the profiles $\mathbf{C}_n^{Q,q}(\phi)$ and $\mathbf{S}_n^{Q,q}(\phi)$ becomes independent of the mass terms entering the EOMs. We regularize the δ -functions, switch to t coordinates and integrate these equations from t to 1, taking into account that the odd fermion profiles vanish identically on the IR brane, *i.e.*, $\mathbf{S}_n^{Q,q}(1) = 0$. In this way we find

$$\begin{aligned}
\mathbf{S}_n^Q(t)\vec{a}_n^Q &= \frac{v}{\sqrt{2}M_{\text{KK}}}\mathbf{Y}_{\bar{q}}\int_t^1 dt' [\delta^\eta(t' - 1)\mathbf{C}_n^q(t')]\vec{a}_n^q, \\
\mathbf{S}_n^q(t)\vec{a}_n^q &= -\frac{v}{\sqrt{2}M_{\text{KK}}}\mathbf{Y}_{\bar{q}}^\dagger\int_t^1 dt' [\delta^\eta(t' - 1)\mathbf{C}_n^Q(t')]\vec{a}_n^Q, \\
\mathbf{C}_n^Q(t)\vec{a}_n^Q &= \mathbf{C}_n^Q(1)\vec{a}_n^Q - \frac{v}{\sqrt{2}M_{\text{KK}}}\mathbf{Y}_{\bar{q}}\int_t^1 dt' [\delta^\eta(t' - 1)\mathbf{S}_n^q(t')]\vec{a}_n^q, \\
\mathbf{C}_n^q(t)\vec{a}_n^q &= \mathbf{C}_n^q(1)\vec{a}_n^q + \frac{v}{\sqrt{2}M_{\text{KK}}}\mathbf{Y}_{\bar{q}}^\dagger\int_t^1 dt' [\delta^\eta(t' - 1)\mathbf{S}_n^Q(t')]\vec{a}_n^Q. \tag{71}
\end{aligned}$$

In order to solve (71), we first introduce the regularized Heaviside function

$$\bar{\theta}^\eta(x) \equiv 1 - \int_{-\infty}^x dy \delta^\eta(y), \tag{72}$$

which obeys

$$\bar{\theta}^\eta(0) = 0, \quad \bar{\theta}^\eta(-\eta) = 1, \quad \partial_x \bar{\theta}^\eta(x) = -\delta^\eta(x). \quad (73)$$

Using the latter properties it is readily shown that

$$\int_t^1 dt' \delta^\eta(t' - 1) [\bar{\theta}^\eta(t' - 1)]^n = \frac{1}{n+1} [\bar{\theta}^\eta(t - 1)]^{n+1}. \quad (74)$$

It follows that for any arbitrary invertible matrix \mathbf{A} one has

$$\begin{aligned} \int_t^1 dt' \delta^\eta(t' - 1) \sinh(\bar{\theta}^\eta(t' - 1) \mathbf{A}) &= [\cosh(\bar{\theta}^\eta(t - 1) \mathbf{A}) - \mathbf{1}] \mathbf{A}^{-1}, \\ \int_t^1 dt' \delta^\eta(t' - 1) \cosh(\bar{\theta}^\eta(t' - 1) \mathbf{A}) &= \sinh(\bar{\theta}^\eta(t - 1) \mathbf{A}) \mathbf{A}^{-1}, \end{aligned} \quad (75)$$

where the hyperbolic sine and cosine are defined via their power expansions.

The relations (75) now allow to determine the solutions to (71). We find the following expressions

$$\begin{aligned} \mathbf{S}_n^Q(t) \vec{a}_n^Q &= \mathbf{Y}_{\bar{q}} \left(\sqrt{\mathbf{Y}_{\bar{q}}^\dagger \mathbf{Y}_{\bar{q}}} \right)^{-1} \sinh \left(\frac{v}{\sqrt{2} M_{\text{KK}}} \bar{\theta}^\eta(t - 1) \sqrt{\mathbf{Y}_{\bar{q}}^\dagger \mathbf{Y}_{\bar{q}}} \right) \mathbf{C}_n^q(1) \vec{a}_n^q, \\ \mathbf{S}_n^q(t) \vec{a}_n^q &= -\mathbf{Y}_{\bar{q}}^\dagger \left(\sqrt{\mathbf{Y}_{\bar{q}} \mathbf{Y}_{\bar{q}}^\dagger} \right)^{-1} \sinh \left(\frac{v}{\sqrt{2} M_{\text{KK}}} \bar{\theta}^\eta(t - 1) \sqrt{\mathbf{Y}_{\bar{q}} \mathbf{Y}_{\bar{q}}^\dagger} \right) \mathbf{C}_n^Q(1) \vec{a}_n^Q, \\ \mathbf{C}_n^Q(t) \vec{a}_n^Q &= \cosh \left(\frac{v}{\sqrt{2} M_{\text{KK}}} \bar{\theta}^\eta(t - 1) \sqrt{\mathbf{Y}_{\bar{q}} \mathbf{Y}_{\bar{q}}^\dagger} \right) \mathbf{C}_n^Q(1) \vec{a}_n^Q, \\ \mathbf{C}_n^q(t) \vec{a}_n^q &= \cosh \left(\frac{v}{\sqrt{2} M_{\text{KK}}} \bar{\theta}^\eta(t - 1) \sqrt{\mathbf{Y}_{\bar{q}}^\dagger \mathbf{Y}_{\bar{q}}} \right) \mathbf{C}_n^q(1) \vec{a}_n^q. \end{aligned} \quad (76)$$

Since the t -integration has already been performed in (76), one can now safely take the limit $\eta \rightarrow 0^+$ and trade the on-brane values $\mathbf{C}_n^{Q,q}(1)$ for the bulk values $\mathbf{C}_n^{Q,q}(1^-)$ obtained from the solutions to (69) by a limiting procedure. Introducing the rescaled Yukawa matrices⁵

$$\tilde{\mathbf{Y}}_{\bar{q}} \equiv \mathbf{f} \left(\frac{v}{\sqrt{2} M_{\text{KK}}} \sqrt{\mathbf{Y}_{\bar{q}} \mathbf{Y}_{\bar{q}}^\dagger} \right) \mathbf{Y}_{\bar{q}}, \quad \mathbf{f}(\mathbf{A}) = \tanh(\mathbf{A}) \mathbf{A}^{-1}, \quad (77)$$

which coincide at leading order with the original ones, *i.e.*, $\tilde{\mathbf{Y}}_{\bar{q}} = \mathbf{Y}_{\bar{q}} + \mathcal{O}(v^2/M_{\text{KK}}^2)$, it is then easy to show that the sought IR BCs are manifestly regularization independent⁶ and can be

⁵Generalizing this result to the case where Z_2 -even and -odd fermion fields couple differently to the brane-localized Higgs sector only requires to perform the replacements $\mathbf{Y}_{\bar{q}} \rightarrow \mathbf{Y}_{\bar{q}}^C$ and $\mathbf{Y}_{\bar{q}}^\dagger \rightarrow \mathbf{Y}_{\bar{q}}^{S\dagger}$, where the superscript in $\mathbf{Y}_{\bar{q}}^{C,S}$ denotes the fields the Higgs couples to. The same replacement rules also apply in the case of (140) to (144).

⁶It seems instructive to rederive (78) using a rectangular function to regularize the δ -functions appearing in (69). The explicit calculation is presented in Appendix A. There it is also shown how to obtain (140) to (144) using the latter regularization.

written in ϕ coordinates as

$$\begin{aligned}\mathbf{S}_n^Q(\pi^-) \vec{a}_n^Q &= \frac{v}{\sqrt{2}M_{\text{KK}}} \tilde{\mathbf{Y}}_{\bar{q}} \mathbf{C}_n^q(\pi^-) \vec{a}_n^q, \\ -\mathbf{S}_n^q(\pi^-) \vec{a}_n^q &= \frac{v}{\sqrt{2}M_{\text{KK}}} \tilde{\mathbf{Y}}_{\bar{q}}^\dagger \mathbf{C}_n^Q(\pi^-) \vec{a}_n^Q.\end{aligned}\tag{78}$$

They hence take precisely the same form as in [24], with the original Yukawa couplings replaced by the rescaled ones as defined in (77). Since in practice the Yukawa matrices (together with the quark profiles) are chosen such that the zero-mode masses as well as the quark mixing angles match the ones determined by experiment, such a rescaling has no observable effect on the mass spectrum and the mixing pattern. However, as we will explain in detail in Section 6, the inclusion of the Yukawa coupling involving Z_2 -odd fermions alters the form of the tree-level interactions of the Higgs-boson with fermions with respect to the results derived in [24].

The δ -distributions in the 5D action (62) forces one to impose generalized orthonormality conditions for the individual profiles [24],

$$\begin{aligned}\int_{-\pi}^{\pi} d\phi e^{\sigma(\phi)} \mathbf{C}_m^{Q,q}(\phi) \mathbf{C}_n^{Q,q}(\phi) &= \delta_{mn} \mathbf{1} + \Delta \mathbf{C}_{mn}^{Q,q}, \\ \int_{-\pi}^{\pi} d\phi e^{\sigma(\phi)} \mathbf{S}_m^{Q,q}(\phi) \mathbf{S}_n^{Q,q}(\phi) &= \delta_{mn} \mathbf{1} + \Delta \mathbf{S}_{mn}^{Q,q},\end{aligned}\tag{79}$$

where $\mathbf{1}$ is a unit matrix of dimension 3×3 , 6×6 , or 9×9 , depending on the value of the indices Q or q . We then find that the 4D action reduces to the desired canonical form if and only if, in addition to the BCs, the relation

$$\vec{a}_m^{Q,q\dagger} (\delta_{mn} \mathbf{1} + \Delta \mathbf{C}_{mn}^{Q,q}) \vec{a}_n^{Q,q} + \vec{a}_m^{q,Q\dagger} (\delta_{mn} \mathbf{1} + \Delta \mathbf{S}_{mn}^{q,Q}) \vec{a}_n^{q,Q} = \delta_{mn}\tag{80}$$

is fulfilled. It is also straightforward to show that the profiles satisfy

$$m_m \Delta \mathbf{C}_{mn}^{Q,q} - m_n \Delta \mathbf{S}_{mn}^{Q,q} = \pm \frac{2}{r} \mathbf{C}_n^{Q,q}(\pi^-) \mathbf{S}_m^{Q,q}(\pi^-).\tag{81}$$

Since an overall normalization can always be reshuffled between the profiles $\mathbf{C}_n^{Q,q}(\phi)$ and $\mathbf{S}_n^{Q,q}(\phi)$ and the eigenvectors $\vec{a}_n^{Q,q}$, the sum $\Delta \mathbf{C}_{nn}^{Q,q} + \Delta \mathbf{S}_{nn}^{Q,q}$ can be chosen freely without changing the physical result. The option $\Delta \mathbf{C}_{nn}^{Q,q} + \Delta \mathbf{S}_{nn}^{Q,q} = 0$ turns out to be particularly convenient and thus will be adopted hereafter. With this choice (80) splits into

$$\vec{a}_n^{Q\dagger} \vec{a}_n^Q + \vec{a}_n^{q\dagger} \vec{a}_n^q = 1,\tag{82}$$

and

$$\vec{a}_m^{Q,q\dagger} \Delta \mathbf{C}_{mn}^{Q,q} \vec{a}_n^{Q,q} + \vec{a}_m^{q,Q\dagger} \Delta \mathbf{S}_{mn}^{q,Q} \vec{a}_n^{q,Q} = 0.\tag{83}$$

Finally, the mass eigenvalues m_n follow from the solutions to the equation

$$\det \left(\mathbf{1} + \frac{v^2}{2M_{\text{KK}}^2} \tilde{\mathbf{Y}}_{\bar{q}} \mathbf{C}_n^q(\pi^-) [\mathbf{S}_n^q(\pi^-)]^{-1} \tilde{\mathbf{Y}}_{\bar{q}}^\dagger \mathbf{C}_n^Q(\pi^-) [\mathbf{S}_n^Q(\pi^-)]^{-1} \right) = 0.\tag{84}$$

Once they are known, the eigenvectors $\vec{a}_n^{Q,q}$ can be determined from (78). Note that, while it is always possible to work with real and diagonal profiles $\mathbf{C}_n^{Q,q}(\phi)$ and $\mathbf{S}_n^{Q,q}(\phi)$, the vectors $\vec{a}_n^{Q,q}$ are, in general, complex-valued objects.

4.3 Bulk Profiles

The explicit form of the solutions $(C_n^{A(+)}(\phi))_i$ and $(S_n^{A(+)}(\phi))_i$ associated with bulk mass parameters M_{A_i} was obtained in [9, 8]. The functions $(C_n^{A(-)}(\phi))_i$ and $(S_n^{A(-)}(\phi))_i$ can be derived in a similar fashion by requiring a Dirichlet condition for the even mode, $(C_n^{A(-)}(0))_i = 0$, to account for the additional twist of the non-SM-like fermions at the UV boundary. The treatment is therefore analogous to the odd modes of the SM-like fermions, for which $(S_n^{A(+)}(0))_i = 0$. We will drop the label A and the index i for the purposes of most of the discussion, since they should be clear from the context. In terms of $t = \epsilon e^{\sigma(\phi)}$, one finds in the bulk (*i.e.*, for $t \in]\epsilon, 1[$)

$$\begin{aligned} C_n^{(\pm)}(\phi) &= \mathcal{N}_n^{(\pm)}(c) \sqrt{\frac{L\epsilon t}{\pi}} f_n^{(\pm)+}(t, c), \\ S_n^{(\pm)}(\phi) &= \pm \mathcal{N}_n^{(\pm)}(c) \operatorname{sgn}(\phi) \sqrt{\frac{L\epsilon t}{\pi}} f_n^{(\pm)-}(t, c), \end{aligned} \quad (85)$$

where the overall “+” sign entering the Z_2 -odd profiles holds if $c = c_Q \equiv +M_Q/k$ refers to the bi-doublet, while the “-” sign applies in the case of $c = c_A \equiv -M_A/k$, where $A = u^c, \mathcal{T}_1, \mathcal{T}_2$. The functions $f_n^{(\pm)\pm}(t, c)$ are given by

$$\begin{aligned} f_n^{(+)\pm}(t, c) &= J_{-\frac{1}{2}-c}(x_n\epsilon) J_{\mp\frac{1}{2}+c}(x_nt) \pm J_{+\frac{1}{2}+c}(x_n\epsilon) J_{\pm\frac{1}{2}-c}(x_nt), \\ f_n^{(-)\pm}(t, c) &= J_{+\frac{1}{2}-c}(x_n\epsilon) J_{\mp\frac{1}{2}+c}(x_nt) \mp J_{-\frac{1}{2}+c}(x_n\epsilon) J_{\pm\frac{1}{2}-c}(x_nt). \end{aligned} \quad (86)$$

They satisfy the equalities

$$f_n^{(+)+}(t, c) = f_n^{(-)-}(t, -c), \quad f_n^{(+)-}(t, c) = -f_n^{(-)+}(t, -c). \quad (87)$$

The orthonormality relations (79) imply the normalization conditions

$$2 \int_{\epsilon}^1 dt t [f_n^{(a)\pm}(t, c)]^2 = \frac{1}{[\mathcal{N}_n^{(a)}(c)]^2} \pm \frac{f_n^{(a)+}(1, c) f_n^{(a)-}(1^-, c)}{x_n}, \quad (88)$$

where $a = \pm$. From these relations we derive

$$\begin{aligned} [\mathcal{N}_n^{(a)}(c)]^{-2} &= [f_n^{(a)+}(1, c)]^2 + [f_n^{(a)-}(1^-, c)]^2 \\ &\quad - \frac{2c}{x_n} f_n^{(a)+}(1, c) f_n^{(a)-}(1^-, c) - \epsilon^2 \left([f_n^{(a)+}(\epsilon, c)]^2 + [f_n^{(a)-}(\epsilon^+, c)]^2 \right), \end{aligned} \quad (89)$$

which extends the result obtained in [24] to the case of Z_2 -odd profiles with non-zero value at the UV boundary. For the special cases where $c + 1/2$ is an integer, the profiles must be obtained from the above relations by a limiting procedure.

For the SM fermions, it is a very good approximation to expand the profiles in the limit $x_n \ll 1$, since even the top-quark mass is much lighter than the KK scale. We will hereafter

refer to such an expansion as the “zero-mode approximation” (ZMA). Using results from [24] in combination with (87), we obtain

$$\begin{aligned}
C_n^{(+)}(\phi) &\approx \sqrt{\frac{L\epsilon}{\pi}} F(c) t^c, & S_n^{(+)}(\phi) &\approx \pm \text{sgn}(\phi) \sqrt{\frac{L\epsilon}{\pi}} x_n F(c) \frac{t^{1+c} - \epsilon^{1+2c} t^{-c}}{1+2c}, \\
C_n^{(-)}(\phi) &\approx -\sqrt{\frac{L\epsilon}{\pi}} x_n F(-c) \frac{t^{1-c} - \epsilon^{1-2c} t^c}{1-2c}, & S_n^{(-)}(\phi) &\approx \pm \text{sgn}(\phi) \sqrt{\frac{L\epsilon}{\pi}} F(-c) t^{-c},
\end{aligned} \tag{90}$$

where we have introduced the zero-mode profile [9, 8]

$$F(c) \equiv \text{sgn}[\cos(\pi c)] \sqrt{\frac{1+2c}{1-\epsilon^{1+2c}}}. \tag{91}$$

The sign factor in (91) is chosen such that the signs in (90) agree with those derived from the exact profiles (85). Notice that the profiles $C_n^{(+)}(\phi)$ and $S_n^{(-)}(\phi)$ are of $\mathcal{O}(1)$, while $C_n^{(-)}(\phi)$ and $S_n^{(+)}(\phi)$ are of $\mathcal{O}(v/M_{\text{KK}})$. As we will explain in detail in the next section, this feature will allow to partially shield the $Zb_L\bar{b}_L$ and $Zd_L^i\bar{d}_L^j$ vertices from corrections due to mixing of zero-mode quarks with their KK excitations.

The quantity $F(c)$ depends strongly on the value of c . One obtains

$$F(c) \approx \begin{cases} -\sqrt{-1-2c} \epsilon^{-c-\frac{1}{2}}, & -3/2 < c < -1/2, \\ \sqrt{1+2c}, & -1/2 < c < 1/2, \end{cases} \tag{92}$$

which implies that for UV-localized fermions the corresponding zero-mode profile is exponentially small, while it is of $\mathcal{O}(1)$ for IR-localized fields.

5 Gauge Interactions with Fermions

In this section we reexamine how a protection of the left-handed down-type couplings of the Z boson can be achieved by choosing an appropriate embedding of the fermions into the enlarged gauge group in the bulk. We also derive the four-fermion charged-current interactions and show explicitly that a custodial protection is not at work in this case. To start, we give the covariant derivative in the UV basis,

$$\begin{aligned}
D_\mu &= \partial_\mu - i \frac{g_{L5}}{\sqrt{2}} (L_\mu^+ T_L^+ + L_\mu^- T_L^-) + i \frac{g_{R5}}{\sqrt{2}} (R_\mu^+ T_R^+ + R_\mu^- T_R^-) \\
&\quad - i g_{Z5} Q_Z Z_\mu - i g_{Z'5} Q_{Z'} Z'_\mu - i e_5 Q A_\mu.
\end{aligned} \tag{93}$$

The Z -boson couplings to fermionic currents are defined by

$$\begin{aligned}
g_Z &= \sqrt{g_L^2 + g_Y^2}, & g_{Z'} &= \sqrt{g_R^2 + g_X^2}, \\
Q_Z &= T_L^3 - \frac{g_Y}{g_Z} Q, & Q_{Z'} &= -T_R^3 - \frac{g_X}{g_{Z'}} Y.
\end{aligned} \tag{94}$$

At this point we have to specify the form of the $SU(2)_{L,R}$ generators when acting on different fermion representations. Acting on fermion bi-doublets, the generators $T_{L,R}^i$ with $i = 1, 2, 3$ are given by the Pauli matrices in the standard convention times a factor of $1/2$. As usual we define $T_{L,R}^\pm = T_{L,R}^1 \pm iT_{L,R}^2$. If, on the other hand, the generators act on $SU(2)_{L,R}$ triplets, then one has

$$T_{L,R}^+ = \begin{pmatrix} 0 & \sqrt{2} & 0 \\ 0 & 0 & \sqrt{2} \\ 0 & 0 & 0 \end{pmatrix}, \quad T_{L,R}^- = \begin{pmatrix} 0 & 0 & 0 \\ \sqrt{2} & 0 & 0 \\ 0 & \sqrt{2} & 0 \end{pmatrix}, \quad T_{L,R}^3 = \begin{pmatrix} 1 & 0 & 0 \\ 0 & 0 & 0 \\ 0 & 0 & -1 \end{pmatrix}. \quad (95)$$

Note that the current operators involve a trace with respect to the fundamental gauge indices, and that again the $T_{L,R}^i$ act from the right. It will furthermore turn out to be useful to introduce

$$\vec{g}_Z = \begin{pmatrix} g_Z Q_Z \\ g_{Z'} Q_{Z'} \end{pmatrix}, \quad (96)$$

as well as the charged-current vectors

$$\begin{aligned} \vec{J}_{W_Q}^{\mu\pm} &= \frac{1}{\sqrt{2}} (g_L \text{Tr} [\bar{Q} \gamma^\mu T^\pm Q], g_R \text{Tr} [\bar{Q} \gamma^\mu Q T^\pm]), \\ \vec{J}_{W_\tau}^{\mu\pm} &= \frac{1}{\sqrt{2}} (g_L \bar{\mathcal{T}}_1 \gamma^\mu T^\pm \mathcal{T}_1, g_R \text{Tr} [\bar{\mathcal{T}}_2 \gamma^\mu \mathcal{T}_2 T^\pm]), \end{aligned} \quad (97)$$

which act on $(L_\mu^\pm, R_\mu^\pm)^T$ from the left. These latter formulas are needed to calculate the corrections to the quark-mixing matrices, which we postpone until Section 5.4.

5.1 Custodial Protection: Gauge-Boson Contributions

Using (44) and (45), we find that the coupling of the Z boson to a quark current is proportional to

$$(\vec{g}_Z^q)^T \vec{\chi}_0^Z(\phi) = \frac{g_Z Q_Z^q}{\sqrt{2}\pi} \left\{ 1 + \frac{m_Z^2}{4M_{\text{KK}}^2} \left[1 - \frac{1}{L} - 2L t^2 \omega_Z^q + 2t^2 \left(\frac{1}{2} - \ln t \right) \right] \right\} + \mathcal{O} \left(\frac{m_Z^4}{M_{\text{KK}}^4} \right), \quad (98)$$

with

$$\omega_Z^q = 1 - \frac{s_Z}{c_Z} \frac{g_{Z'} Q_{Z'}^q}{g_Z Q_Z^q}. \quad (99)$$

This is an important result, as it allows us to understand the custodial protection of the $Z b_L \bar{b}_L$ vertex. Note that the term in (98) that is enhanced by the volume factor L gets modified by a prefactor ω_Z^q , *i.e.*, a combination of the fundamental charges and couplings. While $\omega_Z^q = 1$ for all quarks in the minimal RS model, it is possible to arrange for

$$\omega_Z^{b_L} = 0 \quad \iff \quad g_Z Q_Z^{b_L} = \frac{s_Z}{c_Z} g_{Z'} Q_{Z'}^{b_L}, \quad (100)$$

by virtue of the extension of the gauge group in the bulk. It is interesting to observe that only the leading term in L can be protected, while no such mechanism is available for the subleading

terms in L , since they arise from the fact that the fields $\chi_0^{(\pm)}(t)$ obey different BCs. The latter effects hence represent an irreducible source of P_{LR} symmetry breaking. Numerically, the corrections to the $Zb_L\bar{b}_L$ vertex arising from the gauge sector are thus suppressed by a factor of $L \approx 37$ in the $SU(2)_L \times SU(2)_R \times P_{LR}$ custodial model relative to the minimal RS model.

Formula (99) can be recast into the form

$$\omega_Z^q = \frac{c_w^2}{2g_L^2} \frac{(g_L^2 + g_R^2)(T_L^{3q} + T_R^{3q}) + (g_L^2 - g_R^2)(T_L^{3q} - T_R^{3q})}{T_L^{3q} - s_w^2 Q_q}, \quad (101)$$

which allows one to read off that the choices

$$T_L^{3q} = T_R^{3q} = 0, \quad (P_C \text{ symmetry}) \quad (102)$$

and

$$g_L = g_R, \quad T_L^{3q} = -T_R^{3q}, \quad (P_{LR} \text{ symmetry}) \quad (103)$$

are suitable to protect the Z -boson vertices from receiving L -enhanced corrections. Since the representation (58) features $T_L^{3dL} = -T_R^{3dL} = -1/2$ and $T_L^{3uR} = T_R^{3uR} = 0$, it is then immediately clear that the $Zd_L^i\bar{d}_L^j$ and $Zu_R^i\bar{u}_R^j$ vertices are protected to leading order in L by the P_{LR} and P_C symmetries, respectively. On the other hand, the $Zd_R^i\bar{d}_R^j$ and $Zu_L^i\bar{u}_L^j$ vertices do receive L -enhanced corrections, since the corresponding quantum numbers are $T_L^{3dR} = 0$, $T_R^{3dR} = 1$ and $T_L^{3uL} = T_R^{3uL} = 1/2$. We also add that devising the quark sector as in (58) implies $\omega_Z^{bR} > 0$, so that the shift in the right-handed Z -boson coupling to bottom quarks arising from the gauge-boson sector is predicted to be strictly negative. This suggests that the well-known tension in the global fit to the $Z \rightarrow b\bar{b}$ pseudo observables cannot be softened in the model under considerations. We will come back to this point in Section 7.1.

5.2 Fermion Couplings to the Z Boson

We turn to the phenomenologically relevant expressions for weak gauge interactions of quark currents in the custodial model and identify the RS contribution at relative order v^2/M_{KK}^2 . The Z -boson couplings to left- and right-handed quarks can be read off the Lagrangian

$$\mathcal{L}_{4\text{D}} \ni \frac{g_L}{c_w} \left[1 + \frac{m_Z^2}{4M_{\text{KK}}^2} \left(1 - \frac{1}{L} \right) \right] \sum_{q,m,n} \left[(g_L^q)_{mn} (\bar{q}_L^m \gamma_\mu q_L^n) + (g_R^q)_{mn} (\bar{q}_R^m \gamma_\mu q_R^n) \right] Z^\mu, \quad (104)$$

where the prefactor accounts for a universal correction due to the t -independent terms in (98). The left- and right-handed couplings $\mathbf{g}_{L,R}^q$ are infinite-dimensional matrices in the space of quark modes, and can be parametrized as

$$\begin{aligned} \mathbf{g}_L^q &= (T_L^{3qL} - s_w^2 Q_q) \left[\mathbf{1} - \frac{m_Z^2}{2M_{\text{KK}}^2} (\omega_Z^{qL} L \Delta_Q - \Delta'_Q) \right] - \delta_Q + \frac{m_Z^2}{2M_{\text{KK}}^2} \left(\frac{c_w^2}{g_L^2} L \epsilon_Q - \epsilon'_Q \right), \\ \mathbf{g}_R^q &= -s_w^2 Q_q \left[\mathbf{1} - \frac{m_Z^2}{2M_{\text{KK}}^2} (\omega_Z^{qR} L \Delta_q - \Delta'_q) \right] + \delta_q - \frac{m_Z^2}{2M_{\text{KK}}^2} \left(\frac{c_w^2}{g_L^2} L \epsilon_q - \epsilon'_q \right), \end{aligned} \quad (105)$$

where the charges appearing in the expressions are understood to be the ones of the zero-mode fermions. In \mathbf{g}_L^q they read $T_L^{3uL}(=T_L^{3u}) = T_R^{3uL}(=T_R^{3u}) = T_R^{3dL}(=T_R^{3d}) = 1/2$ and $T_L^{3dL}(=$

$T_L^{3d} = -1/2$, whereas for \mathbf{g}_R^q one has $T_L^{3u_R}(=T_L^{3u^c}) = T_R^{3u_R}(=T_R^{3u^c}) = T_L^{3d_R}(=T_L^{3D}) = 0$ and $T_R^{3d_R}(=T_R^{3D}) = 1$. The quoted numerical values correspond to the choice (58). We do not consider the sector of λ and $\Lambda^{(\prime)}$ quarks at this point, as these fields do not possess zero modes. The L -enhanced term proportional to ω_Z^q vanishes for the assignments (102) and (103), making the custodial protection explicit. Following [24], we have split the corrections to the Z -boson couplings into leading contributions in the ZMA, denoted by $\Delta_{Q,q}^{(\prime)}$, and subleading ones, parametrized by $\varepsilon_{Q,q}^{(\prime)}$. The elements of the leading-order matrices $\Delta_{Q,q}^{(\prime)}$ are defined as

$$\begin{aligned}
(\Delta_Q)_{mn} &= \frac{2\pi}{L\epsilon} \int_\epsilon^1 dt t^2 \left[\vec{a}_m^{Q\dagger} \mathbf{C}_m^Q(t) \mathbf{C}_n^Q(t) \vec{a}_n^Q + \vec{a}_m^{q\dagger} \mathbf{S}_m^q(t) \mathbf{S}_n^q(t) \vec{a}_n^q \right], \\
(\Delta_q)_{mn} &= \frac{2\pi}{L\epsilon} \int_\epsilon^1 dt t^2 \left[\vec{a}_m^{q\dagger} \mathbf{C}_m^q(t) \mathbf{C}_n^q(t) \vec{a}_n^q + \vec{a}_m^{Q\dagger} \mathbf{S}_m^Q(t) \mathbf{S}_n^Q(t) \vec{a}_n^Q \right], \\
(\Delta'_Q)_{mn} &= \frac{2\pi}{L\epsilon} \int_\epsilon^1 dt t^2 \left(\frac{1}{2} - \ln t \right) \left[\vec{a}_m^{Q\dagger} \mathbf{C}_m^Q(t) \mathbf{C}_n^Q(t) \vec{a}_n^Q + \vec{a}_m^{q\dagger} \mathbf{S}_m^q(t) \mathbf{S}_n^q(t) \vec{a}_n^q \right], \\
(\Delta'_q)_{mn} &= \frac{2\pi}{L\epsilon} \int_\epsilon^1 dt t^2 \left(\frac{1}{2} - \ln t \right) \left[\vec{a}_m^{q\dagger} \mathbf{C}_m^q(t) \mathbf{C}_n^q(t) \vec{a}_n^q + \vec{a}_m^{Q\dagger} \mathbf{S}_m^Q(t) \mathbf{S}_n^Q(t) \vec{a}_n^Q \right],
\end{aligned} \tag{106}$$

while the elements of the matrices $\varepsilon_{Q,q}^{(\prime)}$ describing subleading effects take the form

$$\begin{aligned}
(\varepsilon_Q)_{mn} &= \frac{2\pi}{L\epsilon} \int_\epsilon^1 dt t^2 \left[\vec{a}_m^{Q\dagger} \mathbf{C}_m^Q(t) \left\{ g_L^2 \left(T_L^{3qL} \mathbf{1} - \mathbf{T}_L^{3Q} \right) + g_R^2 \left(T_R^{3qL} \mathbf{1} - \mathbf{T}_R^{3Q} \right) \right\} \mathbf{C}_n^Q(t) \vec{a}_n^Q \right. \\
&\quad \left. + \vec{a}_m^{q\dagger} \mathbf{S}_m^q(t) \left\{ g_L^2 \left(T_L^{3qL} \mathbf{1} - \mathbf{T}_L^{3q} \right) + g_R^2 \left(T_R^{3qL} \mathbf{1} - \mathbf{T}_R^{3q} \right) \right\} \mathbf{S}_n^q(t) \vec{a}_n^q \right], \\
(\varepsilon_q)_{mn} &= \frac{2\pi}{L\epsilon} \int_\epsilon^1 dt t^2 \left[\vec{a}_m^{q\dagger} \mathbf{C}_m^q(t) \left\{ g_L^2 \mathbf{T}_L^{3q} - g_R^2 \left(T_R^{3qR} \mathbf{1} - \mathbf{T}_R^{3q} \right) \right\} \mathbf{C}_n^q(t) \vec{a}_n^q \right. \\
&\quad \left. + \vec{a}_m^{Q\dagger} \mathbf{S}_m^Q(t) \left\{ g_L^2 \mathbf{T}_L^{3Q} - g_R^2 \left(T_R^{3qR} \mathbf{1} - \mathbf{T}_R^{3Q} \right) \right\} \mathbf{S}_n^Q(t) \vec{a}_n^Q \right], \\
(\varepsilon'_Q)_{mn} &= \frac{2\pi}{L\epsilon} \int_\epsilon^1 dt t^2 \left(\frac{1}{2} - \ln t \right) \left[\vec{a}_m^{Q\dagger} \mathbf{C}_m^Q(t) \left(T_L^{3qL} \mathbf{1} - \mathbf{T}_L^{3Q} \right) \mathbf{C}_n^Q(t) \vec{a}_n^Q \right. \\
&\quad \left. + \vec{a}_m^{q\dagger} \mathbf{S}_m^q(t) \left(T_L^{3qL} \mathbf{1} - \mathbf{T}_L^{3q} \right) \mathbf{S}_n^q(t) \vec{a}_n^q \right], \\
(\varepsilon'_q)_{mn} &= \frac{2\pi}{L\epsilon} \int_\epsilon^1 dt t^2 \left(\frac{1}{2} - \ln t \right) \left[\vec{a}_m^{q\dagger} \mathbf{C}_m^q(t) \mathbf{T}_L^{3q} \mathbf{C}_n^q(t) \vec{a}_n^q + \vec{a}_m^{Q\dagger} \mathbf{S}_m^Q(t) \mathbf{T}_L^{3Q} \mathbf{S}_n^Q(t) \vec{a}_n^Q \right].
\end{aligned} \tag{107}$$

Finally, the elements of the matrices $\delta_{Q,q}$, which arise because of the non-orthonormality of the quark profiles and describe mixings between the different multiplets, read

$$\begin{aligned}
(\delta_Q)_{mn} &= \frac{2\pi}{L\epsilon} \int_\epsilon^1 dt \left[\vec{a}_m^{Q\dagger} \mathbf{C}_m^Q(t) \left(T_L^{3qL} \mathbf{1} - \mathbf{T}_L^{3Q} \right) \mathbf{C}_n^Q(t) \vec{a}_n^Q \right. \\
&\quad \left. + \vec{a}_m^{q\dagger} \mathbf{S}_m^q(t) \left(T_L^{3qL} \mathbf{1} - \mathbf{T}_L^{3q} \right) \mathbf{S}_n^q(t) \vec{a}_n^q \right],
\end{aligned}$$

$$(\delta_q)_{mn} = \frac{2\pi}{L\epsilon} \int_\epsilon^1 dt \left[\vec{a}_m^{q\dagger} \mathbf{C}_m^q(t) \mathbf{T}_L^{3q} \mathbf{C}_n^q(t) \vec{a}_n^q + \vec{a}_m^{Q\dagger} \mathbf{S}_m^Q(t) \mathbf{T}_L^{3Q} \mathbf{S}_n^Q(t) \vec{a}_n^Q \right]. \quad (108)$$

In the expressions above we have used the charge matrices $\mathbf{T}_{L,R}^{3Q,q}$, defined as

$$\begin{aligned} \mathbf{T}_{L,R}^{3U} &= \begin{pmatrix} T_{L,R}^{3u} & 0 \\ 0 & T_{L,R}^{3u'} \end{pmatrix}, & \mathbf{T}_{L,R}^{3u} &= \begin{pmatrix} T_{L,R}^{3u^c} & 0 & 0 \\ 0 & T_{L,R}^{3U'} & 0 \\ 0 & 0 & T_{L,R}^{3U} \end{pmatrix}, \\ \mathbf{T}_{L,R}^{3D} &= T_{L,R}^{3d}, & \mathbf{T}_{L,R}^{3d} &= \begin{pmatrix} T_{L,R}^{3D} & 0 \\ 0 & T_{L,R}^{3D'} \end{pmatrix}. \end{aligned} \quad (109)$$

One can easily check that for our choice (58) the quantities $\epsilon_{Q,q}^{(i)}$ are indeed suppressed by v^2/M_{KK}^2 with respect to the matrices $\Delta_{Q,q}^{(i)}$. Note that with the chosen embedding (58), the matrices $\mathbf{T}_{L,R}^{3u}$ vanish identically.

5.3 Custodial Protection: Fermionic Contributions

Finally, we want to have a look at the custodial protection of the $Zb_L\bar{b}_L$ vertex from effects arising from quark mixings, parametrized by $\delta_{Q,q}$. These objects scale in general as v^2/M_{KK}^2 , but as they come with an $\mathcal{O}(1)$ coefficient in (105) they are parametrically of the same order as the matrices $\Delta_{Q,q}^{(i)}$. In the case of the left-handed down-type quark sector, one has

$$\begin{aligned} (\delta_D)_{mn} &= \frac{2\pi}{L\epsilon} \int_\epsilon^1 dt \left[a_m^{D\dagger} \mathbf{S}_m^{\mathcal{T}_2(+)}(t) \left(T_L^{3d_L} - T_L^{3D} \right) \mathbf{S}_n^{\mathcal{T}_2(+)}(t) a_n^D \right. \\ &\quad \left. + a_m^{D'\dagger} \mathbf{S}_m^{\mathcal{T}_1(-)}(t) \left(T_L^{3d_L} - T_L^{3D'} \right) \mathbf{S}_n^{\mathcal{T}_1(-)}(t) a_n^{D'} \right] \\ &= -\frac{1}{2} \frac{2\pi}{L\epsilon} \int_\epsilon^1 dt \left[a_m^{D\dagger} \mathbf{S}_m^{\mathcal{T}_2(+)}(t) \mathbf{S}_n^{\mathcal{T}_2(+)}(t) a_n^D - a_m^{D'\dagger} \mathbf{S}_m^{\mathcal{T}_1(-)}(t) \mathbf{S}_n^{\mathcal{T}_1(-)}(t) a_n^{D'} \right], \end{aligned} \quad (110)$$

where in the second step we have inserted the quantum numbers corresponding to our choice (58) of multiplets.

The relative sign between the two terms in the second line of (110) suggests that also for the corrections due to quark mixing a custodial protection mechanism could be at work. To see if this is indeed the case, let us derive the ZMA expression for δ_D . Using the approximate expressions (90), the system of equations (78) can be brought into the form

$$\frac{\sqrt{2}m_n}{v} \hat{a}_n^d = \mathbf{Y}_d^{\text{eff}} \hat{a}_n^D, \quad \frac{\sqrt{2}m_n}{v} \hat{a}_n^D = (\mathbf{Y}_d^{\text{eff}})^\dagger \hat{a}_n^d, \quad (111)$$

and

$$\hat{a}_n^{D'} = \frac{m_n}{M_{\text{KK}}} \text{diag} \left(F^{-1}(c_{\mathcal{T}_{2i}}) F^{-1}(-c_{\mathcal{T}_{1i}}) \right) \hat{a}_n^D, \quad (112)$$

where the diagonal matrix contains the entries shown in brackets. We have furthermore defined the effective Yukawa couplings

$$(\mathbf{Y}_d^{\text{eff}})_{ij} \equiv F(c_{Q_i}) (Y_d)_{ij} F(c_{\mathcal{T}_{2j}}), \quad (113)$$

and the rescaled vectors $\hat{a}_n^A \equiv \sqrt{2} a_n^A$ with $A = d, D, D'$, which obey the normalization conditions

$$\hat{a}_n^{D\dagger} \hat{a}_n^D = 1, \quad \hat{a}_n^{d\dagger} \hat{a}_n^d + \hat{a}_n^{D'\dagger} \hat{a}_n^{D'} = 1. \quad (114)$$

Moreover, we obtain from (111) the equalities

$$\left(m_n^2 \mathbf{1} - \frac{v^2}{2} \mathbf{Y}_d^{\text{eff}} (\mathbf{Y}_d^{\text{eff}})^\dagger\right) \hat{a}_n^d = 0, \quad \left(m_n^2 \mathbf{1} - \frac{v^2}{2} (\mathbf{Y}_d^{\text{eff}})^\dagger \mathbf{Y}_d^{\text{eff}}\right) \hat{a}_n^D = 0, \quad (115)$$

and the mass eigenvalues are the solutions to the equation

$$\det \left(m_n^2 \mathbf{1} - \frac{v^2}{2} \mathbf{Y}_d^{\text{eff}} (\mathbf{Y}_d^{\text{eff}})^\dagger\right) = 0, \quad (116)$$

which implies that to leading order in v/M_{KK} the values m_n are unaffected by the presence of the D' quarks embedded in the multiplet \mathcal{T}_1 . Notice that in the ZMA, but not in general, the vectors \hat{a}_n^d and \hat{a}_n^D belonging to different n are orthogonal on each other.

The eigenvectors \hat{a}_n^d and \hat{a}_n^D with $n = 1, 2, 3$ of the matrices $\mathbf{Y}_d^{\text{eff}} (\mathbf{Y}_d^{\text{eff}})^\dagger$ and $(\mathbf{Y}_d^{\text{eff}})^\dagger \mathbf{Y}_d^{\text{eff}}$ form the columns of the unitary matrices \mathbf{U}_d and \mathbf{W}_d appearing in the singular-value decomposition

$$\mathbf{Y}_d^{\text{eff}} = \mathbf{U}_d \boldsymbol{\lambda}_d \mathbf{W}_d^\dagger, \quad (117)$$

where

$$\boldsymbol{\lambda}_d = \frac{\sqrt{2}}{v} \text{diag}(m_d, m_s, m_b) \quad (118)$$

is a diagonal matrix containing the masses of the SM down-type quarks in units of $v/\sqrt{2}$. Similar relations hold in the up-type quark sector and will be given explicitly in Section 6. It follows that in the ZMA the relations between the original 5D fields and the SM mass eigenstates involve the matrices $\mathbf{U}_{u,d}$ and $\mathbf{W}_{u,d}$. In particular, the Cabibbo-Kobayashi-Maskawa (CKM) matrix is given by $\mathbf{V}_{\text{CKM}} = \mathbf{U}_u^\dagger \mathbf{U}_d$.

With these results at hand, it is a matter of simple algebra to find the expression for $\boldsymbol{\delta}_D$ in the ZMA. Working to first order in v^2/M_{KK}^2 , and using (90) and (112) we arrive at

$$\boldsymbol{\delta}_D = -\frac{1}{2} \mathbf{x}_d \mathbf{W}_d^\dagger \text{diag} \left[\frac{1}{1 - 2c_{\mathcal{T}_{2i}}} \left(\frac{1}{F^2(c_{\mathcal{T}_{2i}})} \left[1 - \frac{1 - 2c_{\mathcal{T}_{2i}}}{F^2(-c_{\mathcal{T}_{1i}})} \right] - 1 + \frac{F^2(c_{\mathcal{T}_{2i}})}{3 + 2c_{\mathcal{T}_{2i}}} \right) \right] \mathbf{W}_d \mathbf{x}_d, \quad (119)$$

where $\mathbf{x}_d \equiv \text{diag}(m_d, m_s, m_b)/M_{\text{KK}}$. Compared to the ZMA result in the minimal RS model [24], this relation contains an additional term involving the zero-mode profile $F(-c_{\mathcal{T}_{1i}})$. It stems from the admixture of the \mathcal{T}_1 multiplet in the zero mode, which is parametrized by the value of $\hat{a}_n^{D'}$. Notice that although this admixture is suppressed by v/M_{KK} , the fact that the profile $\mathbf{S}_n^{\mathcal{T}_1^{(-)}}(t)$ is enhanced with respect to $\mathbf{S}_n^{\mathcal{T}_2^{(+)}}(t)$ by the reciprocal factor promotes the second term in the last line of (110) to a leading contribution.

The relations (111) and (112) are valid to leading order in v/M_{KK} . Beyond that order the first relation in (111) receives corrections from the profiles $\mathbf{C}_n^{\mathcal{T}_i^{(-)}(1^-)$ which scale like $x_n/F(-c_{\mathcal{T}_i})$ as can be seen from (90). Thus in order to avoid exponentially enhanced terms of the form $v/M_{\text{KK}} \epsilon^{1-2c_{\mathcal{T}_i}}$ in the mass eigenvalues m_n , which, barring accidental cancellations, would make it impossible to reproduce the observed zero-mode down-type quark masses, one has to require that all the bulk mass parameters belonging to the multiplet \mathcal{T}_1 obey the relation $c_{\mathcal{T}_i} < 1/2$. In this case the profiles $\mathbf{C}_n^{\mathcal{T}_i^{(-)}(t)$ are IR localized and one has to an excellent accuracy

$$\boldsymbol{\delta}_D = -\frac{1}{2} \mathbf{x}_d \mathbf{W}_d^\dagger \text{diag} \left[\frac{1}{1-2c_{\mathcal{T}_2i}} \left(\frac{1}{F^2(c_{\mathcal{T}_2i})} \left[1 - \frac{1-2c_{\mathcal{T}_2i}}{1-2c_{\mathcal{T}_1i}} \right] - 1 + \frac{F^2(c_{\mathcal{T}_2i})}{3+2c_{\mathcal{T}_2i}} \right) \right] \mathbf{W}_d \mathbf{x}_d. \quad (120)$$

This result implies that the leading term in $\boldsymbol{\delta}_D$, *i.e.*, the contribution inversely proportional to $F^2(c_{\mathcal{T}_2i})$, is absent if the bulk mass parameters $c_{\mathcal{T}_i}$ satisfy

$$c_{\mathcal{T}_1i} = c_{\mathcal{T}_2i}. \quad (121)$$

Unlike in the case of the gauge-boson corrections (98), the conditions (102) and (103) alone are thus not sufficient to entirely shield the $Z b_L \bar{b}_L$ vertex from the leading corrections due to quark mixing. However, since for $c_{\mathcal{T}_2i} \approx -1/2$ and $c_{\mathcal{T}_1i} \lesssim 0$ the first term in (120) is smaller in magnitude than 1, a partial protection is in place for a large range of bulk parameters. In consequence, effects due to quark mixing entering the Z -boson couplings are generically suppressed in the custodial RS model relative to the minimal scenario as long as the Z_2 -odd quark fields are not too far localized in the UV. The subleading terms in $\boldsymbol{\delta}_D$ are independent of $c_{\mathcal{T}_1i}$ and therefore not protected even if $c_{\mathcal{T}_1i} = c_{\mathcal{T}_2i}$. They embody irreducible sources of symmetry breaking, originating from the different BCs of the Z_2 -even and -odd quark fields.

Notice that (121) can be enforced by requiring that the action (62) be invariant under the exchange of the D' and D quark fields,

$$P_{LR}(D') = D, \quad (\text{extended } P_{LR} \text{ symmetry}) \quad (122)$$

which extends the P_{LR} symmetry to the part of the quark sector that mixes with the left-handed down-type zero modes. Notice that while (121) can always be accommodated, the extended symmetry will be necessarily broken by the different BCs of D' and D . The symmetry (122) can also be broken softly by choosing bulk masses for D' that differ from those of D , which is a phenomenological viable option as long as $c_{\mathcal{T}_i} < 1/2$, because it does not affect the SM down-type quark masses in an appreciable way. The protection mechanism discussed here has also been studied in [39] employing a perturbative approach. Our analysis based on the exact solution of the EOMs (69) including the BCs (78) goes beyond the latter work in the sense that it makes explicit the dependence of $\boldsymbol{\delta}_D$ on the bulk masses $\mathbf{M}_{\mathcal{T}_{1,2}}$. It therefore allows for a transparent understanding of the custodial protection mechanism in two respects. First, it makes clear which are the requirements that need to be satisfied to achieve a protection and, second, which are the terms in $\boldsymbol{\delta}_D$ that inevitably escape protection. Compared to the perturbative approach, the exact solution thus has again the salient advantage that the protection of the $Z d_L^i \bar{d}_L^j$ vertices from effects due to quark mixing can be clearly deciphered.

5.4 Four-Fermion Charged-Current Interactions

Hereafter we derive the effective four-fermion interactions induced by the exchange of charged weak W bosons and their KK excitations. In this case, of course, flavor-changing effects are unsuppressed already in the SM. Restricting ourselves to the phenomenologically most relevant case with leptons in the final state, and including corrections up to $\mathcal{O}(v^2/M_{\text{KK}}^2)$, we obtain

$$\mathcal{H}_{\text{eff}}^{(W)} = 2\sqrt{2}G_F \sum_l \left\{ [\bar{u}_L \gamma^\mu \mathbf{V}_L d_L + \bar{u}_R \gamma^\mu \mathbf{V}_R d_R] (\bar{l}_L \gamma_\mu \nu_{lL}) + \text{h.c.} \right\}, \quad (123)$$

where the elements of the mixing matrices $\mathbf{V}_{L,R}$ are computed from (97) and take the form

$$\begin{aligned} \mathbf{V}_L &= \Delta^{+Q} + \sqrt{2}\epsilon^{+q} - \frac{m_W^2}{2M_{\text{KK}}^2} L \left(\bar{\Delta}^{+Q} + \sqrt{2}\bar{\epsilon}^{+q} \right), \\ \mathbf{V}_R &= \sqrt{2}\Delta^{+q} + \epsilon^{+Q} - \frac{m_W^2}{2M_{\text{KK}}^2} L \left(\sqrt{2}\bar{\Delta}^{+q} + \bar{\epsilon}^{+Q} \right), \end{aligned} \quad (124)$$

with

$$\begin{aligned} \Delta_{mn}^{+Q,q} &= \frac{2\pi}{L\epsilon} \int_\epsilon^1 dt \bar{a}_m^{U,u\dagger} \mathbf{C}_m^{U,u}(t) \Omega^{Q,q} \mathbf{C}_n^{D,d}(t) \bar{a}_n^{D,d}, \\ \epsilon_{mn}^{+Q,q} &= \frac{2\pi}{L\epsilon} \int_\epsilon^1 dt \bar{a}_m^{U,u\dagger} \mathbf{S}_m^{U,u}(t) \Omega^{Q,q} \mathbf{S}_n^{D,d}(t) \bar{a}_n^{D,d}, \\ \bar{\Delta}_{mn}^{+Q,q} &= \frac{2\pi}{L\epsilon} \int_\epsilon^1 dt t^2 \bar{a}_m^{U,u\dagger} \mathbf{C}_m^{U,u}(t) \bar{\Omega}^{Q,q} \mathbf{C}_n^{D,d}(t) \bar{a}_n^{D,d}, \\ \bar{\epsilon}_{mn}^{+Q,q} &= \frac{2\pi}{L\epsilon} \int_\epsilon^1 dt t^2 \bar{a}_m^{U,u\dagger} \mathbf{S}_m^{U,u}(t) \bar{\Omega}^{Q,q} \mathbf{S}_n^{D,d}(t) \bar{a}_n^{D,d}, \end{aligned} \quad (125)$$

and

$$\Omega^Q = \begin{pmatrix} \mathbf{1} \\ \mathbf{0} \end{pmatrix}, \quad \Omega^q = \begin{pmatrix} \mathbf{0} & \mathbf{0} \\ \mathbf{0} & \mathbf{1} \\ \mathbf{0} & \mathbf{0} \end{pmatrix}, \quad \bar{\Omega}^Q = \begin{pmatrix} \mathbf{1} \\ -\frac{g_R^2}{g_L^2} \mathbf{1} \end{pmatrix}, \quad \bar{\Omega}^q = \begin{pmatrix} \mathbf{0} & \mathbf{0} \\ \mathbf{0} & \mathbf{1} \\ -\frac{g_R^2}{g_L^2} \mathbf{1} & \mathbf{0} \end{pmatrix}. \quad (126)$$

Notice that the definition of $\mathbf{V}_{L,R}$ includes the exchange of the entire tower of W bosons and their KK excitations and therefore differs from the definition of the CKM matrix employed in [24, 39], which is based on the $Wu_L^i d_L^j$ and $Wu_R^i d_R^j$ vertices. Because an extraction of CKM elements generically involves the normalization of the semileptonic amplitude to the Fermi constant, we have included in G_F in (123) a universal factor $(1 + m_W^2/(2M_{\text{KK}}^2)(1 - 1/(2L)))$ which describes the finite correction to muon decay in the RS model [24] and is independent of the gauge group. Proceeding in this way renders the individual factors in the combination $G_F \mathbf{V}_{L,R}$ physically observable [20]. We note finally that in order to arrive at the effective Hamiltonian (123), we have made the simplified assumption that the left- and right-handed 5D

leptonic fields all have the same bulk mass parameter, and that they are localized sufficiently close to the UV brane so as not to violate the constraints imposed by the electroweak precision tests. By construction, the interactions of the SM leptons with the W boson and its KK excitations are therefore flavor universal and numerically insignificant.

From the formulas (124) it is evident that no custodial protection mechanism is at work in the charged-current sector. This is due to the embedding of the up-type quarks (58) and has already been pointed out in [16]. The leading contribution to $(V_L)_{mn}$ stems from Δ_{mn}^{+Q} , which is unitary to very good approximation. Corrections of order v^2/M_{KK}^2 arise from the non-universality of KK gauge bosons encoded in $\bar{\Delta}_{mn}^{+Q}$ as well as the admixture from U' and D' quarks described by ϵ_{mn}^{+q} . Contributions arising from the admixture of U , D , and u' quarks are of order v^4/M_{KK}^4 and will be neglected in the following. The full expression for \mathbf{V}_L obtained by employing the ZMA reads

$$\mathbf{V}_L = \mathbf{U}_u^\dagger \left[\mathbf{1} - \frac{m_W^2}{2M_{\text{KK}}^2} L \text{diag} \left(\frac{F^2(c_{Q_i})}{3 + 2c_{Q_i}} \right) + \frac{v^2}{2M_{\text{KK}}^2} \text{diag} (F(c_{Q_i})) \mathbf{Y}_d \text{diag} (F^{-2}(-c_{\mathcal{T}_{1i}})) \mathbf{Y}_d^\dagger \text{diag} (F(c_{Q_i})) \right] \mathbf{U}_d, \quad (127)$$

which is obviously not unitary. As far as $(V_R)_{mn}$ is concerned, the dominant contribution is given by ϵ_{mn}^{+Q} , which is suppressed both by v^2/M_{KK}^2 and a chiral factor $m_m^u m_n^d/v^2$. The chiral suppression present in each of the terms contributing to \mathbf{V}_R reflects the mere fact that they all originate from quark mixing. In consequence, right-handed charged-current interactions are too small to give rise to any observable effect [24].

As a measure of unitarity violation, we consider the deviation from unity of the sum of the squares of the matrix elements in the first row of \mathbf{V}_L ,

$$\Delta_1^{\text{non}} = 1 - (|V_{ud}|^2 + |V_{us}|^2 + |V_{ub}|^2) = \left(\mathbf{1} - \mathbf{V}_L \mathbf{V}_L^\dagger \right)_{11}. \quad (128)$$

After expanding the mixing matrices $\mathbf{U}_{u,d}$ in powers of the Cabibbo angle λ (using the warped-space Froggatt-Nielsen formulas given in [24]) and normalizing the result to the typical value of the bulk mass parameter $c_{Q_1} \approx -0.63$, we obtain

$$\Delta_1^{\text{non}} \approx 2 \cdot 10^{-6} \left(\frac{F(c_{Q_1})}{F(-0.63)} \right)^2 \left(\frac{M_{\text{KK}}}{\text{TeV}} \right)^{-2} \times \left[\left| \text{diag} \left(\sqrt{\frac{2}{3 + 2c_{Q_i}}} \right) \vec{u} \right|^2 - \frac{1}{4} \left| \text{diag} \left(\sqrt{\frac{2}{1 - 2c_{\mathcal{T}_{1i}}} } \right) \mathbf{Y}_d^T \vec{u} \right|^2 \right], \quad (129)$$

where the vector \vec{u} is given by

$$\vec{u} = (1, -(M_u)_{21}/(M_u)_{11}, (M_u)_{31}/(M_u)_{11}). \quad (130)$$

Here \mathbf{M}_u denotes the matrix of minors of \mathbf{Y}_u . The first contribution in the square brackets in (129) stems from the exchange of the whole tower of W bosons and is also present in the

minimal RS model. It gives a strictly positive contribution to Δ_1^{non} , which is typically well below the current experimental uncertainty of $6.5 \cdot 10^{-4}$ [20]. However, the effects due to the admixture of U' and D' quarks contribute to (129) with opposite sign and can in principle lead to negative values of Δ_1^{non} . This is not possible in the minimal RS model. A detailed discussion of the breakdown of the unitarity of the quark mixing matrix in the framework of the RS model with custodial protection has been presented in [39]. Unfortunately, in that paper the CKM matrix is defined via the $W u_L^i d_L^j$ vertex and not the effective four-fermion interactions induced by the exchange of the W boson and its KK excitations. This difference prevents us from a straightforward comparison of the results in [39] with ours.

6 Fermion Couplings to the Higgs Boson

The mixing of fermion zero-modes with their KK excitations leads to flavor-changing Higgs couplings in scenarios with warped extra dimensions [40]. Analytic expressions for the relevant interactions have been presented first within the minimal RS model in [24], which however did not include the Yukawa couplings that involve Z_2 -odd fermion profiles. This omission has been noticed in [37], where it has been pointed out that the latter terms provide the dominant corrections to tree-level Higgs FCNCs in the case of light quark flavors. We confirm the $\mathcal{O}(v^2/M_{\text{KK}}^2)$ result for a brane-localized Higgs sector obtained in the latter work and generalize it to our exact treatment of KK profiles and thus to all orders in v/M_{KK} for both the minimal as well as the custodial RS model.

Working in unitary gauge, we first identify the relevant terms in the 4D Lagrangian describing the couplings of the Higgs boson to quarks. They read

$$\mathcal{L}_{4\text{D}} \ni - \sum_{q,m,n} (g_h^q)_{mn} h \bar{q}_L^m q_R^n + \text{h.c.}, \quad (131)$$

and the couplings $(g_h^q)_{mn}$ are given by

$$(g_h^q)_{mn} = \frac{\sqrt{2}\pi}{L} \int_{-\pi}^{\pi} d\phi \delta(|\phi| - \pi) e^{\sigma(\phi)} \left[\bar{a}_m^{Q\dagger} \mathbf{C}_m^Q(\phi) \mathbf{Y}_{\bar{q}} \mathbf{C}_n^q(\phi) \bar{a}_n^q + \bar{a}_m^{q\dagger} \mathbf{S}_m^q(\phi) \mathbf{Y}_{\bar{q}}^\dagger \mathbf{S}_n^Q(\phi) \bar{a}_n^Q \right]. \quad (132)$$

To simplify this expression, we follow [37] and observe that the EOMs (69) imply

$$\begin{aligned} m_n e^{\sigma(\phi)} \bar{a}_m^{Q\dagger} \mathbf{C}_m^Q(\phi) \mathbf{C}_n^Q(\phi) \bar{a}_n^Q - \bar{a}_m^{Q\dagger} \mathbf{S}_m^Q(\phi) \mathbf{S}_n^Q(\phi) \bar{a}_n^Q e^{\sigma(\phi)} m_m - \frac{1}{r} \partial_\phi \bar{a}_m^{Q\dagger} \mathbf{C}_m^Q(\phi) \mathbf{S}_n^Q(\phi) \bar{a}_n^Q \\ - \frac{\sqrt{2}\pi v}{L} \delta(|\phi| - \pi) e^{\sigma(\phi)} \left[\bar{a}_m^{Q\dagger} \mathbf{C}_m^Q(\phi) \mathbf{Y}_{\bar{q}} \mathbf{C}_n^q(\phi) \bar{a}_n^q - \bar{a}_m^{q\dagger} \mathbf{S}_m^q(\phi) \mathbf{Y}_{\bar{q}}^\dagger \mathbf{S}_n^Q(\phi) \bar{a}_n^Q \right] = 0. \end{aligned} \quad (133)$$

After integrating this relation over the whole orbifold, the total derivative in (133) does not contribute since the Z_2 -odd profiles obey $\mathbf{S}_n^{Q,q}(0) = \mathbf{S}_n^{Q,q}(\pm\pi) = 0$. One thus finds, after making use of the canonical normalization of the kinetic terms, as encoded in (79) and (80),

the following expression

$$\begin{aligned}
m_m \delta_{mn} = & \int_{-\pi}^{\pi} d\phi \left\{ m_n e^{\sigma(\phi)} \vec{a}_m^{q\dagger} \mathbf{S}_m^q(\phi) \mathbf{S}_n^q(\phi) \vec{a}_n^q + \vec{a}_m^{Q\dagger} \mathbf{S}_m^Q(\phi) \mathbf{S}_n^Q(\phi) \vec{a}_n^Q e^{\sigma(\phi)} m_m \right. \\
& \left. + \frac{\sqrt{2}\pi v}{L} \delta(|\phi| - \pi) e^{\sigma(\phi)} \left[\vec{a}_m^{Q\dagger} \mathbf{C}_m^Q(\phi) \mathbf{Y}_{\bar{q}} \mathbf{C}_n^q(\phi) \vec{a}_n^q - \vec{a}_m^{q\dagger} \mathbf{S}_m^q(\phi) \mathbf{Y}_{\bar{q}}^\dagger \mathbf{S}_n^Q(\phi) \vec{a}_n^Q \right] \right\}. \tag{134}
\end{aligned}$$

This result allows to eliminate the term bi-linear in the Z_2 -even profiles from (132) and to express the tree-level Higgs FCNCs solely in terms of overlap integrals involving Z_2 -odd fields.

Defining the misalignment $(\Delta g_h^q)_{mn}$ between the SM masses and the Yukawa couplings via

$$(g_h^q)_{mn} \equiv \delta_{mn} \frac{m_m^q}{v} - (\Delta g_h^q)_{mn}, \tag{135}$$

it is then easy to show, by combining the latter definition with (132) and (134), that

$$(\Delta g_h^q)_{mn} = \frac{m_m^q}{v} (\Phi_q)_{mn} + (\Phi_Q)_{mn} \frac{m_n^q}{v} + (\Delta \tilde{g}_h^q)_{mn}, \tag{136}$$

where in t notation

$$(\Phi_q)_{mn} = \frac{2\pi}{L\epsilon} \int_{\epsilon}^1 dt \vec{a}_m^{Q\dagger} \mathbf{S}_m^Q(t) \mathbf{S}_n^Q(t) \vec{a}_n^Q, \quad (\Phi_Q)_{mn} = \frac{2\pi}{L\epsilon} \int_{\epsilon}^1 dt \vec{a}_m^{q\dagger} \mathbf{S}_m^q(t) \mathbf{S}_n^q(t) \vec{a}_n^q, \tag{137}$$

and

$$(\Delta \tilde{g}_h^q)_{mn} = -\sqrt{2} \frac{2\pi}{L\epsilon} \int_{\epsilon}^1 dt \delta(t-1) \vec{a}_m^{q\dagger} \mathbf{S}_m^q(t) \mathbf{Y}_{\bar{q}}^\dagger \mathbf{S}_n^Q(t) \vec{a}_n^Q. \tag{138}$$

Notice that the latter contribution is absent in [24], because this work did not include operators of the form $(Y_q^{(5D)})_{ij} (\bar{Q}_R^i)_{a\alpha} q_L^{c,j} \Phi_{a\alpha}$ in the 5D action. While omitting these operators is technically possible, since they are not needed to generate the SM fermion masses, an omission seems unnatural in the sense that there is no symmetry that would forbid these Z_2 -odd Yukawa couplings.

In order to evaluate the contribution $(\Delta \tilde{g}_h^q)_{mn}$ one again has to regularize the δ -function appearing in (138). Following the detailed explanations given in Section 4.2 and employing

$$\int_t^1 dt' \delta^\eta(t'-1) [\sinh(\bar{\theta}^\eta(t'-1)\mathbf{A})]^2 = \frac{1}{2} \left[\sinh(\bar{\theta}^\eta(t-1)2\mathbf{A})(2\mathbf{A})^{-1} - \bar{\theta}^\eta(t-1)\mathbf{1} \right], \tag{139}$$

we obtain after some simple algebra the following regularization independent result

$$(\Delta \tilde{g}_h^q)_{mn} = \frac{1}{\sqrt{2}} \frac{2\pi}{L\epsilon} \frac{v^2}{3M_{\text{KK}}^2} \vec{a}_m^{Q\dagger} \mathbf{C}_m^Q(1^-) \mathbf{Y}_{\bar{q}} \mathbf{Y}_{\bar{q}}^\dagger \mathbf{g} \left(\frac{v}{\sqrt{2}M_{\text{KK}}} \sqrt{\mathbf{Y}_{\bar{q}} \mathbf{Y}_{\bar{q}}^\dagger} \right) \mathbf{Y}_{\bar{q}} \mathbf{C}_n^q(1^-) \vec{a}_n^q, \tag{140}$$

with

$$\mathbf{g}(\mathbf{A}) = \frac{3}{2} \left[\sinh(2\mathbf{A})(2\mathbf{A})^{-1} - \mathbf{1} \right] (\cosh(\mathbf{A})\mathbf{A})^{-2}. \tag{141}$$

It is also straightforward to express (140) in terms of the rescaled Yukawa matrices introduced in (77). Using

$$\frac{v}{\sqrt{2}M_{\text{KK}}} \sqrt{\mathbf{Y}_{\vec{q}} \mathbf{Y}_{\vec{q}}^\dagger} = \tanh^{-1} \left(\frac{v}{\sqrt{2}M_{\text{KK}}} \sqrt{\tilde{\mathbf{Y}}_{\vec{q}} \tilde{\mathbf{Y}}_{\vec{q}}^\dagger} \right), \quad (142)$$

we obtain

$$(\Delta \tilde{g}_h^q)_{mn} = \frac{1}{\sqrt{2}} \frac{2\pi}{L\epsilon} \frac{v^2}{3M_{\text{KK}}^2} \tilde{a}_m^{Q\dagger} \mathbf{C}_m^Q(1^-) \tilde{\mathbf{Y}}_{\vec{q}} \tilde{\mathbf{Y}}_{\vec{q}}^\dagger \tilde{\mathbf{Y}}_{\vec{q}} \mathbf{C}_n^q(1^-) \tilde{a}_n^q, \quad (143)$$

where

$$\tilde{\mathbf{Y}}_{\vec{q}}^\dagger \equiv \tilde{\mathbf{Y}}_{\vec{q}}^\dagger \mathbf{h} \left(\frac{v}{\sqrt{2}M_{\text{KK}}} \sqrt{\tilde{\mathbf{Y}}_{\vec{q}} \tilde{\mathbf{Y}}_{\vec{q}}^\dagger} \right), \quad \mathbf{h}(\mathbf{A}) = \frac{3}{2} \left[\mathbf{A}^{-2} + \tanh^{-1}(\mathbf{A}) \mathbf{A}^{-1} (\mathbf{1} - \mathbf{A}^{-2}) \right]. \quad (144)$$

In practice, we compute the relevant matrix-valued functions by introducing the unitary matrices $\mathbf{U}_{\vec{q}}$ and $\mathbf{V}_{\vec{q}}$ which diagonalize the hermitian products $\tilde{\mathbf{Y}}_{\vec{q}} \tilde{\mathbf{Y}}_{\vec{q}}^\dagger$ and $\tilde{\mathbf{Y}}_{\vec{q}}^\dagger \tilde{\mathbf{Y}}_{\vec{q}}$,

$$\tilde{\mathbf{Y}}_{\vec{q}} \tilde{\mathbf{Y}}_{\vec{q}}^\dagger = \mathbf{U}_{\vec{q}} \tilde{\mathbf{y}}_{\vec{q}} \tilde{\mathbf{y}}_{\vec{q}}^T \mathbf{U}_{\vec{q}}^\dagger, \quad \tilde{\mathbf{Y}}_{\vec{q}}^\dagger \tilde{\mathbf{Y}}_{\vec{q}} = \mathbf{V}_{\vec{q}} \tilde{\mathbf{y}}_{\vec{q}}^T \tilde{\mathbf{y}}_{\vec{q}} \mathbf{V}_{\vec{q}}^\dagger, \quad (145)$$

where $\tilde{\mathbf{y}}_{\vec{q}}$ is, depending on the value of the index \vec{q} , a matrix of dimension 3×6 or 6×9 containing the non-negative eigenvalues of $\sqrt{\tilde{\mathbf{Y}}_{\vec{q}} \tilde{\mathbf{Y}}_{\vec{q}}^\dagger}$ on its diagonal. It then follows that

$$\tilde{\mathbf{Y}}_{\vec{q}} \tilde{\mathbf{Y}}_{\vec{q}}^\dagger \tilde{\mathbf{Y}}_{\vec{q}} = \mathbf{U}_{\vec{q}} \tilde{\mathbf{y}}_{\vec{q}} \tilde{\mathbf{y}}_{\vec{q}}^T \mathbf{h} \left(\frac{v}{\sqrt{2}M_{\text{KK}}} \sqrt{\tilde{\mathbf{y}}_{\vec{q}} \tilde{\mathbf{y}}_{\vec{q}}^T} \right) \tilde{\mathbf{y}}_{\vec{q}} \mathbf{V}_{\vec{q}}^\dagger. \quad (146)$$

Notice finally that the Yukawa matrices introduced in (77) and (144) satisfy $\tilde{\mathbf{Y}}_{\vec{q}} = \mathbf{Y}_{\vec{q}} + \mathcal{O}(v^2/M_{\text{KK}}^2)$ and $\tilde{\mathbf{Y}}_{\vec{q}}^\dagger = \mathbf{Y}_{\vec{q}}^\dagger + \mathcal{O}(v^2/M_{\text{KK}}^2)$. This implies that as long as one is interested in the ZMA results for $(\Delta \tilde{g}_h^q)_{mn}$ only, one can simply replace $\tilde{\mathbf{Y}}_{\vec{q}} \tilde{\mathbf{Y}}_{\vec{q}}^\dagger \tilde{\mathbf{Y}}_{\vec{q}}$ by the combination $\mathbf{Y}_{\vec{q}} \mathbf{Y}_{\vec{q}}^\dagger \mathbf{Y}_{\vec{q}}$ of original Yukawa matrices.

It will be useful to derive ZMA results for the elements $(\Delta g_h^q)_{mn}$. For this purpose, we still need the $\mathcal{O}(v^2/M_{\text{KK}}^2)$ expressions for the rescaled eigenvectors \hat{a}_n^A with $A = u, u', u^c, U', U$. First note that the relations (111), (113), and (115) to (117) also hold in the up-type quark sector after the replacements $d \rightarrow u, D \rightarrow u^c, c_{\mathcal{T}_{2i}} \rightarrow c_{u_i^c}$ with $\boldsymbol{\lambda}_u = \sqrt{2}/v \text{diag}(m_u, m_c, m_t)$. The remaining \hat{a}_n^A are found to satisfy

$$\begin{aligned} \hat{a}_n^{u'} &= x_n \text{diag} \left(F^{-1}(-c_{Q_i}) F^{-1}(c_{Q_i}) \right) \hat{a}_n^u, \\ \hat{a}_n^{U'} &= \text{diag} \left(F(-c_{\mathcal{T}_{2i}}) F^{-1}(-c_{\mathcal{T}_{1i}}) \right) \hat{a}_n^U, \\ \hat{a}_n^U &= \frac{x_n}{\sqrt{2}} \text{diag} \left(F^{-1}(-c_{\mathcal{T}_{2i}}) \right) \mathbf{Y}_d^\dagger [\mathbf{Y}_u^\dagger]^{-1} \text{diag} \left(F^{-1}(c_{u_i^c}) \right) \hat{a}_n^{u^c}. \end{aligned} \quad (147)$$

It is also easy to show that the eigenvectors satisfy the sum rules

$$\hat{a}_n^{u^c \dagger} \hat{a}_n^{u^c} + \hat{a}_n^{u' \dagger} \hat{a}_n^{u'} = 1, \quad \hat{a}_n^{u \dagger} \hat{a}_n^u + \hat{a}_n^{U \dagger} \hat{a}_n^U + \hat{a}_n^{U' \dagger} \hat{a}_n^{U'} = 1. \quad (148)$$

With these relations at hand, it is straightforward to derive analytic expressions for the $\mathcal{O}(v^2/M_{\text{KK}}^2)$ corrections to Φ_q , Φ_Q , and $\Delta\tilde{g}_h^q$. In the case of down-type quarks, we find

$$\begin{aligned}\Phi_d &= \mathbf{x}_d \mathbf{U}_d^\dagger \text{diag} \left[\frac{1}{1-2c_{Q_i}} \left(\frac{1}{F^2(c_{Q_i})} - 1 + \frac{F^2(c_{Q_i})}{3+2c_{Q_i}} \right) \right] \mathbf{U}_d \mathbf{x}_d, \\ \Phi_D &= \mathbf{x}_d \mathbf{W}_d^\dagger \text{diag} \left[\frac{1}{1-2c_{\mathcal{T}_{2i}}} \left(\frac{1}{F^2(c_{\mathcal{T}_{2i}})} \left[1 + \frac{1-2c_{\mathcal{T}_{2i}}}{F^2(-c_{\mathcal{T}_{1i}})} \right] - 1 + \frac{F^2(c_{\mathcal{T}_{2i}})}{3+2c_{\mathcal{T}_{2i}}} \right) \right] \mathbf{W}_d \mathbf{x}_d, \\ \Delta\tilde{g}_h^d &= \frac{\sqrt{2}v^2}{3M_{\text{KK}}^2} \mathbf{U}_d^\dagger \text{diag} [F(c_{Q_i})] \mathbf{Y}_d \mathbf{Y}_d^\dagger \mathbf{Y}_d \text{diag} [F(c_{\mathcal{T}_{2i}})] \mathbf{W}_d,\end{aligned}\tag{149}$$

while for up-type quarks we obtain

$$\begin{aligned}\Phi_u &= \mathbf{x}_u \mathbf{U}_u^\dagger \text{diag} \left[\frac{1}{1-2c_{Q_i}} \left(\frac{1}{F^2(c_{Q_i})} \left[1 + \frac{1-2c_{Q_i}}{F^2(-c_{Q_i})} \right] - 1 + \frac{F^2(c_{Q_i})}{3+2c_{Q_i}} \right) \right] \mathbf{U}_u \mathbf{x}_u, \\ \Phi_U &= \mathbf{x}_u \mathbf{W}_u^\dagger \left\{ \text{diag} \left[\frac{1}{1-2c_{u_i^c}} \left(\frac{1}{F^2(c_{u_i^c})} - 1 + \frac{F^2(c_{u_i^c})}{3+2c_{u_i^c}} \right) \right] + \frac{1}{2} \text{diag} (F^{-1}(c_{u_i^c})) \mathbf{Y}_u^{-1} \mathbf{Y}_d \right. \\ &\quad \left. \times \text{diag} \left(\frac{1}{F^2(-c_{\mathcal{T}_{2i}}} + \frac{1}{F^2(-c_{\mathcal{T}_{1i}})} \right) \mathbf{Y}_d^\dagger [\mathbf{Y}_u^\dagger]^{-1} \text{diag} (F^{-1}(c_{u_i^c})) \right\} \mathbf{W}_u \mathbf{x}_u,\end{aligned}\tag{150}$$

$$\Delta\tilde{g}_h^u = \frac{\sqrt{2}v^2}{3M_{\text{KK}}^2} \mathbf{U}_u^\dagger \text{diag} [F(c_{Q_i})] \mathbf{Y}_u \mathbf{Y}_u^\dagger \mathbf{Y}_u \text{diag} [F(c_{u_i^c})] \mathbf{W}_u,$$

with $\mathbf{x}_u \equiv \text{diag}(m_u, m_c, m_t)/M_{\text{KK}}$. Here \mathbf{U}_u (\mathbf{W}_u) are the left- (right-) handed rotation matrices diagonalizing the effective up-type Yukawa coupling.

At this point some comments are in order. First, notice that compared to the ZMA results in the minimal RS model [24] the expressions for Φ_D , Φ_u , and Φ_U contain additional terms, whereas Φ_d is unchanged. The new terms in (149) and (150) are the ones involving the zero-mode profiles $F(-c_{\mathcal{T}_{1i}})$, $F(-c_{\mathcal{T}_{2i}})$, and $F(-c_{Q_i})$. They arise from the admixture of the $\mathcal{S}_n^{\mathcal{T}_{1i}(-)}(t)$, $\mathcal{S}_n^{\mathcal{T}_{2i}(-)}(t)$, and $\mathcal{S}_n^{Q(-)}(t)$ profiles in the corresponding zero-mode wave functions. In each case, the suppression by v/M_{KK} due to the admixture is offset by the $\mathcal{O}(M_{\text{KK}}/v)$ enhancement of the Z_2 -odd ($-$) profile relative to its ($+$) counterpart. For $c_{Q_i} < 1/2$, the leading contribution in Φ_u is numerically enhanced by a factor of 2 with respect to the minimal model. If the $Z d_L^i \bar{d}_L^j$ vertices are protected from fermion mixing by (121) and $c_{\mathcal{T}_{1i}} < 1/2$, then the same is true for Φ_D . Depending on the structure of the Yukawa matrices and bulk masses, a similar enhancement is possible in Φ_U . Notice that the extra suppression by factors of m_n^q/v in $\Phi_{d,D,u,U}$ imply that for light quark flavors the Higgs-boson FCNCs arising from the latter terms are parametrically suppressed relative to those mediated by the exchange of a Z boson. This makes the chirally unsuppressed contributions $\Delta\tilde{g}_h^{d,u}$, that arise from the Z_2 -odd Yukawa couplings, the dominant sources of flavor violation in the Higgs sector [37]. As far as the $\mathcal{O}(v^2/M_{\text{KK}}^2)$ corrections to $\Delta\tilde{g}_h^{d,u}$ as given in (149) and (150) are concerned, we find perfect agreement with the results presented in the latter article for the case of a brane-localized Higgs sector. Compared to the minimal RS model the corrections $\Delta\tilde{g}_h^{d,u}$ are again bigger

by a factor of 2 in the extended scenario. Notice also that the factor of $1/3$ arising in the ZMA expressions for $\Delta\tilde{g}_h^{d,u}$ follows immediately if one applies (74) to a composite operator containing two Z_2 -odd fermion profiles.

Let us finally mention, that a model-independent analysis of the flavor misalignment of the SM fermion masses and the Yukawa couplings has been presented in [41]. There it has been shown that at the level of dimension six, chirally unsuppressed contributions to flavor-changing Higgs-boson vertices generically will arise from composite operators like $\bar{q}_L^i H q_R^j (H^\dagger H)$ in models where the Higgs is a bound state of a new strongly-interacting theory. If present, the latter terms will dominate over the chirally suppressed contributions originating from operators of the form $\bar{q}_L^i \not{D} q_L^j (H^\dagger H)$, because the couplings y_{q^*} of the composite Higgs to the other strong interacting states can be large, resulting in $y_{q^*}^2/(16\pi^2) \gg m_q/v$. Notice that in our concrete model, considering all relevant dimension-six operators in lowest-order of the mass insertion approximation, allows to recover the ZMA results (149) and (150) quantifying the misalignment between the Yukawa couplings and the zero-mode masses (see [37] for a illuminating discussion). We emphasize that in our exact solution (135), (136), (137), and (143), all new-physics effects induced by the mass insertions, corresponding to both the non-derivative and derivative dimension-six operators, the former of which in fact lead to the chirally unsuppressed terms in (136), are resummed to all orders in v^2/M_{KK}^2 at tree level. Before presenting a comprehensive analysis of the phenomenological impact of Higgs effects in the rare decay $t \rightarrow ch$ as well as Higgs-boson production and decay (see Sections 7.3 to 7.5), we add that in the case of $\Delta F = 2$ processes, *i.e.*, neutral meson mixing, the importance of Higgs FCNCs turns out to be limited. The most pronounced effects occur in the case of the CP-violating parameter ϵ_K , but even here they are typically smaller than the corrections due to KK gluon exchange [42].

7 Phenomenological Applications

In the following we consider some applications of our results. We begin with a discussion of the constraints imposed by the precision measurements of the bottom-quark pseudo observables. In particular, we show that the tension in the global $Z \rightarrow b\bar{b}$ fit is not significantly relaxed for a light Higgs boson with mass $m_h \approx 100$ GeV. A perfect fit can, however, be obtained for $m_h \lesssim 1$ TeV, which is the naturally expected mass range for the Higgs boson in models with a brane-localized scalar sector. We furthermore discuss the phenomenology of rare top-quark decays in the custodial model and compare it to the one of the minimal RS model. The experimental prospects for observing the rare FCNC transitions $t \rightarrow cZ$ and $t \rightarrow ch$ at the LHC turn out to be more favorable in extended RS scenarios than in the minimal model. The first complete one-loop calculation of all relevant Higgs-boson production and decay channels at hadron colliders represents the highlight of our phenomenological investigations. We find that, due to the composite nature of the Higgs boson, the top quark, and the KK gauge bosons and fermions, observable effects in both production and decay can naturally occur in RS scenarios. This observation could potentially have a tangible impact on the LHC physics program.

7.1 Bottom-Quark Pseudo Observables

In order to derive explicit expressions for $g_L^b \equiv (g_L^d)_{33}$ and $g_R^b \equiv (g_R^d)_{33}$ in the ZMA, we first need formulas for the leading contributions to the overlap integrals $(\Delta_{D,d}^{(j)})_{33}$. We find to the order considered

$$\begin{aligned}
\Delta_D &= \mathbf{U}_d^\dagger \text{diag} \left[\frac{F^2(c_{Q_i})}{3 + 2c_{Q_i}} \right] \mathbf{U}_d, \\
\Delta_d &= \mathbf{W}_d^\dagger \text{diag} \left[\frac{F^2(c_{\mathcal{T}_{2i}})}{3 + 2c_{\mathcal{T}_{2i}}} \right] \mathbf{W}_d, \\
\Delta'_D &= \mathbf{U}_d^\dagger \text{diag} \left[\frac{5 + 2c_{Q_i}}{2(3 + 2c_{Q_i})^2} F^2(c_{Q_i}) \right] \mathbf{U}_d, \\
\Delta'_d &= \mathbf{W}_d^\dagger \text{diag} \left[\frac{5 + 2c_{\mathcal{T}_{2i}}}{2(3 + 2c_{\mathcal{T}_{2i}})^2} F^2(c_{\mathcal{T}_{2i}}) \right] \mathbf{W}_d.
\end{aligned} \tag{151}$$

Notice that these expressions have exactly the same form as in the minimal model [24].

The matrices $\epsilon_{D,d}^{(j)}$ vanish at leading order in the ZMA, meaning that they are suppressed by an extra factor of v^2/M_{KK}^2 . We consequently neglect them. The matrices $\delta_{D,d}$, on the other hand, are of the same order as the $\Delta_{D,d}^{(j)}$ contributions. The ZMA expression for δ_D has already been given in (120), and the last missing ingredient takes the form $\delta_d = -1/2 \Phi_d$ and resembles the ZMA result found in the RS model with $SU(2)_L \times U(1)_Y$ bulk gauge symmetry [24].

After Taylor expansion of the mixing matrices \mathbf{U}_d and \mathbf{W}_d in powers of the Cabibbo angle λ [24], we finally arrive for $c_{b'_R}, c_{\mathcal{T}_{1i}} < 1/2$ at

$$\begin{aligned}
g_L^b &= \left(-\frac{1}{2} + \frac{s_w^2}{3} \right) \left[1 - \frac{m_Z^2}{2M_{\text{KK}}^2} \frac{F^2(c_{b_L})}{3 + 2c_{b_L}} \left(\omega_Z^{b_L} L - \frac{5 + 2c_{b_L}}{2(3 + 2c_{b_L})} \right) \right] \\
&+ \frac{m_b^2}{2M_{\text{KK}}^2} \left\{ \frac{1}{1 - 2c_{b_R}} \left(\frac{1}{F^2(c_{b_R})} \left[1 - \frac{1 - 2c_{b_R}}{1 - 2c_{b'_R}} \right] - 1 + \frac{F^2(c_{b_R})}{3 + 2c_{b_R}} \right) \right. \\
&\quad \left. + \sum_{i=1}^2 \frac{|(Y_d)_{3i}|^2}{|(Y_d)_{33}|^2} \frac{1}{1 - 2c_{\mathcal{T}_{2i}}} \frac{1}{F^2(c_{b_R})} \left[1 - \frac{1 - 2c_{\mathcal{T}_{2i}}}{1 - 2c_{\mathcal{T}_{1i}}} \right] \right\},
\end{aligned} \tag{152}$$

$$\begin{aligned}
g_R^b &= \frac{s_w^2}{3} \left[1 - \frac{m_Z^2}{2M_{\text{KK}}^2} \frac{F^2(c_{b_R})}{3 + 2c_{b_R}} \left(\omega_Z^{b_R} L - \frac{5 + 2c_{b_R}}{2(3 + 2c_{b_R})} \right) \right] \\
&- \frac{m_b^2}{2M_{\text{KK}}^2} \left\{ \frac{1}{1 - 2c_{b_L}} \left(\frac{1}{F^2(c_{b_L})} - 1 + \frac{F^2(c_{b_L})}{3 + 2c_{b_L}} \right) + \sum_{i=1}^2 \frac{|(Y_d)_{i3}|^2}{|(Y_d)_{33}|^2} \frac{1}{1 - 2c_{Q_i}} \frac{1}{F^2(c_{b_L})} \right\},
\end{aligned}$$

where $c_{b_L} \equiv c_{Q_3}$, $c_{b_R} \equiv c_{\mathcal{T}_{23}}$, and $c_{b'_R} \equiv c_{\mathcal{T}_{13}}$. Furthermore, $m_b \equiv m_b(M_{\text{KK}})$ denotes the bottom-quark $\overline{\text{MS}}$ mass evaluated at the KK scale. Notice that we kept $c_{\mathcal{T}_{1i}} \neq c_{\mathcal{T}_{2i}}$, thereby allowing

the P_{LR} symmetry to be broken by the triplet bulk masses. We also retained the parameters ω_Z^{bL} and ω_Z^{bR} . In the custodial RS model one has $\omega_Z^{bL} = 0$ and

$$\omega_Z^{bR} = \frac{3c_w^2}{s_w^2} \approx 10.0, \quad (153)$$

where in order to arrive at the numerical values we have employed $s_w^2 \approx 0.23$, corresponding to the value of the weak mixing angle at the Z -pole.⁷

By inspection of (152), we observe that the non-universal corrections to the $Zb\bar{b}$ couplings reduce both g_L^b and g_R^b if the extended P_{LR} symmetry (122) is at work. If one allows the P_{LR} symmetry to be broken by $c_{\mathcal{T}_{1i}} \neq c_{\mathcal{T}_{2i}}$, then the shift in g_L^b can also be positive as a result of fermion mixing. As we will see in a moment, this always aggravates the quality of the $Z \rightarrow b\bar{b}$ fit. It is also evident that with respect to the minimal model, where the shift δg_L^b is large and positive while δg_R^b is small and negative [24], the constraints arising from the bottom-quark pseudo observables are naively much less stringent. Yet in order to gauge the improvement and to fully understand the parameter dependence, in particular the one on the bulk mass parameters $c_{\mathcal{T}_{1i}}$, one has to perform a detailed numerical analysis. Such an exercise is the subject of the remainder of this subsection.

Consider the ratio of the width of the Z -boson decay into bottom quarks and the total hadronic width, R_b^0 , the bottom-quark left-right asymmetry, A_b , and the forward-backward asymmetry for bottom quarks, $A_{\text{FB}}^{0,b}$. The dependences of these quantities on the left- and right-handed bottom-quark couplings are given by [43]

$$R_b^0 = \left[1 + \frac{4 \sum_{q=u,d} [(g_L^q)^2 + (g_R^q)^2]}{\eta_{\text{QCD}} \eta_{\text{QED}} [(1 - 6z_b)(g_L^b - g_R^b)^2 + (g_L^b + g_R^b)^2]} \right]^{-1},$$

$$A_b = \frac{2\sqrt{1 - 4z_b} \frac{g_L^b + g_R^b}{g_L^b - g_R^b}}{1 - 4z_b + (1 + 2z_b) \left(\frac{g_L^b + g_R^b}{g_L^b - g_R^b} \right)^2}, \quad A_{\text{FB}}^{0,b} = \frac{3}{4} A_e A_b. \quad (154)$$

Radiative QCD and QED corrections are encoded by the factors $\eta_{\text{QCD}} = 0.9954$ and $\eta_{\text{QED}} = 0.9997$, while the parameter $z_b \equiv m_b^2(m_Z)/m_Z^2 = 0.997 \cdot 10^{-3}$ describes the effects of the non-zero bottom-quark mass. Since to an excellent approximation one can neglect the RS contributions to the left- and right-handed couplings of the light quarks, $g_{L,R}^q$, and to the asymmetry parameter of the electron, A_e , we will fix these quantities to their SM values $(g_L^u)_{\text{SM}} = 0.34674$, $(g_R^u)_{\text{SM}} = -0.15470$, $(g_L^d)_{\text{SM}} = -0.42434$, $(g_R^d)_{\text{SM}} = 0.077345$ [44], and $(A_e)_{\text{SM}} = 0.1462$ [45]. The quoted values correspond to the SM input parameters given in Appendix B.

⁷The electromagnetic coupling and the weak mixing angle are running parameters in the low-energy effective theory obtained after decoupling the RS contributions at the scale M_{KK} . The associated large logarithms can be effectively included by replacing $s_w^2(M_{\text{KK}})$ by $s_w^2(m_Z)$ in the couplings $g_{L,R}^b$. On the other hand, the value of the bottom-quark mass entering the matching is frozen at the high scale and does not evolve in the effective theory.

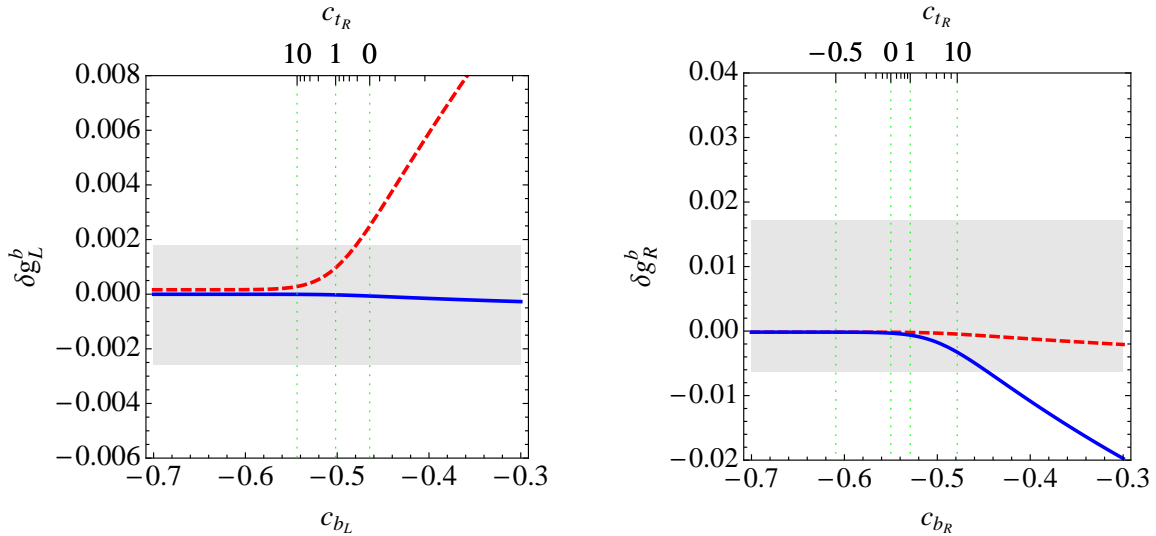


Figure 2: Anomalous couplings δg_L^b (left) and δg_R^b (right) as functions of c_{b_L} and c_{b_R} . The blue solid (red dashed) lines correspond to the predictions obtained in the RS model with extended P_{LR} symmetry (minimal RS model). Bulk mass parameters not explicitly shown are set to $-1/2$, and all elements of the down-type Yukawa matrix are taken to be equal to 1 in magnitude. The light gray bands indicate the experimentally allowed 99% CL ranges. See text for details.

Evaluating the relations (154) using $(g_L^b)_{\text{SM}} = -0.42114$ and $(g_R^b)_{\text{SM}} = 0.077420$ [44], we obtain for the central values of the bottom-quark pseudo observables

$$(R_b^0)_{\text{SM}} = 0.21578, \quad (A_b)_{\text{SM}} = 0.935, \quad (A_{\text{FB}}^{0,b})_{\text{SM}} = 0.1025. \quad (155)$$

One should compare these numbers with the experimental results [44]

$$\begin{aligned} (R_b^0)_{\text{exp}} &= 0.21629 \pm 0.00066, \\ (A_b)_{\text{exp}} &= 0.923 \pm 0.020, \\ (A_{\text{FB}}^{0,b})_{\text{exp}} &= 0.0992 \pm 0.0016, \end{aligned} \quad \rho = \begin{pmatrix} 1.00 & -0.08 & -0.10 \\ -0.08 & 1.00 & 0.06 \\ -0.10 & 0.06 & 1.00 \end{pmatrix}, \quad (156)$$

where ρ is the correlation matrix. While the R_b^0 and A_b measurements agree within $+0.8\sigma$ and -0.6σ with their SM predictions for $m_h = 150 \text{ GeV}$, the $A_{\text{FB}}^{0,b}$ measurement is almost -2.1σ away from its SM expectation.⁸ Shifts of order $+20\%$ and -0.5% in the right- and left-handed bottom-quark couplings relative to the SM could explain the observed discrepancy. Such a pronounced correction in g_R^b would affect A_b and $A_{\text{FB}}^{0,b}$, which both depend linearly on the ratio g_R^b/g_L^b , in a significant way, while it would not spoil the good agreement in $R_b^0 \propto (g_L^b)^2 + (g_R^b)^2$.

In Figure 2 we show our predictions for the anomalous couplings $\delta g_{L,R}^b \equiv g_{L,R}^b - (g_{L,R}^b)_{\text{SM}}$ as functions of the bulk mass parameters $c_{b_{L,R}}$. Similar plots have been presented in [34]. The shown curves correspond to $c_{Q_i} = c_{T_{1i}} = c_{T_{2i}} = -1/2$ and $|(Y_d)_{3i}| = |(Y_d)_{i3}| = |(Y_d)_{33}| = 1$ with $i = 1, 2$. We see that compared to the minimal case (red dashed line) the prediction for δg_L^b in the RS model with extended P_{LR} symmetry (blue solid line) is, owing to (100), essentially

⁸For $m_h = 115 \text{ GeV}$ the discrepancy in $A_{\text{FB}}^{0,b}$ would amount to around -2.5σ .

independent of c_{b_L} .⁹ The predictions for the anomalous coupling δg_L^b are thus easily within the experimental 99% confidence level (CL) bound (light gray band), which gives a strong motivation to protect the $Zb_L\bar{b}_L$ vertex through the mechanism of [16]. Notice that in the case of the minimal RS model, δg_L^b can be suppressed by localizing the right-handed top quark very close to the IR brane. This feature is illustrated by the ticks on the upper border of the frame in the left panel. The given values of $c_{t_R} \equiv c_{u_3^c}$ have been obtained by solving $m_t = v/\sqrt{2} |(Y_u)_{33}| |F(c_{b_L})F(c_{t_R})|$ for the bulk mass parameter c_{t_R} , evaluating the top-quark $\overline{\text{MS}}$ mass at $M_{\text{KK}} = 1 \text{ TeV}$ and setting $|(Y_u)_{33}| = 3$. For smaller (larger) values of $|(Y_u)_{33}|$ the ticks are shifted to the right (left).

In the case of δg_R^b we observe instead that, as a result of (153), the corrections to the anomalous coupling are always larger in the RS model with extended P_{LR} symmetry (blue solid line) than in the minimal formulation (red dashed line).¹⁰ It is however important to remark that even in the former case the $Zb_R\bar{b}_R$ coupling is predicted to be SM-like, since shifts in δg_R^b outside the experimental 99% CL range (light gray band) would require the bulk mass parameter of the right-handed top quark to be significantly larger than 1. Such a choice appears unnatural, since $c_{t_R} > 1$ implies that the corresponding bulk mass exceeds the curvature scale, in which case the right-handed top quark should be treated as a brane-localized and not a bulk fermion. The latter feature can be inferred from the ticks on the upper border of the frame in the right panel. They have been obtained by combining the equality $m_b = v/\sqrt{2} |(Y_d)_{33}| |F(c_{b_L})F(c_{b_R})|$ with the one for m_t given earlier, solving again for c_{t_R} . The Yukawa parameters have been fixed to $|(Y_d)_{33}| = 1$ and $|(Y_u)_{33}| = 3$. For smaller (larger) values of $|(Y_d)_{33}|$ the ticks move to the right (left). Rescaling $|(Y_u)_{33}|$ has the opposite effect. This observation leads us to the conclusion that, irrespectively of the bulk gauge group, naturalness in combination with the requirement to reproduce the observed top- and bottom-quark masses excludes large corrections to δg_R^b in models of warped extra dimensions in which the left-handed bottom and top quark reside in the same multiplet. This model-independent conclusion should be contrasted with the analysis [46], which finds sizable corrections in δg_R^b . The values of the bulk mass parameters $c_{b_{L,R}}$ and c_{t_R} considered in the latter article lead however to bottom- and top-quark masses of $m_b \approx 40 \text{ GeV}$ and $m_t \approx 75 \text{ GeV}$, which are in conflict with observation. We finally remark that if the left-handed bottom and top quarks arise as an admixture of the zero-mode fields of two $SU(2)_L$ doublets, then the bottom- and top-quark masses are determined by two independent sets of bulk mass parameters, so that it is possible to account simultaneously for the quark masses and mixings as well as the $A_{\text{FB}}^{0,b}$ anomaly [47].

The left panel of Figure 3 illustrates the impact of a possible breaking of the P_{LR} symmetry by the bulk masses parameters $c_{\mathcal{T}_i}$. The plot shows the regions of 99% probability in the $c_{b_L} - c_{b_R}$ plane for $M_{\text{KK}} = 1 \text{ TeV}$ under the restriction $0.1 < |(Y_d)_{33}| < 3$. The colored contours indicate the magnitude $|(Y_d)_{33}|$ necessary to achieve the correct value of the bottom-quark mass. Requiring in addition a consistent value of the quark masses and mixings restricts the parameter space further. This is indicated by the green dashed, fin-shaped region in the left

⁹In order not to induce unacceptably large corrections to δg_R^b induced by effects due to fermion mixing, one has to require $c_{b_L} \gtrsim -0.55$.

¹⁰Notice that in order to reproduce the large top-quark mass with Yukawa couplings of $\mathcal{O}(1)$ one has to require $c_{t_R} > -1/2$, corresponding to $c_{b_R} \gtrsim -0.6$.

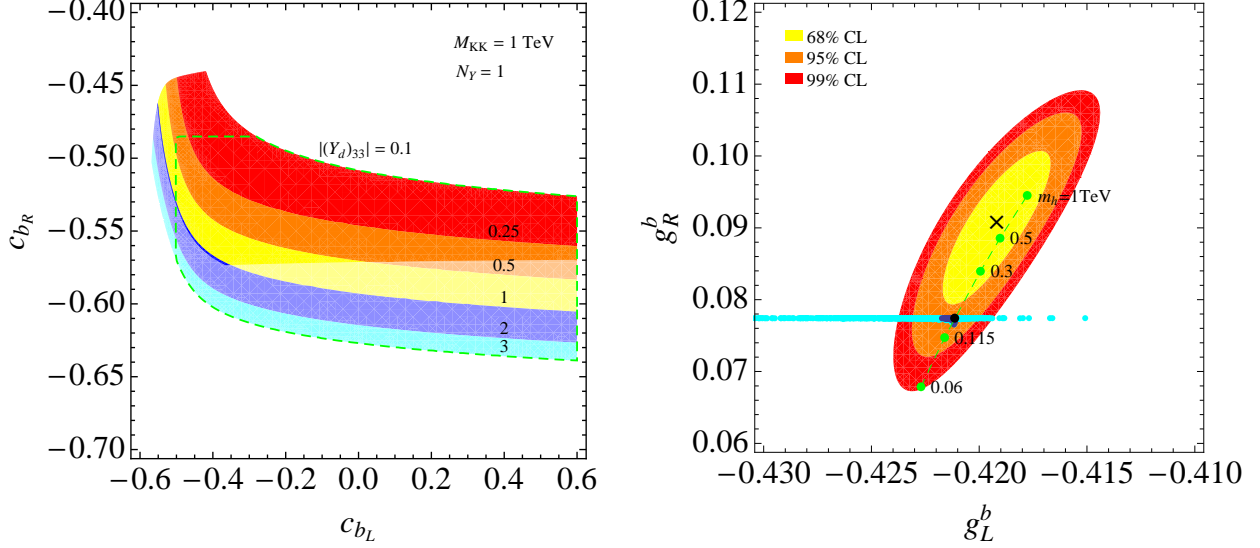


Figure 3: Left: Region of 99% probability in the c_{b_L} - c_{b_R} plane for $M_{KK} = 1$ TeV. We set $c_{Q_i} = c_{\mathcal{T}_{1i}} = c_{\mathcal{T}_{2i}} = -1/2$ and $N_Y \equiv |(Y_d)_{ij}|/|(Y_d)_{33}| = 1$ for $i, j = 1, 2$. The colored contours indicate the value of $|(Y_d)_{33}|$ necessary to reproduce the value of the bottom-quark mass. While the whole colored region corresponds to the RS results with $c_{b'_R} = c_{b_R}$, only the parameter space indicated by bright colors is accessible for $c_{b'_R} = 0$. The green dashed, fin-shaped region contains 99% of the parameter points that lead to consistent values of the quark masses and mixings. Right: Regions of 68%, 95%, and 99% probability in the g_L^b - g_R^b plane. The horizontal stripe consists of a large number of points in parameter space. The blue (cyan) points represent the RS result $c_{b'_R} = c_{b_R}$ ($c_{b'_R} \neq c_{b_R}$). The black dot is the SM expectation for the reference point, and the green dashed line indicates the SM predictions for $m_h \in [0.06, 1]$ TeV. See text for details.

panel of Figure 3, which contains 99% of the allowed parameter points. While in the case of an extended P_{LR} symmetry the whole colored region is accessible, allowing for $c_{b'_R} \neq c_{b_R}$ can cut away a sizable part of parameter space. This is demonstrated by the bright colored region, which corresponds to the choice $c_{b'_R} = 0$. Notice that the P_{LR} breaking correction to g_{b_L} in (152) arising from $c_{b'_R} \neq c_{b_R}$ scales like $-v^2/M_{KK}^2 |(Y_d)_{33}|^2 F^2(c_{b_L})$. This explains why values $|(Y_d)_{33}| \gtrsim 1$ are not compatible with the $Z \rightarrow b\bar{b}$ data in the case $c_{b'_R} = 0$.

The possible size of P_{LR} symmetry-breaking corrections is shown in the right panel of Figure 3, which displays the regions of 68%, 95%, and 99% CL obtained from a global fit to the $Z \rightarrow b\bar{b}$ pseudo observables (156). The predictions in the RS model with (without) extended P_{LR} symmetry are superimposed as blue (cyan) scatter points. The shown points correspond to 10000 random choices of parameters with $M_{KK} = [1, 10]$ TeV, $|(Y_{u,d})_{ij}| \in [0.1, 3]$, $\arg((Y_{u,d})_{ij}) \in [0, 2\pi[$, and $c_{t_R} \in]-1/2, 1]$ that reproduce the quark masses and mixings with a global χ^2/n_{dof} better than 11.5/10, corresponding to 68% CL. The cyan points have been obtained by allowing the bulk mass parameters $c_{\mathcal{T}_i}$ with $i = 1, 2, 3$ to take any value in the range $[-1, 0]$. We see that in the former case the small RS contributions always drive g_L^b to smaller values with respect to the SM reference point (black dot), while in the latter case

moderate positive and large negative corrections in g_L^b are possible, leading further away from the best fit values $g_L^b = -0.41918$ and $g_R^b = 0.090677$ (black cross). In both cases g_R^b remains essentially unaffected. Thus, like in the minimal model [24], the corrections (152) alone cannot account for the positive shift in g_R^b needed to explain the anomaly in $A_{\text{FB}}^{0,b}$.¹¹

A perfect fit to the $Z \rightarrow b\bar{b}$ data can however be achieved by allowing for a heavy Higgs boson, because the shifts

$$\Delta g_L^b = 1.77 \cdot 10^{-3} \ln \frac{m_h}{m_h^{\text{ref}}}, \quad \Delta g_R^b = 0.92 \cdot 10^{-2} \ln \frac{m_h}{m_h^{\text{ref}}} \quad (157)$$

in $g_{L,R}^b$ due to a Higgs-boson mass different from the reference value $m_h^{\text{ref}} = 150$ GeV are both positive for $m_h > m_h^{\text{ref}}$. The latter relations parametrize the leading logarithmic Higgs-mass dependences of $g_{L,R}^b$ and have been derived with the help of ZFITTER [45].¹² The exact shifts in the $Zb\bar{b}$ couplings for $m_h \in [0.06, 1]$ TeV are indicated by the green dashed line in the right panel of Figure 3. One observes that a Higgs-boson mass in the ballpark of $m_h = 0.5$ TeV would bring the predictions of $g_{L,R}^b$ so close to the best fit values that already the small corrections in the RS model with extended P_{LR} symmetry are sufficient to reach the minimum of the χ^2 distribution. Warped models with the Higgs field localized in the IR might thus indirectly allow for an explanation of the $A_{\text{FB}}^{0,b}$ anomaly, since in these set-ups the Higgs boson is naturally expected to be heavy, which leads to a good agreement between the $Z \rightarrow b\bar{b}$ data and theory. Such an option is however not unproblematic, since the presence of a heavy Higgs boson can potentially spoil the global electroweak fit in RS models with custodial protection of the T parameter [24].

7.2 Rare Decay $t \rightarrow cZ$

As the top quark, being the heaviest fermion in the SM, is localized closest to the IR brane, it couples most strongly to the KK excitations of the gauge bosons. It is thus natural to expect sizable effects in processes involving flavor-violating top-quark couplings. Since FCNCs in the up-type quark sector are less constrained by K - and B -meson physics than those in the down-type quark sector, the decay $t \rightarrow cZ$ provides a promising test of RS models.

From (104) we derive the branching ratio for this decay, which is given to excellent approximation by [24]

$$\begin{aligned} \mathcal{B}(t \rightarrow cZ) &= \frac{2(1 - r_Z^2)^2(1 + 2r_Z^2)}{(1 - r_W^2)^2(1 + 2r_W^2)} \\ &\times \left\{ |(g_L^u)_{23}|^2 + |(g_R^u)_{23}|^2 - \frac{12r_c r_Z^2}{(1 - r_Z^2)(1 + 2r_Z^2)} \text{Re}[(g_L^u)_{23}^* (g_R^u)_{23}] \right\} \\ &\approx 1.842 \left[|(g_L^u)_{23}|^2 + |(g_R^u)_{23}|^2 \right] - 0.048 \text{Re}[(g_L^u)_{23}^* (g_R^u)_{23}], \end{aligned} \quad (158)$$

¹¹The corrections to g_R^b are always negative but small and hence hardly visible in the figure.

¹²The default flags of ZFITTER version 6.42 are used, except for setting ALEM=2 to take into account the externally supplied value of $\Delta\alpha_{\text{had}}^{(5)}(m_Z)$.

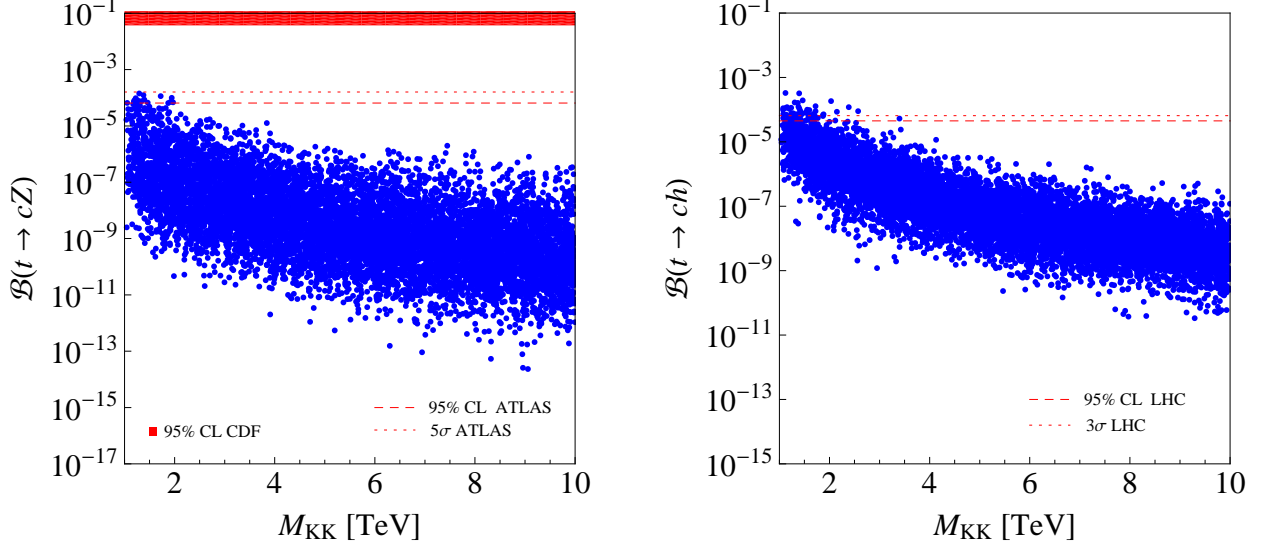


Figure 4: Branching ratio of the rare decays $t \rightarrow cZ$ (left) and $t \rightarrow ch$ (right) as functions of M_{KK} in the RS model with extended custodial protection $c_{\mathcal{T}_{1i}} = c_{\mathcal{T}_{2i}}$. The red band in the left panel is excluded at 95% CL by the CDF search for $t \rightarrow u(c)Z$. The red dotted and dashed lines in the left (right) plot indicate the expected discovery and exclusion sensitivities of ATLAS (LHC) for 100 fb^{-1} integrated luminosity. All scatter points reproduce the correct quark masses, mixing angles, and the CKM phase. See text for details.

where $r_i \equiv m_i^{\text{pole}}/m_t^{\text{pole}}$, and for simplicity we have only kept terms up to first order in v^2/M_{KK}^2 and the charm-quark mass ratio $r_c \approx 8.7 \cdot 10^{-3}$. The flavor-changing couplings in the custodial model are given by

$$\begin{aligned}
 (g_L^u)_{23} &= -\frac{m_Z^2}{2M_{\text{KK}}^2} \left(\frac{1}{2} - \frac{2}{3}s_w^2 \right) \left[\omega_Z^{uL} L(\Delta_U)_{23} - (\Delta'_U)_{23} \right] - (\delta_U)_{23} , \\
 (g_R^u)_{23} &= -\frac{m_Z^2}{2M_{\text{KK}}^2} \frac{2}{3}s_w^2 (\Delta'_u)_{23} + (\delta_u)_{23} .
 \end{aligned}
 \tag{159}$$

The ZMA expressions for the matrices Δ_U , Δ'_U , and Δ'_u are obtained from (151) by the replacements $c_{\mathcal{T}_{2i}} \rightarrow c_{u_i^c}$, $\mathbf{U}_d \rightarrow \mathbf{U}_u$, and $\mathbf{W}_d \rightarrow \mathbf{W}_u$. In the same approximation one has $\delta_U = 1/2 \Phi_U$ with Φ_U introduced in (150) and

$$\delta_u = \frac{1}{2} \mathbf{x}_u \mathbf{U}_u^\dagger \text{diag} \left[\frac{1}{1 - 2c_{Q_i}} \left(\frac{1}{F^2(c_{Q_i})} \left[1 - \frac{1 - 2c_{Q_i}}{F^2(-c_{Q_i})} \right] - 1 + \frac{F^2(c_{Q_i})}{3 + 2c_{Q_i}} \right) \right] \mathbf{U}_u \mathbf{x}_u . \tag{160}$$

Notice that, compared to the ZMA result in the minimal RS model [24], the mixing matrix δ_u contains an additional term involving the zero-mode profile $F(-c_{Q_i})$.

Inserting the quantum numbers of the representation (58) into (101), we see that the leading contribution to $(g_L^u)_{23}$ is enhanced by a factor

$$\omega_Z^{uL} = \frac{2c_w^2}{1 - \frac{4}{3}s_w^2} \approx 2.2 . \tag{161}$$

In contrast to the minimal model [24], the right-handed coupling does not receive an L -enhanced contribution, because $\omega_Z^{uR} = 0$. Moreover, the contribution inversely proportional to $F^2(c_{Q_i})$ in δ_u is highly suppressed if $c_{Q_i} < 1/2$, since $F^2(-c_{Q_i}) \approx 1 - 2c_{Q_i}$ in such a case. The leading corrections to the $Zu_R^i \bar{u}_R^j$ vertices due to quark mixing are therefore protected by the custodial symmetry. While these features remove a possible source of large effects associated with the composite nature of the right-handed top quark, they imply that the chirality of the Ztc interactions in the model under consideration is predicted not to be right-handed, as argued in [40], but left-handed. Of course, other choices of the quantum numbers of the right-handed up-type quarks than those in Table 2 are possible, so that the RS framework does not lead to a firm prediction of the chirality of the Ztc interactions.

The predictions for $\mathcal{B}(t \rightarrow cZ)$ in the custodial RS model with extended P_{LR} symmetry as a function of M_{KK} are shown in the left panel of Figure 4. The experimental upper bound on FCNC $t \rightarrow u(c)Z$ from the CDF experiment amounts to $\mathcal{B}(t \rightarrow u(c)Z) < 3.7\%$ at 95% CL [49] and is shown as a band. At the LHC, one can search for rare FCNC top-quark transitions in top-quark production and decays. The ATLAS [50] and CMS [51] collaborations have examined this possibility in simulation studies. The minimal branching ratio $\mathcal{B}(t \rightarrow cZ)$ allowing for a 5σ signal discovery with 100 fb^{-1} integrated luminosity is expected to be $1.6 \cdot 10^{-4}$ at ATLAS. In the absence of a signal, the expected upper bound at 95% CL is $6.5 \cdot 10^{-5}$. These values are visualized by the red dotted and dashed lines in the plot. Our numerical studies show that for low KK mass scales in the ballpark of 2 TeV,¹³ which is a realistic possibility in RS models with custodial protection, the branching ratio $\mathcal{B}(t \rightarrow cZ)$ can come close to the region which can be probed at the LHC.¹⁴ In the minimal RS model the possible branching ratios are smaller, since the strong correlation between the Ztc and $Zb\bar{b}$ couplings generically leads to a rejection of points with large $\mathcal{B}(t \rightarrow cZ)$ [24]. The custodial protection of the $Zb_L \bar{b}_L$ vertex thus leads indirectly to improved prospects of a detection of the decay $t \rightarrow cZ$ at the LHC.

7.3 Rare Decay $t \rightarrow ch$

The general form of the interactions of fermions with the Higgs boson has been given in (131). These couplings allow for the flavor-changing decay $t \rightarrow ch$ with a branching ratio

$$\mathcal{B}(t \rightarrow ch) = \frac{2(1 - r_h^2)^2 r_W^2}{(1 - r_W^2)^2 (1 + 2r_W^2) g^2} \left\{ |(g_h^u)_{23}|^2 + |(g_h^u)_{32}|^2 + \frac{4r_c}{1 - r_h^2} \text{Re}[(g_h^u)_{23} (g_h^u)_{32}] \right\}, \quad (162)$$

where as before $r_i \equiv m_i^{\text{pole}}/m_t^{\text{pole}}$, and g is the $SU(2)_L$ gauge coupling. Again, we have included terms up to first order in the charm-quark mass. In our numerical analysis we will use $r_h = 0.87$, corresponding to a Higgs-boson mass $m_h = 150 \text{ GeV}$.

The predictions for $\mathcal{B}(t \rightarrow ch)$ in the custodial RS model with extended P_{LR} symmetry as a function of M_{KK} are shown in the right panel of Figure 4. The LHC is expected to provide

¹³Corresponding to masses of the lightest KK gauge bosons of around 5 TeV.

¹⁴As a result of $|F(c_{Q_1})|/|F(c_{Q_2})| \sim \lambda$ the branching ratio of $t \rightarrow uZ$ is typically suppressed by two orders of magnitude compared to $t \rightarrow cZ$, rendering the former mode unobservable at the LHC. Similar statements apply to the branching ratio of $t \rightarrow uh$.

a 3σ evidence for $\mathcal{B}(t \rightarrow ch)$ larger than $6.5 \cdot 10^{-5}$ or set an upper bound of $4.5 \cdot 10^{-5}$ with 95% CL if the decay is not observed [52]. These limits are indicated by the red dotted and dashed lines in the plot. We see that for low KK mass scales values of the branching ratio can even exceed the LHC reach, so that a detection of a possible RS signal with $t \rightarrow ch$ could become reality. Let us add that without inclusion of the Yukawa couplings involving Z_2 -odd fermion profiles the obtained branching fractions would be typically smaller by almost two orders of magnitude. In the minimal RS model the prospects for an observation of $t \rightarrow ch$ turn out to be less favorable, since the constraints from $Z \rightarrow b\bar{b}$ typically eliminate those points in parameter space that would show pronounced effects [24].

7.4 Higgs-Boson Production

At hadron colliders such as the Tevatron or the LHC the leading production mechanism of the Higgs boson is gluon-gluon fusion, which receives its dominant contribution from a top-quark triangle loop. Within the RS framework, one has to take into account the whole KK tower of the top as well as the other quark flavors, since all these modes contribute to the $gg \rightarrow h$ amplitude at $\mathcal{O}(v^2/M_{\text{KK}}^2)$. The relevant Feynman diagrams are shown on the very left in the top row of Figure 5 and on the left-hand side of Figure 6.

In order to calculate the $gg \rightarrow h$ production cross section in the RS model, we rescale the SM prediction, employing

$$\sigma(gg \rightarrow h)_{\text{RS}} = |\kappa_g|^2 \sigma(gg \rightarrow h)_{\text{SM}}, \quad (163)$$

where

$$\kappa_g = \frac{\sum_{i=t,b} \kappa_i A_q^h(\tau_i) + \sum_{j=u,d,\lambda} \nu_j}{\sum_{i=t,b} A_q^h(\tau_i)}, \quad (164)$$

with $\tau_i \equiv 4m_i^2/m_h^2$. The first term in the numerator encodes the effects due to zero modes running in the loop and the corresponding sum includes both the virtual top- and bottom-quark contributions. The form factor $A_q^h(\tau_i)$ approaches 1 for $\tau_i \rightarrow \infty$ and vanishes proportional to τ_i for $\tau_i \rightarrow 0$. Its analytic form is given in Appendix C. As they are power suppressed, the only phenomenologically relevant correction in $\sigma(gg \rightarrow h)_{\text{SM}}$ due to lighter quarks is the interference term of the bottom- and top-quark amplitudes. Its effect can be approximated by multiplying the cross section $\sigma(gg \rightarrow h)_{\text{SM}}$ without the bottom-quark corrections by $(1 + 2 \text{Re} A_q^h(\tau_b))$. Numerically, this approximate treatment decreases the SM cross section by about 9%, 2%, and below 1% for $m_h = 100$ GeV, 300 GeV, and 600 GeV, in good agreement with the next-to-leading order calculation including the exact mass dependence [53]. In our numerical evaluation of the SM Higgs-boson production cross section via $gg \rightarrow h$, the bottom-quark contribution will be included using the lowest-order approximation.

The quantities

$$\kappa_t = 1 - \frac{v}{m_t} (\Delta g_h^u)_{33}, \quad \kappa_b = 1 - \frac{v}{m_b} (\Delta g_h^d)_{33} \quad (165)$$

appearing in (164) describe the ratios of Higgs-boson couplings to heavy quarks in the custodial RS model relative to the corresponding SM values. In Figure 7 we show the real parts of these

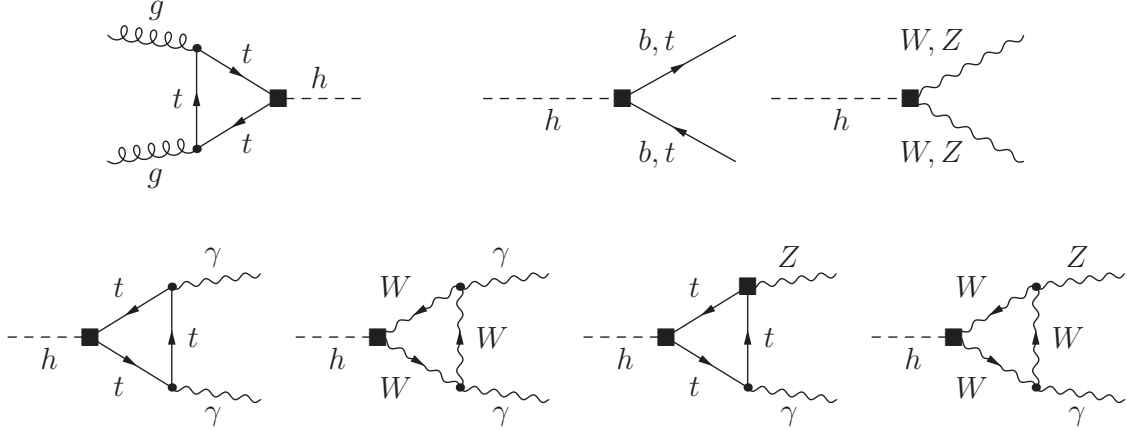


Figure 5: Examples of Feynman diagrams involving zero-mode fields only that contribute to the production and the decay of the Higgs boson at leading order of perturbation theory. Vertices indicated by a black square can receive sizable shifts in the RS model relative to the SM couplings. See text for details.

ratios as a function of M_{KK} for a set of 150 random parameter points corresponding to the model with the extended P_{LR} symmetry (122), which we will always employ in our numerical analysis. The same sample of model parameter points will be used in the remainder of this paper. Since the imaginary parts of $\kappa_{t,b}$ turn out to be small (the origin of this feature will be explained below), they are not shown in the figures. We observe that both the $ht\bar{t}$ and the $hb\bar{b}$ coupling are reduced in the RS scenario with respect to the SM, resulting in $\text{Re } \kappa_{t,b} \leq 1$. The same conclusion has been reached in [37] for the minimal RS model. Numerically, we find that for $M_{\text{KK}} = 2 \text{ TeV}$ ($M_{\text{KK}} = 3 \text{ TeV}$) the average corrections amount to around -25% and -15% (-10% and -5%) in the top- and bottom-quark sectors, respectively. Since the RS corrections to the Yukawa couplings scale as v^2/M_{KK}^2 , the average value of the ratios $\kappa_{t,b}$ can be parametrized by $1 - a_{t,b} v^2/M_{\text{KK}}^2$ with the coefficients $a_{t,b}$ given in Table 3. The quoted values of $a_{t,b}$ have been obtained from the best fits to the shown sample of scatter points.

The suppression of the Yukawa couplings of the third-generation quarks, $\text{Re } \kappa_{t,b} \leq 1$, as well as the feature $|\text{Im } \kappa_{t,b}| \ll 1$ are not difficult to understand. First, one has $m_3^q/v ((\Phi_q)_{33} + (\Phi_Q)_{33}) \geq 0$ since the diagonal elements of the matrices $\Phi_{q,Q}$ introduced in (137) are absolute squares. Second, the third term in (136) can be written in the ZMA as

$$(\Delta \tilde{g}_h^u)_{33} = \frac{4m_t^2}{3vM_{\text{KK}}^2} \sum_{j=1}^3 m_j^u \left(\mathbf{U}_u^\dagger \text{diag} [F^{-2}(c_{Q_i})] \mathbf{U}_u \right)_{j3} \left(\mathbf{W}_u^\dagger \text{diag} [F^{-2}(c_{u_i^c})] \mathbf{W}_u \right)_{3j}. \quad (166)$$

A similar formula applies to the case of $(\Delta \tilde{g}_h^d)_{33}$. Because the diagonal elements of the matrices $\mathbf{U}_u^\dagger \text{diag} [F^{-2}(c_{Q_i})] \mathbf{U}_u$ and $\mathbf{W}_u^\dagger \text{diag} [F^{-2}(c_{u_i^c})] \mathbf{W}_u$ are absolute squares, the term with $j = 3$ is obviously positive semi-definite. The terms with $j = 1, 2$, on the other hand, can have an arbitrary complex phase. Yet, due to the strong chiral suppression, $m_c/m_t \approx 1/275$ and $m_u/m_t \approx 10^{-5}$, the imaginary part of (166) turns out to be negligibly small, leaving us with

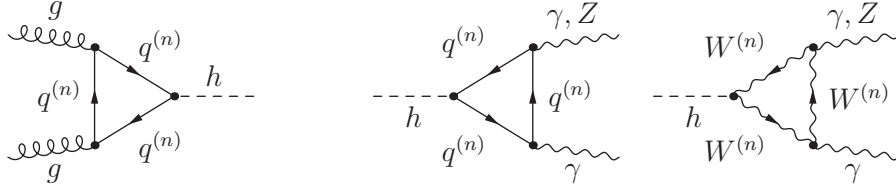


Figure 6: Examples of one-loop contributions involving KK excitations that contribute to the production and the decay of the Higgs boson at leading order of perturbation theory. See text for details.

$(\Delta\tilde{g}_h^u)_{33} \geq 0$. The same holds true for $(\Delta\tilde{g}_h^d)_{33}$, although the chiral suppression is weaker in this case, $m_s/m_b \approx 1/50$ and $m_d/m_b \approx 1/800$. Recalling that $(\Delta g_h^q)_{33} = m_3^q/v ((\Phi_q)_{33} + (\Phi_Q)_{33}) + (\Delta\tilde{g}_h^q)_{33} \geq 0$ enters (135) with a minus sign, we conclude that the $ht\bar{t}$ and $hb\bar{b}$ couplings are predicted to be suppressed relative to their SM values in both the minimal and the extended RS set-ups. We believe that this finding is model-independent and holds in a wide class of RS set-ups. The same conclusion has been drawn in the context of models where the Higgs arises as a pseudo Nambu-Goldstone boson [54, 55].

The second term in the numerator of (164) represents the contribution to the $gg \rightarrow h$ amplitude arising from the virtual exchange of KK quarks. The corresponding Feynman graph is shown on the very left in Figure 6. In the up-type quark sector the associated coefficient takes the form

$$\begin{aligned} \nu_u &= v \sum_{n=4}^{\infty} \frac{(g_h^u)_{nn}}{m_n^u} A_q^h(\tau_n^u) \\ &= \frac{2\pi}{\epsilon L} \sum_{n=4}^{\infty} \frac{\bar{a}_n^{U\dagger} \mathbf{C}_n^U(\pi^-) \left(\mathbf{1} - \frac{v^2}{3M_{\text{KK}}^2} \tilde{\mathbf{Y}}_{\bar{u}} \tilde{\mathbf{Y}}_{\bar{u}}^\dagger \right) \mathbf{S}_n^U(\pi^-) \bar{a}_n^U}{x_n^u} A_q^h(\tau_n^u). \end{aligned} \quad (167)$$

Similar relations hold in the sector of down-type and λ quarks.¹⁵ Since the mass of the first KK up-type quark is already much larger than the Higgs-boson mass, $m_4^u/M_{\text{KK}} = \mathcal{O}(\text{a few}) \gg m_h/M_{\text{KK}}$, it is an excellent approximation to replace the function $A_q^h(\tau_n^u)$ by its asymptotic value of 1 obtained for $\tau_n^u \equiv 4(m_n^u)^2/m_h^2 \rightarrow \infty$.

Before presenting our numerical results for these contributions, we would like to add some comments about the convergence of the sum in (167). In the SM, the top-quark contribution to the $gg \rightarrow h$ amplitude is proportional to y_t/m_t in the decoupling limit. In this limit the amplitude can be described by the effective operator $h/v G_{\mu\nu}^a G^{a\mu\nu}$, whose Wilson coefficient is related to the QCD β -function. This relationship arises through low-energy theorems appropriate to external Higgs bosons with vanishing momentum [55, 56, 57, 58], which apply to any quantum field theory. In the context of the RS framework they imply that the sum in (167) must be convergent, because the running of α_s can be shown to be logarithmic in

¹⁵With λ quarks we denote all fermionic KK excitations with electric charge 5/3.

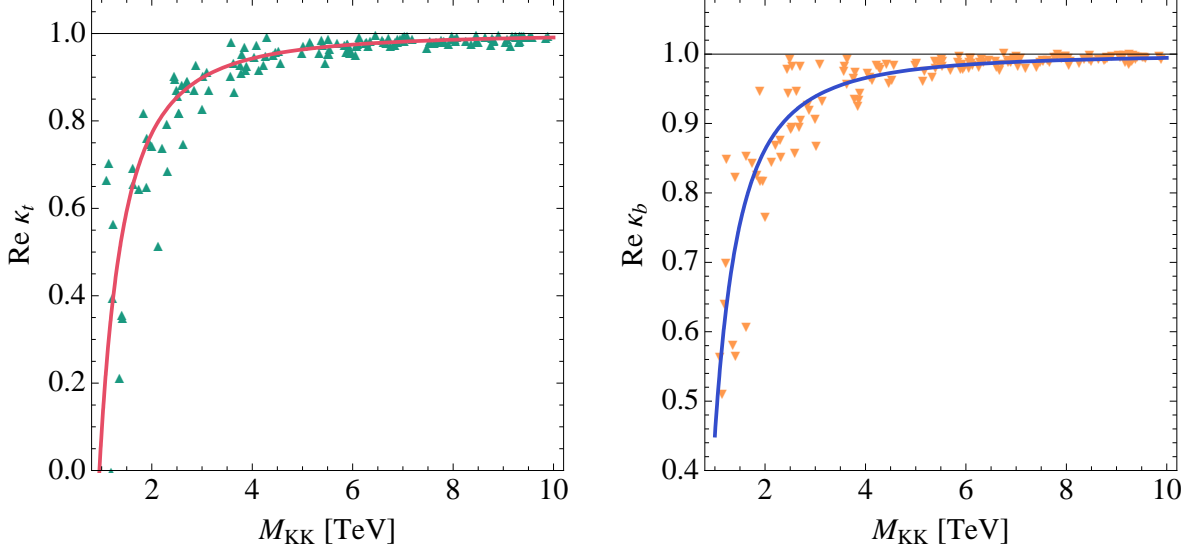


Figure 7: Predictions for the real parts of the ratios of the $ht\bar{t}$ (left) and $hb\bar{b}$ (right) coupling in the custodial RS model relative to the SM value. The solid lines show fits to the samples of parameter points. See text for details.

warped extra-dimension models [27, 59, 60, 61, 62, 63, 64, 65]. While the finiteness of the effective hgg coupling is thus guaranteed on general grounds, an explicit calculation of (167) in the KK decomposed 4D theory turns out to be non-trivial. This is due to the fact that the Higgs VEV induces $\mathcal{O}(1)$ mixings between the various modes of a single KK level [24]. For example, in the up-type quark sector there are five types of fields, namely u , u' , u^c , U' , and U . Each of them exists in three different flavors, so that there are altogether 15 KK modes of similar mass in each level. In the down-type quark sector, one instead ends up with nine modes, while in the minimal RS model one has six states per KK level in both the up- and the down-type quark sectors (corresponding to $SU(2)_L$ doublets and singlets). Finally, in the λ -type quark sector one again faces nine KK excitations per level. In contrast, exotic matter is not present in the minimal RS model. Since the mixing effects among the states of the same KK level, encoded in the eigenvectors \vec{a}_n^A , are large, they cannot be treated perturbatively, and one has to resort to numerical methods as long as one is interested in the case of three families. However, restricting oneself to the simpler case of a single generation, it turns out to be possible to derive an analytic expression for (167). This formula will be given in a companion paper.

In order to calculate the KK sum numerically, one first has to find the solutions to the eigenvalue equation (84).¹⁶ In the case of the up-type quark sector, this requires determining the roots of a 6×6 determinant, which in practice turns out to be intricate, because one

¹⁶In the absence of soft P_{LR} breaking, $c_{\mathcal{T}_{1i}} = c_{\mathcal{T}_{2i}}$, three out of the 15 (9) states in each up-type (λ -type) quark KK level will have masses that resemble the ones found in the spectrum for $(Y_{u,d})_{ij} = 0$. This feature is easy to understand, because a unitary transformation \mathcal{U} acting on the quarks $(U, U')^T \rightarrow \mathcal{U}(U, U')^T$ reshuffles only the Yukawa interactions but leaves all other bi-linear terms in the action (62) as well as the BCs invariant. The combinations $(U - U')/\sqrt{2}$ and $(\Lambda - \Lambda')/\sqrt{2}$ are thus unaffected by the Higgs mechanism.

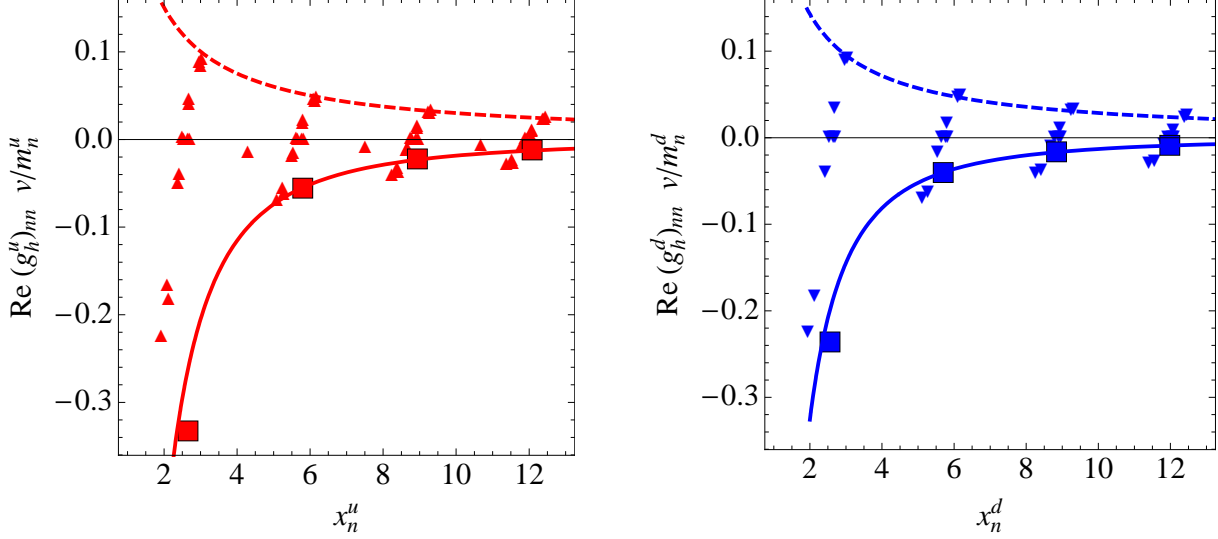


Figure 8: Numerical results for the real parts of the coefficients $\nu_{u,d}$ corresponding to a specific parameter point with $M_{\text{KK}} = 2 \text{ TeV}$. The red (blue) dots in the left (right) panel display the first 60 (36) terms in the KK sum for up- (down-type) quarks, while the red (blue) filled boxes indicate the sums over a complete KK level. See text for details.

needs to find suitable starting points to search for the roots. We obtain these starting values by diagonalizing a truncated mass matrix obtained in the perturbative approach [11, 25, 66]. In Figure 8 we display the results of our numerical calculations for one parameter point with $M_{\text{KK}} = 2 \text{ TeV}$. The dots correspond to the real parts of individual terms in the sum (167) for up- and down-type quarks, while the filled boxes indicate the values obtained by summing up the contributions of one KK level. Results for the exotic λ -type quarks are not shown, since they resemble those found in the down-type quark sector. By inspection of the two panels one immediately notices two important features of the KK contributions. First, even though the contribution of an individual mode can be positive and negative, the sum over an entire KK level is strictly negative. Second, the importance of higher-level KK sums decreases quadratically, ensuring that (167) converges to a finite value. This feature is indicated by the solid lines, which represent the best fits to $1/x_n^2$ including the results of the second, third, and fourth KK-level sums.¹⁷ In order to calculate (167), we then evaluate the corresponding fit at $\bar{x}_1^u + (k-1)\pi$ and resum the resulting series ($k = 1, \dots, \infty$) into a trigamma function, $\psi^{(1)}(\bar{x}_1^u/\pi)$. Here \bar{x}_1^u denotes the mean mass value of the first up-type quark KK level in units of the KK scale. In this way, we effectively include the entire tower of KK quarks in our result for ν_u . The same procedure is applied in the case of the coefficients ν_d and ν_λ .

In Figure 9 we display the real parts of the coefficients ν_u and ν_d as a function of the KK scale for a set of 150 randomly chosen parameter points. The results for the coefficient ν_λ are almost identically to those of ν_d , and we thus do not show them explicitly. We see that the

¹⁷The dashed lines depict the $1/x_n$ behavior of the sum over a single fermion tower. The convergence of the total sum is guaranteed by cancellations between different modes of the same KK level.

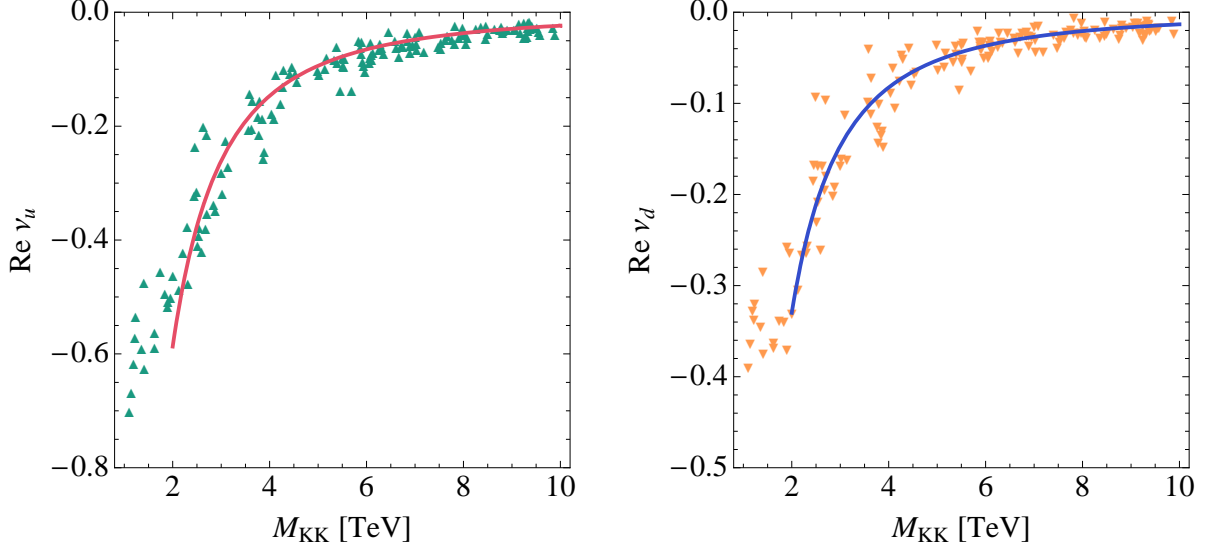


Figure 9: Predictions for the real parts of the coefficients ν_u and ν_d in the custodial RS model. The solid lines indicate the best fits to the shown sample of parameter points lying in the range $M_{\text{KK}} = [2, 10]$ TeV. See text for details.

corrections to the effective hgg coupling arising from triangle diagrams involving KK quarks are all strictly negative. In the up-type quark sector the corrections are almost a factor of 2 larger than those appearing in the down- and λ -type quark sectors. This feature can be traced back to the higher multiplicity of states in the former relative to the later sectors, which suggests that $\nu_u/\nu_{d,\lambda} = 15/9 \approx 1.7$. Numerically, we find that for $M_{\text{KK}} = 2$ TeV ($M_{\text{KK}} = 3$ TeV) the average value of the real parts of ν_u and $\nu_{d,\lambda}$ amounts to about -0.59 and -0.34 (-0.26 and -0.15) with the ratio of the values being quite close to the naive estimate. We also observe that the imaginary parts of the coefficients $\nu_{u,d,\lambda}$ are orders of magnitude smaller than the real parts. This feature can be understood from (135) and (136). Obviously, the only term in these equations that has a phase is $(\Delta\tilde{g}_h^q)_{nm}$. This contribution is however suppressed by v^2/M_{KK}^2 relative to the leading term of $\mathcal{O}(1)$. Since the leading KK quark corrections to the effective hgg vertex decouple as v^2/M_{KK}^2 , we parametrize the average values of $\nu_{u,d,\lambda}$ as $a_{u,d,\lambda} v^2/M_{\text{KK}}^2$ and determine the values of $a_{u,d,\lambda}$ from the best fit to the shown sample of points restricted to the range $M_{\text{KK}} = [2, 10]$ TeV. The obtained values for the coefficients $a_{u,d,\lambda}$ are collected in Table 3. Points with KK scale below 2 TeV have been excluded in the fit, since they depend sensitively on higher-order terms in v/M_{KK} . This feature is noticeable in the plots, which show that for very low KK scale the exact results for $\nu_{u,d}$ are typically above the solid lines indicating our fits. This should be kept in mind when using the parameterizations $a_{u,d,\lambda} v^2/M_{\text{KK}}^2$ to calculate $\nu_{u,d,\lambda}$ for KK scales below 2 TeV.

Our numerical results for the Higgs-boson production cross sections at the Tevatron and LHC for the center-of-mass energy $\sqrt{s} = 1.96$ TeV and $\sqrt{s} = 10$ TeV are shown in Figure 10. The calculation of $\sigma(gg \rightarrow h)_{\text{SM}}$ is based on [67], which combines the next-to-next-to-leading fixed-order corrections [68, 69, 70] with resummation of both threshold logarithms from soft-gluon emission [71, 72, 73, 74, 75] and terms of the form $(N_c \pi \alpha_s)^n$ [76]. In the evaluation of the

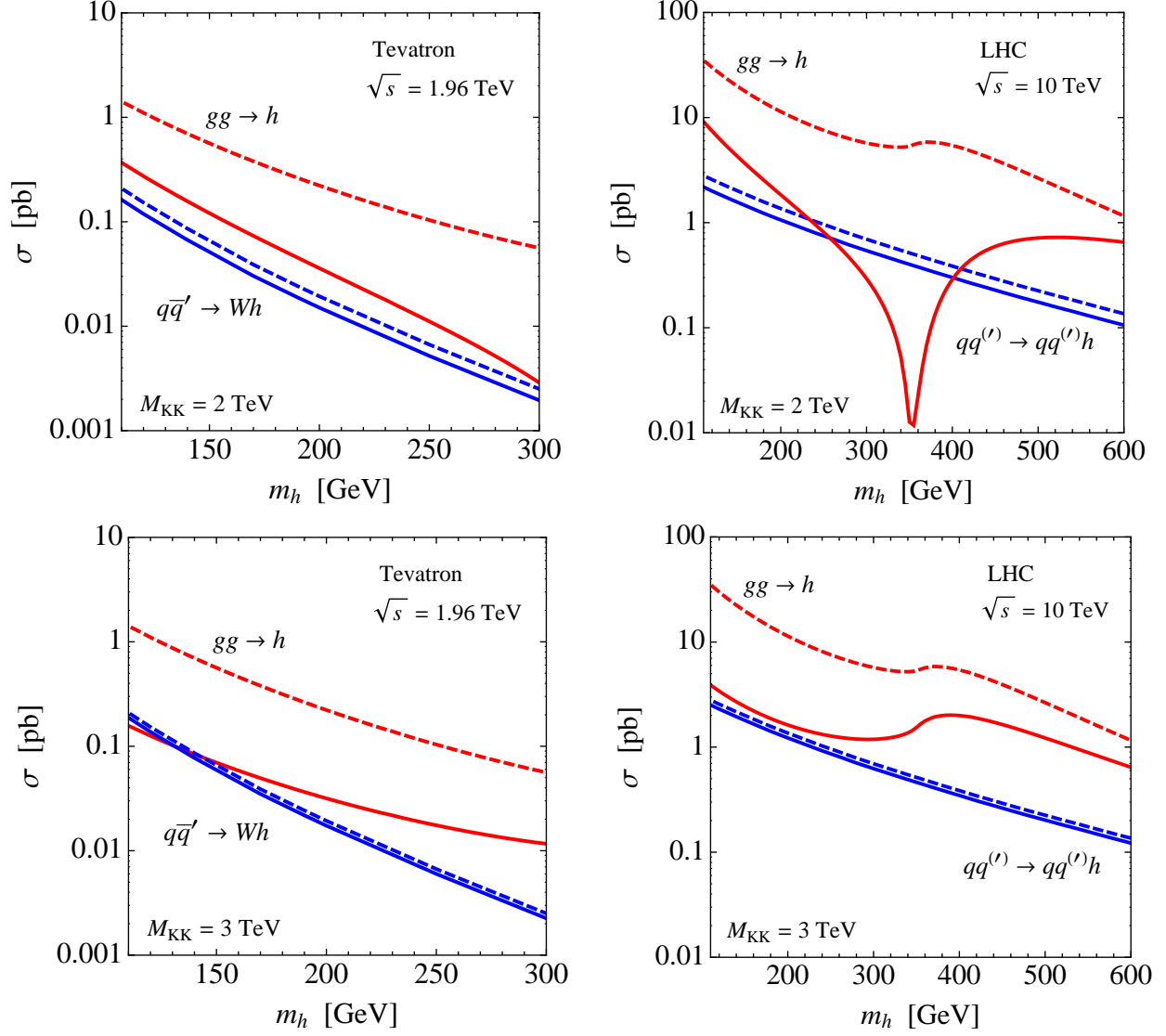


Figure 10: Main Higgs-boson production cross sections at the Tevatron (left) and the LHC (right) for center-of-mass energies of $\sqrt{s} = 1.96$ TeV and $\sqrt{s} = 10$ TeV, employing $M_{\text{KK}} = 2$ TeV (upper row) and $M_{\text{KK}} = 3$ TeV (lower row). In the case of the Tevatron the panels show gluon-gluon fusion (red) and associated W -boson production (blue), while for the LHC the dominant channels are gluon-gluon (red) and weak gauge-boson fusion (blue). The dashed lines illustrate the SM predictions, while the solid lines indicate the results obtained in the custodial RS model. See text for details.

SM Higgs-boson production cross section, the MRST2006NNLO parton distribution functions [77] and the associated normalization $\alpha_s(m_Z) = 0.1191$ for the strong coupling constant are used. The SM predictions are depicted by red dashed lines, whereas the solid red lines correspond to the RS results. The latter predictions have been obtained by employing (163) and (164) using the fit formulas for $\kappa_{t,b}$ and $\nu_{u,d,\lambda}$ discussed before. The relevant values for $a_{t,b,u,d,\lambda}$ can be found

a_t	a_b	a_t^V
$15.08 - 0.79i$	$9.08 + 0.43i$	3.63

a_u	a_d	a_λ	$a_{\gamma Z}^u$	$a_{\gamma Z}^d$	$a_{\gamma Z}^\lambda$	$a_{\gamma Z}^W$
-38.80	-21.80	-22.58	$-46.46 - 0.02i$	17.98	-6.38	10.76

Table 3: Fit coefficients in units of v^2/M_{KK}^2 entering the various contributions to Higgs-boson production and decay. Corrections due to zero and KK modes are displayed in the upper and lower table, respectively. See text for details.

in Table 3. All four panels show clearly that the Higgs production cross sections in gluon-gluon fusion experience a significant reduction in the custodial RS model. We emphasize that the destructive interference between the SM and the KK-quark contributions to the $gg \rightarrow h$ amplitude has been conjectured in [54, 55] to be a general feature of new-physics models where new colored fermions add to the quadratic divergence of the Higgs-boson mass (which is the case in RS set-ups [24]). For the considered Higgs-boson masses, we find in the case of $M_{\text{KK}} = 2 \text{ TeV}$ ($M_{\text{KK}} = 3 \text{ TeV}$) suppressions that range between -65% and -95% (-80% and -90%) and from -45% to almost -100% (-45% to -90%) at the Tevatron and LHC, respectively (see also Figure 12). Interestingly, the found depletions survive even at $M_{\text{KK}} = 5 \text{ TeV}$, still reaching up to -40% at both colliders. Since both the theoretical accuracy [67, 68, 69, 70] and the expected experimental precision [51, 78] are at the level of 10%, such pronounced reductions in Higgs events from gluon-gluon fusion should be observable at the LHC. The non-trivial Higgs-mass dependence of the displayed RS curves results from the interplay between the RS zero- and KK-mode contributions. The real part of the zero-mode amplitude increases until the $t\bar{t}$ threshold is reached and decreases above threshold quadratically with m_h (modulo logarithmic effects). It is positive for all values of the Higgs-boson mass. On the contrary, the real part of the amplitude associated to the virtual exchange of KK quarks is negative and a constant in the heavy-mass limit. Since for $M_{\text{KK}} \lesssim 2 \text{ TeV}$ the latter contribution is always dominant, the correction arising from KK-quark triangle diagrams effectively flips the sign of the real part of the total $gg \rightarrow h$ amplitude with respect to the SM expectation for small and high Higgs masses. In the threshold region, $m_h \approx 2m_t$, the destructive interference between the individual contributions can, on the other hand, become almost perfect, leading to a strong suppression of Higgs production via gluon-gluon fusion. This feature is nicely illustrated by the upper right panel of Figure 10. Because the RS contributions decouple rapidly for increasing KK scale, a complete extinction of the sum of individual amplitudes is not possible for $M_{\text{KK}} \gtrsim 2 \text{ TeV}$. In this case, the zero-mode contribution to $gg \rightarrow h$ dominates, and the Higgs-mass dependence of the RS prediction is similar to the one of the SM result. We emphasize that in spite of the many parameters in the fermion sector of the custodial RS model, the shown results for the Higgs-boson production cross section depend to first order only on the overall KK-mass scale. This claim is supported by the narrow spread of scatter points depicted in the two panels of Figure 9.

Compared to gluon-gluon fusion, Higgs-boson production through weak gauge-boson fu-

sion, $qq^{(\prime)} \rightarrow qq^{(\prime)}V^*V^* \rightarrow qq^{(\prime)}h$ with $V = W, Z$, which is known to be extremely useful for discovery at the LHC, receives only moderate corrections of around -20% (-10%) for $M_{\text{KK}} = 2 \text{ TeV}$ ($M_{\text{KK}} = 3 \text{ TeV}$). The same reduction will affect associated W -boson production, $q\bar{q}' \rightarrow W^* \rightarrow Wh$, which is the only channel that in principle would allow for a Higgs discovery at the Tevatron. The RS predictions for the production cross section for $q\bar{q}' \rightarrow Wh$ at the Tevatron and for $qq^{(\prime)} \rightarrow qq^{(\prime)}h$ at the LHC are illustrated by the solid blue lines in the left and right panels of Figure 10, respectively. The corresponding SM predictions are taken from [79] and represented by the blue dashed lines. Finally, the cross section of associated top-quark pair production, $q\bar{q} \rightarrow t\bar{t}^* \rightarrow t\bar{t}h$, will also experience a reduction. For values of the KK scale in the ballpark of 2 TeV , this suppression can amount up to -40% . Since $qq^{(\prime)} \rightarrow qq^{(\prime)}h$, $q\bar{q}' \rightarrow Wh$, and $q\bar{q} \rightarrow t\bar{t}h$ are tree-level processes, their RS predictions have all been obtained by a simple rescaling of the corresponding SM results.

In summary, we find that the main Higgs-boson production modes at hadron colliders are suppressed in the custodial RS model relative to the SM. Suppression effects in $gg \rightarrow h$ were also reported in [37, 54, 80].¹⁸ A direct numerical comparison with our findings is however not possible, since [37] only included zero-mode corrections, while [54, 80] studied RS variants that differ from the specific set-up considered here. In [82] the authors studied corrections to gluon-gluon fusion arising from virtual exchange of light fermionic KK modes. There it has been claimed that for a heavy bottom-quark partner with a mass $m_{b'}$ of a few hundred GeV the Higgs-boson production cross section via $gg \rightarrow h$ can be significantly enhanced. We would like to point out in this context that in order to achieve $m_{b'} \ll M_{\text{KK}}$ with the embedding of quarks as chosen in (58), the P_{LR} symmetry has to be broken strongly via the bulk mass parameters of the \mathcal{T}_1 multiplets by choosing $c_{\mathcal{T}_1}$ rather far away from $c_{\mathcal{T}_2}$. While for $c_{\mathcal{T}_1} > 1/2$ it is possible to achieve $\text{Re}\nu_d > 0$ and thus an enhancement of the $gg \rightarrow h$ cross section, such choices of parameters need to be fine-tuned to reproduce the measured mass spectrum of the SM quarks for anarchic Yukawa couplings. If, on the other hand, $c_{\mathcal{T}_1} < 1/2$, we find that $\text{Re}\nu_d$ remains strictly negative, and as a result the $gg \rightarrow h$ channel experiences a reduction. We furthermore add that choices of $c_{\mathcal{T}_1}$ corresponding to a strong breaking of the P_{LR} symmetry lead, barring an accidental cancellation, to a sizable negative shift in the $Zb_L\bar{b}_L$ coupling through (120), which is problematic in view of the stringent constraints arising from the $Z \rightarrow b\bar{b}$ pseudo observables. To which extent electroweak precision measurements constrain the masses of light fermionic KK partners deserves further study.

7.5 Higgs-Boson Decay

We now move on to study the decay modes of the Higgs boson. In this context, we will consider all processes with quarks and gauge bosons in the final state that can receive important RS corrections and have a branching fraction larger than 10^{-4} . As we have not explicitly specified the embedding of the fermions in the lepton sector, we ignore decays into taus and muons. Due to the UV localization of the leptonic fields, we however expect that the decay widths of the Higgs into charged leptons are all SM-like. Furthermore, we will not include loop contributions

¹⁸See also [81] for a recent detailed analysis of Higgs-boson production cross sections and decay rates in a related context.

of KK leptons in our analysis of the $h \rightarrow \gamma\gamma$ and $h \rightarrow \gamma Z$ decay channels. We will comment on the potential impact of this omission below.

In order to be able to calculate the decay rates of the Higgs boson into massive gauge bosons, we still need to evaluate the RS corrections to the $WW h$, $ZZ h$, and $WW Z$ tree-level vertices. Due to the unbroken $U(1)_{\text{EM}}$ gauge group, the $WW\gamma$ coupling is unchanged with respect to the SM to all orders in v^2/M_{KK}^2 . The weak couplings involving the Higgs boson are derived from the cubic and quartic interactions due to (9). In unitary gauge, the relevant terms in the Lagrangian read

$$\mathcal{L}_{4\text{D}} \ni (h^2 + 2vh) \left[\frac{g_L^2}{4} (1 - \Delta g_h^W) W_\mu^+ W^{-\mu} + \frac{g_L^2 + g_Y^2}{8} (1 - \Delta g_h^Z) Z_\mu Z^\mu \right], \quad (168)$$

where

$$\Delta g_h^V = x_V^2 \left[L \left(1 + \frac{s_V^2}{c_V^2} \right) - 1 + \frac{1}{2L} \right] + \mathcal{O}(x_V^4), \quad (169)$$

and $x_V \equiv m_V/M_{\text{KK}}$ for $V = W, Z$. In the case of the P_{LR} symmetry (103), one has $s_W^2/c_W^2 = 1$ and $s_Z^2/c_Z^2 = 1 - 2s_w^2$, which implies that the leading correction due to $\Delta g_h^{W,Z}$ takes the form $-2m_W^2/M_{\text{KK}}^2 L$. For $M_{\text{KK}} = 2 \text{ TeV}$ ($M_{\text{KK}} = 3 \text{ TeV}$) these terms lead to a suppression of the $WW h$ and $ZZ h$ couplings by about -10% (-5%) compared to the SM. Notice that in the minimal RS model the expressions (169) hold in the limit $s_{W,Z} \rightarrow 0$, and consequently the corrections to the couplings of the Higgs to massive gauge bosons are smaller by about a factor of 2. Our finding that the couplings $WW h$ and $ZZ h$ experience a reduction from their SM expectations confirms the model-independent statements made in [55].

The partial decay widths $\Gamma(h \rightarrow f)$ of the Higgs boson decaying to a final state f are again obtained by rescaling the SM decay widths. We use

$$\Gamma(h \rightarrow f)_{\text{RS}} = |\kappa_f|^2 \Gamma(h \rightarrow f)_{\text{SM}}, \quad (170)$$

with

$$\kappa_W = 1 - \Delta g_h^W, \quad \kappa_Z = 1 - \Delta g_h^Z, \quad (171)$$

in the case of the decay of the Higgs boson into a pair of W and Z bosons, respectively. The relevant $\kappa_{g,t,b}$ parameters for decays into two gluons, top or bottom quarks have already been given in (164) and (165). In Figure 5 the diagrams inducing the decay into a pair of heavy quarks and massive gauge bosons are shown on the right in the top row. Apart from the change in the $ht\bar{t}$ coupling, we neglect RS corrections to the three-body decay $h \rightarrow t\bar{t}^*(WW^*) \rightarrow tbW$, which relative to the two-body mode $h \rightarrow t\bar{t}$ amounts to a correction of (far below) 1% in the SM. Given the smallness of this effect, the omission of possible new-physics effects in the Wtb coupling that would affect the $h \rightarrow tbW$ channel is for all practical purposes irrelevant.

In the case of the final state with two photons, we employ

$$\kappa_\gamma = \frac{\sum_{i=t,b} N_c Q_i^2 \kappa_i A_q^h(\tau_i) + \kappa_W A_W^h(\tau_W) + \sum_{j=u,d,\lambda} N_c Q_j^2 \nu_j + \nu_\gamma^W}{\sum_{i=t,b} N_c Q_i^2 A_q^h(\tau_i) + A_W^h(\tau_W)}, \quad (172)$$

in (170), where $N_c = 3$, $Q_{t,u} = 2/3$, $Q_{b,d} = -1/3$, $Q_\lambda = 5/3$, $\tau_W \equiv 4m_W^2/m_h^2$, and the explicit expression for the form factor $A_W^h(\tau_W)$, encoding the W -boson contribution, can be found in Appendix C. The first, second, and third terms in the numerator describe the effects of virtual heavy-quark, W -boson, and KK-quark exchange, respectively. The corresponding one-loop graphs are shown on the left in the bottom row of Figure 5 and in the center plot of Figure 6. The amplitude $A_W^h(\tau_W)$ interferes destructively with the quark contribution $A_q^h(\tau_i)$, falling from $-21/4$ for $\tau_W \rightarrow \infty$ to $-15/4 - 9\pi^2/16$ at the WW threshold $\tau_W = 1$ and finally approaching $-3/2$ in the limit $\tau_W \rightarrow 0$. Comparing these numbers with the ones for $A_q^h(\tau_i)$ quoted earlier, one observes that within the SM the W -boson contribution to the $h \rightarrow \gamma\gamma$ decay amplitude is always dominant below threshold.

We emphasize that in (172) contributions from leptonic KK modes are not included. While the precise impact of these effects depends on the exact realization of the lepton sector (which we have not specified), it is possible to predict their relative sign as well as estimate their size. Generalizing the result (172) to include contributions from triangle diagrams with KK leptons only requires to perform the replacement

$$\sum_{j=u,d,\lambda} N_c Q_j^2 \nu_j \rightarrow \sum_{j=u,d,\lambda} N_c Q_j^2 \nu_j + Q_l^2 \nu_l = \frac{4\nu_u}{3} + \frac{\nu_d}{3} + \frac{25\nu_\lambda}{3} + \nu_l, \quad (173)$$

where $\nu_u \approx 2\nu_d \approx 2\nu_\lambda$ and the parameter ν_l encodes the effects due to KK-lepton loops. Under the reasonable assumption that $\nu_l \approx \nu_u/2$, we conclude from (173) that the KK lepton contribution to the $h \rightarrow \gamma\gamma$ amplitude amounts to approximately 10% of the KK quark corrections and interferes constructively with the latter. Based on this estimate we expect that an omission of KK lepton effects in the calculation of κ_γ has only a minor numerical impact on the obtained Higgs-boson branching fractions.

The quantity ν_γ^W representing the one-loop contribution of the W -boson KK modes can be calculated analytically in the decoupling limit. The corresponding Feynman diagram is displayed on the very right in Figure 6. Employing the results for the KK sums derived in Section 3.5, we obtain

$$\begin{aligned} \nu_\gamma^W &= \frac{2\pi x_W^2 (g_L^2 + g_R^2)}{g_L^2} \sum_{n=1}^{\infty} \frac{\vec{d}_W^T \vec{\chi}_n^W(1) \vec{\chi}_n^{WT}(1) \vec{d}_W}{(x_n^W)^2} A_W^h(\tau_n^W) \\ &= \frac{2\pi x_W^2 (g_L^2 + g_R^2)}{g_L^2} \vec{d}_W^T [\Sigma_W(1, 1) - \Pi_W(1, 1)] \vec{d}_W \left(-\frac{21}{4} + \mathcal{O}(1/\tau_n^W) \right) \\ &= -\frac{21}{8} \Delta g_h^W (1 + \mathcal{O}(1/\tau_n^W)), \end{aligned} \quad (174)$$

where $\vec{d}_W = (c_W, -s_W)^T$ and $\tau_n^W \equiv 4(m_n^W)^2/m_h^2$. Since already $m_1^W \approx 2.5M_{\text{KK}} \gg m_h$, the terms suppressed by powers of τ_n^W in (174) can be ignored in practice. The result for Δg_h^W can be found in (169).

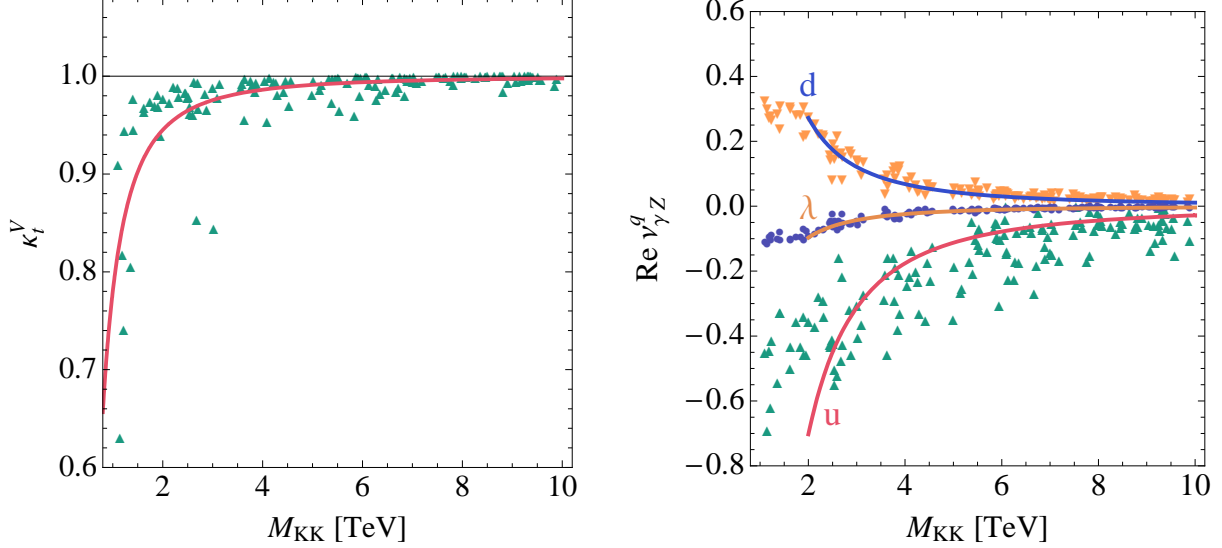


Figure 11: Predictions for the vector couplings of the Z boson to top and bottom quarks (left) and for the various types of KK-quark contributions to the effective $h\gamma Z$ coupling (right) in the custodial RS model. The solid lines show fits to the scatter points. See text for details.

In order to compute the last missing decay channel, namely $h \rightarrow \gamma Z$, we use

$$\kappa_{\gamma Z} = \frac{\sum_{i=t,b} N_c \frac{2Q_i v_i}{c_w} \kappa_i \kappa_i^V A_q^h(\tau_i, \lambda_i) + \kappa_W A_W^h(\tau_W, \lambda_W) + \sum_{j=u,d,\lambda} N_c \frac{2Q_j v_j}{c_w} \nu_{\gamma Z}^j + \nu_{\gamma Z}^W}{\sum_{i=t,b} N_c \frac{2Q_i v_i}{c_w} A_q^h(\tau_i, \lambda_i) + A_W^h(\tau_W, \lambda_W)}, \quad (175)$$

in (170). Here $v_i \equiv T_L^{3i} - 2s_w^2 Q_i$, and $\lambda_i \equiv 4m_i^2/m_Z^2$ for $i = t, b, W$. The amplitudes $A_{q,W}^h(\tau_i, \lambda_i)$ encoding the effects of virtual quarks and W bosons in $h \rightarrow \gamma Z$ are collected in Appendix C. The corresponding Feynman diagrams are shown on the right in the bottom row of Figure 5. Like in the case of $h \rightarrow \gamma\gamma$, the SM decay rate for $h \rightarrow \gamma Z$ is in large parts of the parameter space dominated by the W -boson loop contribution. One has $A_q^h(\tau_i, \lambda_i) = -1/3$ for $\tau_i, \lambda_i \rightarrow \infty$ and $A_q^h(\tau_i, \lambda_i) = 0$ for $\tau_i, \lambda_i \rightarrow 0$. On the other hand, the function $A_W^h(\tau_W, \lambda_W)$ rises from around 4.6 to 9.8 between $\tau_W \rightarrow \infty$ and $\tau_W = 1$, and then falls to approximately 0.6 in the limit $\tau_W \rightarrow 0$.

The first term in the numerator of (175) depends on the ratios

$$\kappa_t^V = \frac{(g_L^u)_{33} + (g_R^u)_{33}}{v_t}, \quad \kappa_b^V = \frac{(g_L^d)_{33} + (g_R^d)_{33}}{v_b}, \quad (176)$$

which quantify the relative shift in the vector coupling of the Z boson to top and bottom quarks. In the left panel of Figure 11 we show the predictions for κ_t^V versus M_{KK} for 150 randomly chosen model parameter points. It is evident from the plot that the vector coupling of the Z boson to top quarks is always reduced in the custodial RS model relative to the SM.

Numerically, the suppression amounts to a moderate effect of -5% (-2.5%) for $M_{\text{KK}} = 2 \text{ TeV}$ ($M_{\text{KK}} = 3 \text{ TeV}$). In contrast, the Z -boson coupling to bottom-quark pairs is larger than its SM value, but numerically the resulting effects turn out to be negligibly small due to the custodial protection mechanism. Consequently, we will set κ_b^V to 1 in our numerical analysis. Parameterizing the average value of the relative shift κ_t^V by $(1 - a_t^V v^2/M_{\text{KK}}^2)$ the coefficient a_t^V can again be determined through a fit. Employing the shown set of parameter points, we obtain the value for a_t^V given in Table 3.

The second term in the numerator of (175) encodes the contribution to the $h \rightarrow \gamma Z$ transition arising from the W -boson triangle graph. The calculation of this zero-mode contribution is greatly simplified by the following two observations. First, one has

$$\frac{2\pi}{L} \int_{\epsilon}^1 \frac{dt}{t} \chi_0^{(+)}(t) = \sqrt{2\pi} + \mathcal{O}\left(\frac{v^4}{M_{\text{KK}}^4}\right), \quad (177)$$

and second $[(\vec{A}_0^a)_2 \chi_0^{(-)}(t)]^2 = \mathcal{O}(v^4/M_{\text{KK}}^4)$. The expressions for $\chi_0^{(\pm)}(t)$ and \vec{A}_0^a necessary to derive these results can be found in (44) and (45). In combination these two relations imply that the triple gauge-boson vertex involving two W - and one Z -boson fields does not receive corrections at $\mathcal{O}(v^2/M_{\text{KK}}^2)$ in the RS model, regardless of the specific gauge group. By the same line of reasoning, it is also readily seen that all quartic gauge-boson vertices first differ at order v^4/M_{KK}^4 from the corresponding SM expressions. In view of this extra suppression, we will set the triple gauge-boson couplings of the zero modes to their SM values when evaluating the Higgs-boson branching fractions. In this approximation the effect of virtual W -boson exchange to (175) is simply given by the combination $\kappa_W A_W^h(\tau_W, \lambda_W)$, which up to the different form factor resembles the form of the corresponding term in (172).

The third term in the numerator of (175) describes the contribution to the $h \rightarrow \gamma Z$ amplitude stemming from the virtual exchange of KK quarks. The corresponding one-loop diagram is displayed in the middle of Figure 6. In the up-type quark sector we find

$$\begin{aligned} \nu_{\gamma Z}^u &= v \sum_{n=4}^{\infty} \frac{(g_h^u)_{nn}}{m_n^u} \kappa_n^{u,V} A_q^h(\tau_n^u, \lambda_n^u) \\ &= \frac{2\pi}{\epsilon L} \sum_{n=4}^{\infty} \frac{\vec{a}_n^{U\dagger} \mathbf{C}_n^U(\pi^-) \left(\mathbf{1} - \frac{v^2}{3 M_{\text{KK}}^2} \tilde{\mathbf{Y}}_{\vec{u}} \tilde{\mathbf{Y}}_{\vec{u}}^\dagger \right) \mathbf{S}_n^U(\pi^-) \vec{a}_n^U}{x_n^u} \kappa_n^{u,V} A_q^h(\tau_n^u, \lambda_n^u), \end{aligned} \quad (178)$$

where $\kappa_n^{u,V}$ denotes the relative strength of vector coupling of the Z boson to the n^{th} up-type quark KK mode defined in analogy to (176), and $\lambda_n^u \equiv 4(m_n^u)^2/m_Z^2$. Analog expressions apply in the case of down- and λ -type quark KK modes. Since an analytic calculation of (178) turns out to be impractical, we resort to a numerical evaluation of the KK sum employing the method described in Section 7.4. The predictions for the real parts of $\nu_{\gamma Z}^u$, $\nu_{\gamma Z}^d$, and $\nu_{\gamma Z}^\lambda$ corresponding to a set of 150 random model parameter points are depicted in the right panel of Figure 11. The solid lines displayed there indicate the best fit of the form $a_{\gamma Z}^{u,d,\lambda} v^2/M_{\text{KK}}^2$ to the sample of points with KK scales in the range $[2, 10] \text{ TeV}$. As before, points with $M_{\text{KK}} < 2 \text{ TeV}$ have been excluded in the fit, since they are subject to significant higher-order corrections.

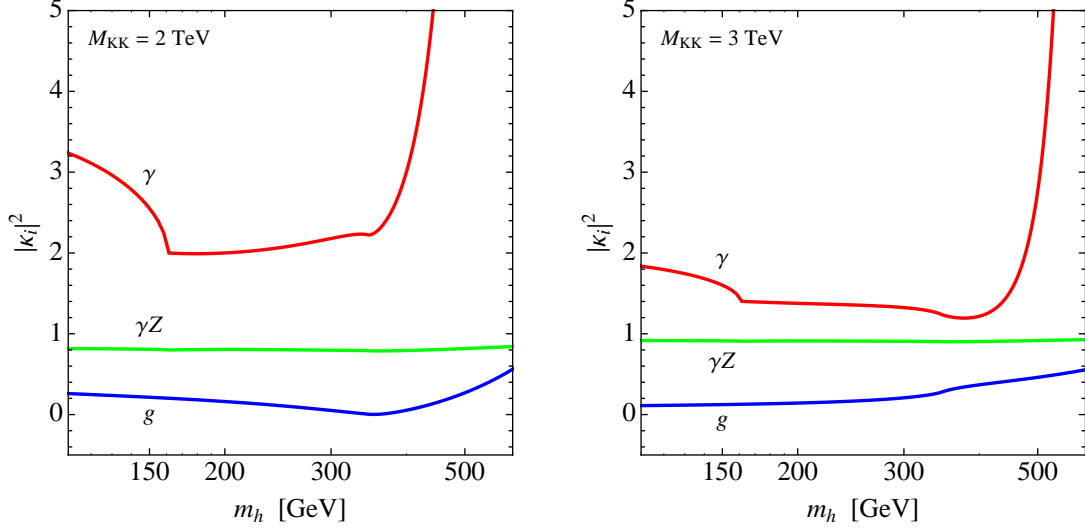


Figure 12: Relative corrections $|\kappa_g|^2$ (blue line), $|\kappa_\gamma|^2$ (red line), and $|\kappa_{\gamma Z}|^2$ (green line) as functions of the Higgs-boson mass, employing $M_{\text{KK}} = 2 \text{ TeV}$ (left panel) and $M_{\text{KK}} = 3 \text{ TeV}$ (right panel). See text for details.

The corresponding coefficients $a_{\gamma Z}^{u,d,\lambda}$ can be found in Table 3. The average values of the real parts of $\nu_{\gamma Z}^u$, $\nu_{\gamma Z}^d$, and $\nu_{\gamma Z}^\lambda$ obtained from the fit formulas are -0.70 (-0.31), 0.27 (0.12), and -0.10 (-0.04) for $M_{\text{KK}} = 2 \text{ TeV}$ ($M_{\text{KK}} = 3 \text{ TeV}$), respectively. The imaginary parts $\text{Im} \nu_{\gamma Z}^{u,d,\lambda}$ turn out to be tiny. The reason for this feature has already been discussed in Section 7.4.

Contributions from KK-lepton triangle graphs have again not been incorporated in (175). Denoting these corrections by $\nu_{\gamma Z}^l$, they can be included via the simple replacement

$$\sum_{j=u,d,\lambda} N_c \frac{2Q_j v_j}{c_w} \nu_{\gamma Z}^j \rightarrow \sum_{j=u,d,\lambda} N_c \frac{2Q_j v_j}{c_w} \nu_{\gamma Z}^j + \frac{2Q_l v_l}{c_w} \nu_{\gamma Z}^l. \quad (179)$$

In order to estimate the typical size of $\nu_{\gamma Z}^l$ we need an analytic formula for the relative strength of the vector coupling between the Z boson and fermionic KK modes appearing in (178). We find

$$\kappa_n^{f,V} = 1 - \frac{(\delta_F)_{nn} - (\delta_f)_{nn}}{v_f} + \mathcal{O}\left(\frac{m_Z^2}{M_{\text{KK}}^2}\right), \quad (180)$$

where the expressions for $\delta_{F,f}$ can be found in (108). In the case of extended P_{LR} symmetry (122), it turns out that for down- and λ -type KK quarks the result for $\kappa_n^{f,V}$ can be expressed in terms of the electric charge and the third component of the weak isospin of the involved fermion, while no such formula can be derived for up-type quark KK modes. We obtain to excellent approximation ($f = d, \lambda$)

$$\kappa_n^{f,V} = 1 + \frac{T_L^{3fL}}{v_f}, \quad (181)$$

which implies that all down-type (λ -type) KK-quark modes couple with universal strength to the vector part of the Z -boson coupling. It follows that in the decoupling limit, $\tau_n^f, \lambda_n^f \rightarrow \infty$, one has

$$\left(1 + \frac{T_L^{3fL}}{v_f}\right) \frac{A_f^h(\tau_n^f, \lambda_n^f)}{A_f^h(\tau_n^f)} = \frac{a_{\gamma Z}^f}{a_f}. \quad (182)$$

From the numbers of the fit coefficients given in Table 3, we see that this relation is satisfied to an accuracy of around 1%. The KK-fermion effects in the down- and λ -type quark sectors that contribute to $h \rightarrow gg, \gamma\gamma$, and γZ are thus universal, in the sense that they can be simply obtained from each other by an appropriate replacement of the vector couplings of the external fields.

Making now the plausible assumption that in the decoupling limit the sums $\nu_{\gamma Z}^d$ and $\nu_{\gamma Z}^l$ differ only by the presence of the vector couplings $\kappa_n^{d,V}$ and $\kappa_n^{l,V}$, we obtain the following estimate for the contribution to (179) from leptonic relative to down-type quark KK modes:

$$\frac{Q_l v_l \nu_{\gamma Z}^l}{N_c Q_d v_d \nu_{\gamma Z}^d} \approx \frac{Q_l v_l \kappa_n^{l,V}}{N_c Q_d v_d \kappa_n^{d,V}} = \frac{3 - 6s_w^2}{3 - 2s_w^2} \approx 0.64. \quad (183)$$

As a result, the sum (179) can be approximated as

$$\sum_{j=u,d,\lambda} N_c \frac{2Q_j v_j}{c_w} \nu_{\gamma Z}^j + \frac{2Q_l v_l}{c_w} \nu_{\gamma Z}^l \approx 0.88 \nu_{\gamma Z}^u + 0.79 \nu_{\gamma Z}^d - 3.04 \nu_{\gamma Z}^\lambda + 0.50 \nu_{\gamma Z}^d, \quad (184)$$

where the last term on the right-hand side encodes the effects due to KK leptons, and in order to obtain the numerical values we have inserted the relevant electroweak quantum numbers and used $s_w^2 \approx 0.23$. For $M_{\text{KK}} = 2 \text{ TeV}$, the real part of the relation (184) evaluates to -0.11 (0.03) if effects due to KK leptons are excluded (included). While these numbers imply that an omission of KK lepton effects can change the numerical value of the KK fermion contribution notably, it is not difficult to see that the impact on (175) itself is limited, since the coefficient $\kappa_{\gamma Z}$ is dominated by the W -boson triangle contribution. We thus conclude that the absence of KK-lepton contributions in our prediction for $h \rightarrow \gamma Z$ (which is anyhow difficult to study at the LHC) will not change any of the conclusions drawn below.

The coefficient $\nu_{\gamma Z}^W$ in (175) incorporates the effects in $h \rightarrow \gamma Z$ due to charged KK-boson excitations in the loop. The associated Feynman graph is displayed on the very right in Figure 6. This contribution can be written as

$$\nu_{\gamma Z}^W = \frac{2\pi x_W^2 (g_L^2 + g_R^2)}{g_L^2} \sum_{n=1}^{\infty} \frac{\vec{d}_W^T \vec{\chi}_n^W(1) \vec{\chi}_n^{WT}(1) \vec{d}_W}{(x_n^W)^2} \mathcal{I}_{nn0}^{WWZ} A_W^h(\tau_n^W, \lambda_n^W), \quad (185)$$

with

$$\begin{aligned} \mathcal{I}_{nn0}^{WWZ} = & \frac{(2\pi)^{3/2}}{L} \int_{\epsilon}^1 \frac{dt}{t} \left[\chi_0^{(+Z)}(\vec{A}_0^Z)_1 \left(\chi_n^{(+W)^2}(\vec{A}_n^W)_1^2 + \frac{g_Y^2}{g_L^2} \chi_n^{(-W)^2}(\vec{A}_n^W)_2^2 \right) \right. \\ & \left. - \sqrt{1 - g_Y^4/g_L^4} \chi_0^{(-Z)}(\vec{A}_0^Z)_2 \chi_n^{(-W)^2}(\vec{A}_n^W)_2^2 \right], \end{aligned} \quad (186)$$

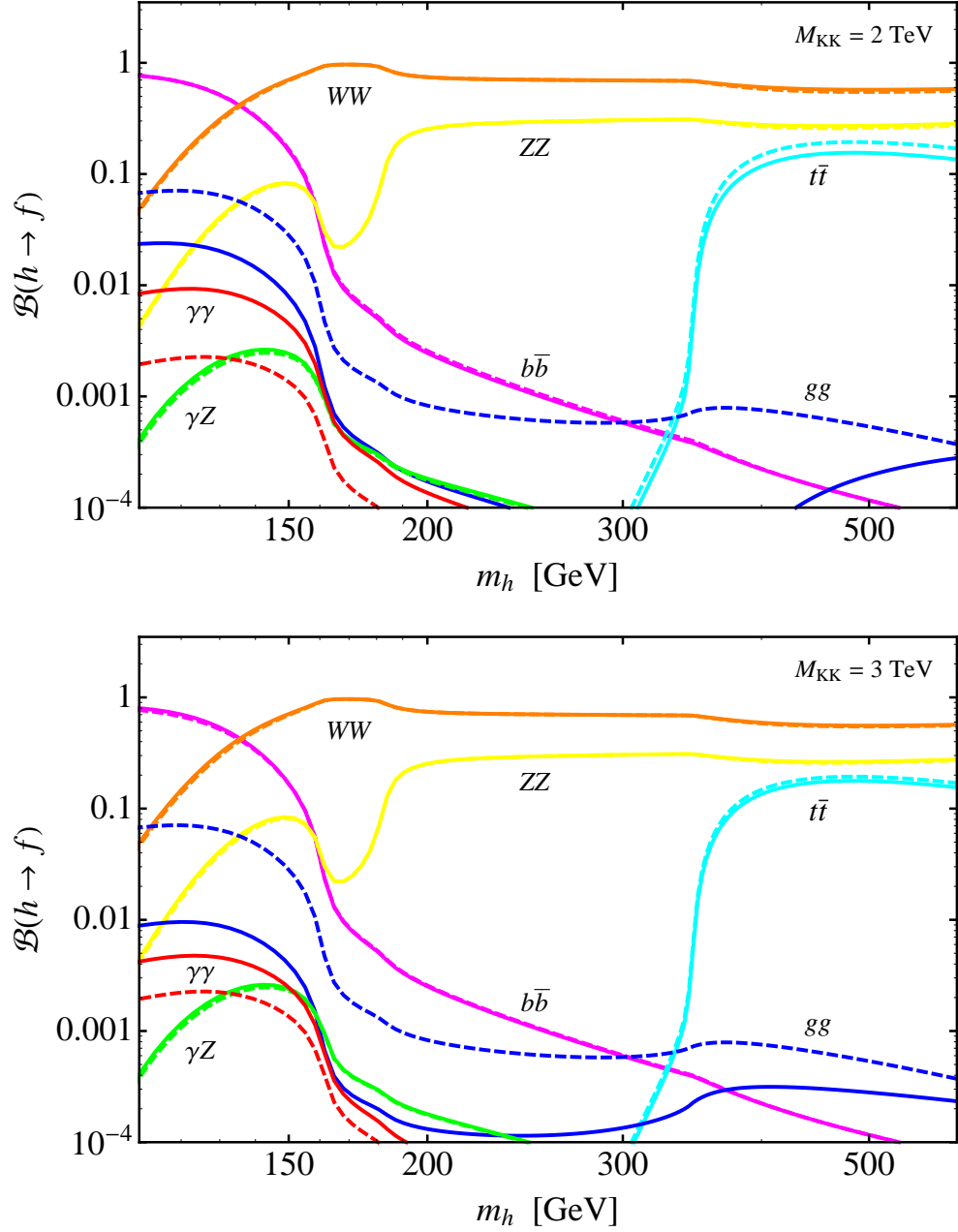


Figure 13: Branching ratios for $h \rightarrow f$ as functions of the Higgs-boson mass for $M_{\text{KK}} = 2 \text{ TeV}$ (upper panel) and $M_{\text{KK}} = 3 \text{ TeV}$ (lower panel). The dashed lines indicate the SM predictions, while the solid lines show the corresponding RS expectations. Branching fractions of less than 10^{-4} and decay channels into final states with muon, tau, charm-, and strange-quark pairs, which are all expected to remain SM-like, are not shown. See text for details.

and $\lambda_n^W \equiv 4(m_n^W)^2/m_Z^2$. Notice that the prefactor in the second line of the above formula corresponds to the choice $g_L = g_R$. Since the first term in the sum of (185) is already suppressed by a factor of v^2/M_{KK}^2 , the computation of $\nu_{\gamma Z}^W$ to this order only requires the knowledge of the overlap integral (186) to zeroth order in the ratio of the weak over the KK scale. We obtain

$$\mathcal{I}_{nn0}^{WWZ} = \frac{2\pi}{L} \int_{\epsilon}^1 \frac{dt}{t} \left(\chi_n^{(+)\text{W}2} (\bar{A}_n^W)_1^2 + \frac{g_Y^2}{g_L^2} \chi_n^{(-)\text{W}2} (\bar{A}_n^W)_2^2 \right) + \mathcal{O}\left(\frac{v^2}{M_{\text{KK}}^2}\right). \quad (187)$$

It is again an excellent approximation to evaluate the loop function $A_W^h(\tau_n^W, \lambda_n^W)$ in the infinite mass limit $\tau_n^W, \lambda_n^W \rightarrow \infty$, in which the form factor approaches $31 c_w/6 - 11 s_w^2/(6 c_w) \approx 4.0$. We perform the sum in (185) numerically, including sufficiently many KK levels until the series converges. In this way, we find $\nu_{\gamma Z}^W = 0.16$ ($\nu_{\gamma Z}^W = 0.07$) for $M_{\text{KK}} = 2 \text{ TeV}$ ($M_{\text{KK}} = 3 \text{ TeV}$). Values for $\nu_{\gamma Z}^W$ corresponding to different KK scales can be obtained by means of the fit formula $a_{\gamma Z}^W v^2/M_{\text{KK}}^2$ with the coefficient $a_{\gamma Z}^W$ given in Table 3.

In the two panels of Figure 12 we display the relative corrections $|\kappa_g|^2$, $|\kappa_\gamma|^2$, and $|\kappa_{\gamma Z}|^2$ for $M_{\text{KK}} = 2 \text{ TeV}$ (left) and $M_{\text{KK}} = 3 \text{ TeV}$ (right). The depicted curves represent the RS results obtained from (169) and (174) as well as the relevant fit formulas with the values of the coefficients collected in Table 3. While the behavior of $|\kappa_g|^2$ has already been explained in Section 7.4, we see that $|\kappa_{\gamma Z}|^2$ is close to 1 and independent of the value of the Higgs-boson mass. This implies that the partial decay width $\Gamma(h \rightarrow \gamma Z)$ in the custodial RS model is essentially unchanged with respect to the SM. The relative correction $|\kappa_\gamma|^2$ is, on the other hand, a non-trivial function of m_h . Below the WW threshold, the W -boson amplitude dominates the SM $h \rightarrow \gamma\gamma$ decay rate and the contributions due to KK quarks and W bosons both interfere constructively with the SM gauge-boson triangle graph. For $m_h = 130 \text{ GeV}$, the new-physics contributions amount to around 70% (30%) of the total SM amplitude for $M_{\text{KK}} = 2 \text{ TeV}$ ($M_{\text{KK}} = 3 \text{ TeV}$), resulting in values $|\kappa_\gamma|^2 \approx 3$ ($|\kappa_\gamma|^2 \approx 1.7$). For $m_h \gtrsim 160 \text{ GeV}$, the Higgs-mass dependence of the SM amplitude becomes less pronounced and the RS prediction stays almost constant. The strong rise of $|\kappa_\gamma|^2$, visible at higher values of the Higgs mass, results from the fact that for $m_h \approx 650 \text{ GeV}$ the top-quark loop nearly cancels the W -boson contribution in the SM. In consequence, for $m_h \gtrsim 500 \text{ GeV}$ the partial width $\Gamma(h \rightarrow \gamma\gamma)$ is almost entirely due to loops involving heavy KK modes, with the contribution from KK quarks being the dominant correction.

The various Higgs-boson branching ratios obtained using the above results are shown in Figure 13. The dashed lines illustrate the SM expectations calculated with the help of HDECAY [83],¹⁹ while the solid lines represent the RS predictions based on the results for $\kappa_{t,b,W,Z}$ quoted above and the curves for $|\kappa_{g,\gamma,\gamma Z}|^2$ displayed in Figure 12. It is evident that in the custodial RS model the branching ratios $h \rightarrow b\bar{b}$, $h \rightarrow WW$, and $h \rightarrow ZZ$ receive only insignificant corrections, not exceeding the level of $\pm 5\%$. For $m_h \gtrsim 180 \text{ GeV}$ the experimentally cleanest signature for the discovery of the Higgs boson at the LHC is its “golden” decay to four leptons, $h \rightarrow Z^{(*)}Z^{(*)} \rightarrow l^+l^-l^+l^-$. Since the $h \rightarrow ZZ$ branching fraction is essential SM-like, the reduction in the $gg \rightarrow h$ production cross section will make an observation of the Higgs boson in the golden channel more difficult. Moderate effects occur in the non-discovery channels $h \rightarrow \gamma Z$ and $h \rightarrow t\bar{t}$. In the relevant ranges for the Higgs mass, the modifications in

¹⁹Expect for the parameters listed in Appendix B, the original input file of HDECAY version 3.51 is used.

the branching ratios amount to around +10% (+10%) and -25% (-10%) for $M_{\text{KK}} = 2 \text{ TeV}$ ($M_{\text{KK}} = 3 \text{ TeV}$). The most pronounced effects are found for $h \rightarrow gg$ and $h \rightarrow \gamma\gamma$. For Higgs masses below the WW threshold, the branching fraction of the former mode is reduced by a factor of almost 4 (8), while the branching ratio of the latter transition is enhanced by a factor of around 4 (2). The corresponding maximal values of $\mathcal{B}(h \rightarrow \gamma\gamma)$ are $9.3 \cdot 10^{-3}$ ($4.8 \cdot 10^{-3}$) for $M_{\text{KK}} = 2 \text{ TeV}$ ($M_{\text{KK}} = 3 \text{ TeV}$) and arise at $m_h \approx 120 \text{ GeV}$. Calculating the rescaling factor $\varkappa = (\sigma_{\text{RS}}(gg \rightarrow h) \mathcal{B}(h \rightarrow \gamma\gamma)_{\text{RS}}) / (\sigma_{\text{SM}}(gg \rightarrow h) \mathcal{B}(h \rightarrow \gamma\gamma)_{\text{SM}})$ for $\sqrt{s} = 10 \text{ TeV}$ and the quoted maximal branching fractions, we obtain the values 1.03 (0.24). These numbers suggest that the statistical significance for a LHC discovery of the Higgs boson in $h \rightarrow \gamma\gamma$ can be enhanced in the custodial RS model for low KK scales. A detailed study of how the deviations found in the RS framework affect the searches for the Higgs boson at the LHC will be presented elsewhere. We add that if the KK scale is lowered to 1 TeV, the branching ratio of $h \rightarrow tc$ can reach values above 10^{-4} for Higgs masses above $m_h \approx 180 \text{ GeV}$.²⁰ For such a low KK scale, also the decay channel $h \rightarrow bs$ can open up below the WW threshold, but typically stays below the level of 10^{-3} . Note that our results for the Higgs-boson branching fractions depend primarily on the value of the KK scale, and are rather insensitive to the other free parameters present in the model. For example, the final results do not strongly depend on the precise localization pattern of the fermionic bulk fields. We also verified that the omission of KK-lepton effects does not have a pronounced effect. RS predictions for the various branching fractions of the Higgs boson have been presented previously in [37]. Yet a direct comparison with our results is difficult, as the latter work only includes RS corrections affecting the tree-level couplings of the Higgs boson to fermions.

8 Conclusions

We have performed a thorough analysis of the structure of tree-level effects in the RS model with enlarged bulk gauge symmetry $SU(2)_L \times SU(2)_R \times U(1)_X \times P_{LR}$ and an IR brane-localized Higgs sector. In contrast to the existing literature, where the Yukawa couplings have always been treated as a perturbation, we have performed the KK decomposition of the gauge fields in a covariant R_ξ gauge within the basis of mass eigenstates, by constructing the exact solutions to the bulk equations of motion augmented with appropriate boundary conditions. The KK decomposition in the matter sector has been performed employing the same formalism and including the mixing of fermionic fields between different representations and generations in a completely general way. By expanding the exact results, we have derived simple analytic expressions for the profiles and masses of the various SM particles as well as for the sums over KK towers of gauge bosons, which include all terms up to second order in the ratio of the Higgs vacuum expectation value v over the KK mass scale M_{KK} .

We have demonstrated that our exact approach is not only more elegant, but also offers some distinct advantages over treating the couplings of the bulk fields to the Higgs sector perturbatively. By expanding the low-energy spectrum as well as the gauge couplings in powers of

²⁰In the limit of vanishing charm-quark mass, $r_c = 0$, the corresponding decay rate is simply obtained from (162) by multiplying the branching fraction for $t \rightarrow ch$ with $g^2(1 - r_W^2)^2(1 + 2r_W^2)/(2r_W^2) m_h/(16\pi)$ and replacing r_h through r_t . Of course, an analogous formula applies in the case of $h \rightarrow bs$.

v^2/M_{KK}^2 , we have obtained analytic formulas which allow not only for a numerical treatment, but for a transparent and explicit understanding of the model-specific protection mechanisms of the Peskin-Takeuchi parameter T and the left-handed Z -boson vertices involving down-type quarks. In the case of the gauge-boson corrections to the $Zd_L^i\bar{d}_L^j$ couplings, we have pointed out all terms that escape the custodial protection and identified them with the irreducible sources of P_{LR} -symmetry breaking, originating from the different boundary conditions of untwisted and twisted gauge-boson profiles on the UV brane. Unlike in the perturbative approach, which in general requires diagonalizing high-dimensional matrices numerically, the interpretation of our results in physical terms is thus very clear. By making the dependence on the implementation of the matter sector explicit, we were also able to address the important question about the model-dependence of the resulting gauge-boson interactions with SM fermions. We have shown in this context, that the P_{LR} symmetry is explicitly broken by the bulk mass parameters of the Z_2 -odd $SU(2)_L$ singlet fields if their values differ from the ones of their Z_2 -even counterparts. Turning our attention to the charged-current interactions, we have then demonstrated that a custodial protection is not at work in this case. We have finally revisited the issue of the flavor-misalignment between fermion zero-mode masses and Yukawa couplings, extending existing analyses of the structure of the flavor-changing Higgs-boson couplings to the case of the RS scenario with custodial protection.

Subsequently we have considered some simple applications of our general results. A thorough discussion of the constraints imposed by the precision measurements of the bottom-quark pseudo observables opened our phenomenological survey. We found that, contrary to the minimal case, the prediction for the correction to the $Zb_L\bar{b}_L$ vertex in the RS model with extended P_{LR} symmetry is essentially independent of the left-handed bulk mass parameter of the third-generation quarks. This feature relaxes the bounds that originate from the precision measurements of the left-handed Z -boson coupling significantly, giving a strong motivation to protect the latter vertex through a suitable embedding of the bottom quarks. We have furthermore pointed out that, irrespectively of the bulk gauge group and barring an unnatural large value of the bulk mass parameter of the right-handed top quark, the requirement to obtain the correct top- and bottom-quark masses excludes large corrections to the $Zb_R\bar{b}_R$ coupling. A direct explanation of the anomaly in the forward-backward asymmetry for bottom quarks seems therefore generically challenging in warped extra-dimension models in which the left-handed bottom and top quark are part of the same multiplet. Allowing for a heavy Higgs boson with a mass in the ballpark of 0.5 TeV (which is the naturally expected mass range for m_h in models with a brane-localized Higgs sector) leads however to a good agreement between $Z \rightarrow b\bar{b}$ data and theory. Yet, a heavy Higgs boson would need tuning in models with custodial symmetry, since the shifts induced by $m_h = 0.5$ TeV in the parameters S and T cannot be compensated by RS tree-level effects, and thus would require the presence of sizable oblique loop corrections in order not to spoil the global electroweak fit. Detailed numerical analyses of the new-physics effects in rare top-quark decays as well as of the changes in the production cross section and branching fractions of the Higgs boson completed our phenomenological investigations. In the former case, we found that due to the protection of the $Zb_L\bar{b}_L$ vertex, the experimental prospects for observing $t \rightarrow cZ$ and $t \rightarrow ch$ are more favorable in the extended than in the minimal RS scenario. In particular, for KK gauge-boson masses below 5 TeV the branching fractions of both $t \rightarrow cZ$ and $t \rightarrow ch$ can be within the reach of the LHC. In

the latter case, our study revealed that due to the composite nature of the Higgs boson, the top quark, and the KK modes, observable effects in Higgs physics can naturally occur in the scenario under consideration. In order to arrive at this conclusion, we have performed the first complete one-loop calculation of all Higgs-boson production and decay channels relevant at hadron colliders, incorporating all effects stemming from the extended electroweak gauge boson and fermion sectors. Concerning the main Higgs-boson production modes at the Tevatron and the LHC, proceeding through $gg \rightarrow h$, $q\bar{q}' \rightarrow Wh$, and $qq^{(\prime)} \rightarrow qq^{(\prime)}h$, we found that they are all suppressed in the custodial RS model relative to the SM. Since the shifts in the production cross sections can exceed the combined experimental and theoretical uncertainties, the reduction in Higgs events predicted in the RS framework might be observable at the LHC. On the other hand, the reduced $gg \rightarrow h$ production cross section should make an observation of the Higgs boson with a mass above the ZZ threshold via the “golden” four-lepton channel more difficult, because the $h \rightarrow ZZ$ branching fraction remains essential SM-like in the custodial RS model. The possible enhancement of the branching ratio for $h \rightarrow \gamma\gamma$ might however lead to a higher statistical significance and a faster LHC discovery of the Higgs boson, if its mass is below the WW threshold. We emphasize that our findings concerning Higgs physics have to be considered robust predictions, since they depend rather weakly on the details of the spectrum (and thus the specific RS parameter values) once the contributions of the entire KK towers have been included.

The analytical and numerical results obtained in this article form the basis for general calculations of flavor-changing processes in the custodial RS model. A detailed phenomenological analysis of the potential new-physics effects in neutral-meson mixing and in rare decays of kaons and B mesons, including both inclusive and exclusive processes, is left for future work.

Acknowledgments

It is a pleasure to thank A. Azatov, M. Toharia, and L. Zhu for helpful correspondence concerning flavor-changing Higgs-boson couplings. We are also grateful to V. Ahrens, M. Benzke, and D. Dolce for useful discussions. The Feynman diagrams shown in this work are drawn using `FeynArts` [84]. The research of S.C. is supported by the DFG cluster of excellence “Origin and Structure of the Universe”. The research of F.G., U.H., M.N., and T.P. is supported in part by the German Federal Ministry for Education and Research grant 05H09UME (“Precision Calculations for Collider and Flavour Physics at the LHC”), and by the Research Centre “Elementary Forces and Mathematical Foundations” funded by the Excellence Initiative of the State of Rhineland-Palatinate. U.H. thanks the Galileo Galilei Institute for Theoretical Physics for the hospitality and the INFN for partial support during the final stage of this work.

A IR BCs and Higgs-Boson FCNCs

In this appendix we rederive (78) and (140) to (144), using the rectangular function

$$\delta^\eta(t-1) = \begin{cases} \frac{1}{\eta}, & t \in [1-\eta, 1], \\ 0, & \text{otherwise,} \end{cases} \quad (\text{A1})$$

to regularize the δ -functions appearing in the EOMs (69).

Keeping only terms relevant in the range $t \in [1-\eta, 1]$, the EOMs (69) close to the IR brane take the simpler form

$$\begin{aligned} -\partial_t \mathbf{S}_n^Q(t) \vec{a}_n^Q &= \delta^\eta(t-1) \frac{v}{\sqrt{2}M_{\text{KK}}} \mathbf{Y}_{\bar{q}} \mathbf{C}_n^q(t) \vec{a}_n^q, \\ \partial_t \mathbf{S}_n^q(t) \vec{a}_n^q &= \delta^\eta(t-1) \frac{v}{\sqrt{2}M_{\text{KK}}} \mathbf{Y}_{\bar{q}}^\dagger \mathbf{C}_n^Q(t) \vec{a}_n^Q, \\ \partial_t \mathbf{C}_n^Q(t) \vec{a}_n^Q &= \delta^\eta(t-1) \frac{v}{\sqrt{2}M_{\text{KK}}} \mathbf{Y}_{\bar{q}} \mathbf{S}_n^q(t) \vec{a}_n^q, \\ -\partial_t \mathbf{C}_n^q(t) \vec{a}_n^q &= \delta^\eta(t-1) \frac{v}{\sqrt{2}M_{\text{KK}}} \mathbf{Y}_{\bar{q}}^\dagger \mathbf{S}_n^Q(t) \vec{a}_n^Q. \end{aligned} \quad (\text{A2})$$

Combining the first (second) with the fourth (third) relation and using (A1), we obtain

$$\left[\partial_t^2 - \left(\frac{\mathbf{X}_{\bar{q}}}{\eta} \right)^2 \right] \mathbf{S}_n^Q(t) = 0, \quad \left[\partial_t^2 - \left(\frac{\tilde{\mathbf{X}}_{\bar{q}}}{\eta} \right)^2 \right] \mathbf{S}_n^q(t) = 0, \quad (\text{A3})$$

where

$$\mathbf{X}_{\bar{q}} \equiv \frac{v}{\sqrt{2}M_{\text{KK}}} \sqrt{\mathbf{Y}_{\bar{q}} \mathbf{Y}_{\bar{q}}^\dagger}, \quad \tilde{\mathbf{X}}_{\bar{q}} \equiv \frac{v}{\sqrt{2}M_{\text{KK}}} \sqrt{\mathbf{Y}_{\bar{q}}^\dagger \mathbf{Y}_{\bar{q}}}. \quad (\text{A4})$$

Imposing now the BCs $\mathbf{S}_n^{Q,q}(1) = 0$ and matching $\mathbf{S}_n^{Q,q}(1-\eta)$ onto the solutions of (69) evaluated in the limit $t \rightarrow 1^-$, we find that the differential equations (A3) are solved by

$$\mathbf{S}_n^Q(t) = \frac{\sinh\left(\frac{\mathbf{X}_{\bar{q}}}{\eta}(1-t)\right)}{\sinh(\mathbf{X}_{\bar{q}})} \mathbf{S}_n^Q(1^-), \quad \mathbf{S}_n^q(t) = \frac{\sinh\left(\frac{\tilde{\mathbf{X}}_{\bar{q}}}{\eta}(1-t)\right)}{\sinh(\tilde{\mathbf{X}}_{\bar{q}})} \mathbf{S}_n^q(1^-). \quad (\text{A5})$$

This implies that in the interval $t \in [1-\eta, 1]$ the Z_2 -even fermion profiles take the form

$$\mathbf{C}_n^Q(t) = \frac{\cosh\left(\frac{\mathbf{X}_{\bar{q}}}{\eta}(1-t)\right)}{\cosh(\mathbf{X}_{\bar{q}})} \mathbf{C}_n^Q(1^-), \quad \mathbf{C}_n^q(t) = \frac{\cosh\left(\frac{\tilde{\mathbf{X}}_{\bar{q}}}{\eta}(1-t)\right)}{\cosh(\tilde{\mathbf{X}}_{\bar{q}})} \mathbf{C}_n^q(1^-). \quad (\text{A6})$$

Reinserting the solutions (A5) and (A6) into (A2), allows us to determine the IR BCs which relate the Z_2 -even profiles with the -odd ones at $t = 1^-$. The resulting expressions read

$$\begin{aligned} \mathbf{S}_n^Q(1^-) \vec{a}_n^Q &= \frac{v}{\sqrt{2}M_{\text{KK}}} \mathbf{Y}_{\bar{q}} (\tilde{\mathbf{X}}_{\bar{q}})^{-1} \tanh(\tilde{\mathbf{X}}_{\bar{q}}) \mathbf{C}_n^q(1^-) \vec{a}_n^q, \\ -\mathbf{S}_n^q(1^-) \vec{a}_n^q &= \frac{v}{\sqrt{2}M_{\text{KK}}} \mathbf{Y}_{\bar{q}}^\dagger (\mathbf{X}_{\bar{q}})^{-1} \tanh(\mathbf{X}_{\bar{q}}) \mathbf{C}_n^Q(1^-) \vec{a}_n^Q, \end{aligned} \quad (\text{A7})$$

which, after introducing the rescaled Yukawa couplings $\tilde{\mathbf{Y}}_{\tilde{q}}$, resembles (78)

Employing the regularization (A1) for the δ -function, the flavor-changing Higgs-boson couplings (138) become

$$(\Delta\tilde{g}_h^q)_{mn} = -\sqrt{2} \frac{2\pi}{L\epsilon} \int_{1-\eta}^1 dt \frac{1}{\eta} \tilde{a}_m^{q\dagger} \mathbf{S}_m^q(t) \mathbf{Y}_{\tilde{q}}^\dagger \mathbf{S}_n^Q(t) \tilde{a}_n^Q. \quad (\text{A8})$$

Combining (A5), (A6), and (A7) and using

$$\int_{1-\eta}^1 dt \frac{1}{\eta} \sinh^2\left(\frac{\mathbf{A}}{\eta}(1-t)\right) = \frac{1}{2} \left(\sinh(2\mathbf{A})(2\mathbf{A})^{-1} - \mathbf{1} \right), \quad (\text{A9})$$

valid for any arbitrary invertible matrix \mathbf{A} , we then obtain (140) to (144).

B Reference Values for the SM Parameters

The central values and errors of the quark masses used in our analysis are

$$\begin{aligned} m_u &= (1.5 \pm 1.0) \text{ MeV}, & m_c &= (520 \pm 40) \text{ MeV}, & m_t &= (144 \pm 5) \text{ GeV}, \\ m_d &= (3.0 \pm 2.0) \text{ MeV}, & m_s &= (50 \pm 15) \text{ MeV}, & m_b &= (2.4 \pm 0.1) \text{ GeV}. \end{aligned} \quad (\text{B1})$$

They correspond to $\overline{\text{MS}}$ masses evaluated at the scale $M_{\text{KK}} = 1 \text{ TeV}$, obtained by using the low-energy values as compiled in [85]. The central values and errors of the Wolfenstein parameters are taken from [86] and read

$$\lambda = 0.2265 \pm 0.0008, \quad A = 0.807 \pm 0.018, \quad \bar{\rho} = 0.141_{-0.017}^{+0.029}, \quad \bar{\eta} = 0.343 \pm 0.016. \quad (\text{B2})$$

The central values and errors for the parameters entering our analysis of the bottom-quark pseudo observables are [44, 48]

$$\begin{aligned} \Delta\alpha_{\text{had}}^{(5)}(m_Z) &= 0.02758 \pm 0.00035, & m_Z &= (91.1875 \pm 0.0021) \text{ GeV}, \\ \alpha_s(m_Z) &= 0.118 \pm 0.003, & m_t &= (172.6 \pm 1.4) \text{ GeV}. \end{aligned} \quad (\text{B3})$$

We refer to the central values for these quantities as SM reference values. Unless noted otherwise, the reference value for the Higgs-boson mass is $m_h = 150 \text{ GeV}$.

C Form Factors for Higgs-Boson Production and Decay

The form factors $A_{q,W}^h(\tau)$ and $A_{q,W}^h(\tau, \lambda)$ describing the effects of quark and W -boson loops in the production and the decay of the Higgs boson are given by [87]

$$\begin{aligned}
 A_q^h(\tau) &= \frac{3\tau}{2} [1 + (1 - \tau) f(\tau)] , \\
 A_W^h(\tau) &= -\frac{3}{4} [2 + 3\tau + 3\tau(2 - \tau) f(\tau)] , \\
 A_q^h(\tau, \lambda) &= -I(\tau, \lambda) + J(\tau, \lambda) , \\
 A_W^h(\tau, \lambda) &= c_w \left\{ 4 \left(3 - \frac{s_w^2}{c_w^2} \right) I(\tau, \lambda) + \left[\left(1 + \frac{2}{\tau} \right) \frac{s_w^2}{c_w^2} - \left(5 + \frac{2}{\tau} \right) \right] J(\tau, \lambda) \right\} .
 \end{aligned} \tag{C1}$$

The functions $I(\tau, \lambda)$ and $J(\tau, \lambda)$ take the form

$$\begin{aligned}
 I(\tau, \lambda) &= -\frac{\tau\lambda}{2(\tau - \lambda)} [f(\tau) - f(\lambda)] , \\
 J(\tau, \lambda) &= \frac{\tau\lambda}{2(\tau - \lambda)} + \frac{\tau^2\lambda^2}{2(\tau - \lambda)^2} [f(\tau) - f(\lambda)] + \frac{\tau^2\lambda}{(\tau - \lambda)^2} [g(\tau) - g(\lambda)] ,
 \end{aligned} \tag{C2}$$

while the functions $f(\tau)$ and $g(\tau)$ read

$$f(\tau) = \begin{cases} -\frac{1}{4} \left[\ln \left(\frac{1 + \sqrt{1 - \tau}}{1 - \sqrt{1 - \tau}} \right) - i\pi \right]^2 , & \tau \leq 1 , \\ \arcsin^2 \left(\frac{1}{\sqrt{\tau}} \right) , & \tau > 1 , \end{cases} \tag{C3}$$

$$g(\tau) = \begin{cases} \sqrt{\tau - 1} \arcsin \left(\frac{1}{\sqrt{\tau}} \right) , & \tau \leq 1 , \\ \frac{1}{2} \sqrt{1 - \tau} \left[\ln \left(\frac{1 + \sqrt{1 - \tau}}{1 - \sqrt{1 - \tau}} \right) - i\pi \right] , & \tau > 1 . \end{cases} \tag{C4}$$

References

- [1] L. Randall and R. Sundrum, Phys. Rev. Lett. **83**, 3370 (1999) [arXiv:hep-ph/9905221].
- [2] J. M. Maldacena, Adv. Theor. Math. Phys. **2**, 231 (1998) [Int. J. Theor. Phys. **38**, 1113 (1999)] [arXiv:hep-th/9711200].
- [3] S. S. Gubser, I. R. Klebanov and A. M. Polyakov, Phys. Lett. B **428**, 105 (1998) [arXiv:hep-th/9802109].
- [4] E. Witten, Adv. Theor. Math. Phys. **2**, 253 (1998) [arXiv:hep-th/9802150].

- [5] H. Davoudiasl, J. L. Hewett and T. G. Rizzo, Phys. Lett. B **473**, 43 (2000) [arXiv:hep-ph/9911262].
- [6] A. Pomarol, Phys. Lett. B **486**, 153 (2000) [arXiv:hep-ph/9911294].
- [7] S. Chang, J. Hisano, H. Nakano, N. Okada and M. Yamaguchi, Phys. Rev. D **62**, 084025 (2000) [arXiv:hep-ph/9912498].
- [8] Y. Grossman and M. Neubert, Phys. Lett. B **474**, 361 (2000) [arXiv:hep-ph/9912408].
- [9] T. Gherghetta and A. Pomarol, Nucl. Phys. B **586**, 141 (2000) [arXiv:hep-ph/0003129].
- [10] S. J. Huber and Q. Shafi, Phys. Lett. B **498**, 256 (2001) [arXiv:hep-ph/0010195].
- [11] S. J. Huber, Nucl. Phys. B **666**, 269 (2003) [arXiv:hep-ph/0303183].
- [12] N. Arkani-Hamed and M. Schmaltz, Phys. Rev. D **61**, 033005 (2000) [arXiv:hep-ph/9903417].
- [13] K. Agashe, G. Perez and A. Soni, Phys. Rev. Lett. **93**, 201804 (2004) [arXiv:hep-ph/0406101].
- [14] K. Agashe, G. Perez and A. Soni, Phys. Rev. D **71**, 016002 (2005) [arXiv:hep-ph/0408134].
- [15] K. Agashe, A. Delgado, M. J. May and R. Sundrum, JHEP **0308**, 050 (2003) [arXiv:hep-ph/0308036].
- [16] K. Agashe, R. Contino, L. Da Rold and A. Pomarol, Phys. Lett. B **641**, 62 (2006) [arXiv:hep-ph/0605341].
- [17] M. Blanke, A. J. Buras, B. Duling, S. Gori and A. Weiler, JHEP **0903**, 001 (2009) [arXiv:0809.1073 [hep-ph]].
- [18] C. Csaki, A. Falkowski and A. Weiler, JHEP **0809**, 008 (2008) [arXiv:0804.1954 [hep-ph]].
- [19] O. Gedalia, G. Isidori and G. Perez, Phys. Lett. B **682**, 200 (2009) [arXiv:0905.3264 [hep-ph]].
- [20] M. Bauer, S. Casagrande, U. Haisch and M. Neubert, arXiv:0912.1625 [hep-ph].
- [21] H. Davoudiasl, J. L. Hewett and T. G. Rizzo, Phys. Rev. D **68**, 045002 (2003) [arXiv:hep-ph/0212279].
- [22] M. S. Carena, E. Ponton, T. M. P. Tait and C. E. M. Wagner, Phys. Rev. D **67**, 096006 (2003) [arXiv:hep-ph/0212307].
- [23] M. S. Carena, A. Delgado, E. Ponton, T. M. P. Tait and C. E. M. Wagner, Phys. Rev. D **68**, 035010 (2003) [arXiv:hep-ph/0305188].

- [24] S. Casagrande, F. Goertz, U. Haisch, M. Neubert and T. Pfoh, JHEP **0810**, 094 (2008) [arXiv:0807.4937 [hep-ph]].
- [25] F. Goertz and T. Pfoh, JHEP **0810** (2008) 035 [arXiv:0809.1378 [hep-ph]].
- [26] M. Bauer, S. Casagrande, L. Gründer, U. Haisch and M. Neubert, Phys. Rev. D **79** (2009) 076001 [arXiv:0811.3678 [hep-ph]].
- [27] L. Randall and M. D. Schwartz, JHEP **0111** (2001) 003 [arXiv:hep-th/0108114].
- [28] M. E. Albrecht, M. Blanke, A. J. Buras, B. Duling and K. Gemmler, JHEP **0909**, 064 (2009) [arXiv:0903.2415 [hep-ph]].
- [29] G. Burdman and L. Da Rold, JHEP **0811** (2008) 025 [arXiv:0809.4009 [hep-ph]].
- [30] M. E. Peskin and T. Takeuchi, Phys. Rev. Lett. **65**, 964 (1990).
- [31] M. E. Peskin and T. Takeuchi, Phys. Rev. D **46** (1992) 381.
- [32] C. Csaki, J. Erlich and J. Terning, Phys. Rev. D **66** (2002) 064021 [arXiv:hep-ph/0203034].
- [33] A. Delgado and A. Falkowski, JHEP **0705**, 097 (2007) [arXiv:hep-ph/0702234].
- [34] M. S. Carena, E. Ponton, J. Santiago and C. E. M. Wagner, Nucl. Phys. B **759** (2006) 202 [arXiv:hep-ph/0607106].
- [35] M. S. Carena, E. Ponton, J. Santiago and C. E. M. Wagner, Phys. Rev. D **76** (2007) 035006 [arXiv:hep-ph/0701055].
- [36] J. Hirn and V. Sanz, Phys. Rev. D **76**, 044022 (2007) [arXiv:hep-ph/0702005].
- [37] A. Azatov, M. Toharia and L. Zhu, Phys. Rev. D **80**, 035016 (2009) [arXiv:0906.1990 [hep-ph]].
- [38] J. A. Bagger, F. Feruglio and F. Zwirner, Phys. Rev. Lett. **88** (2002) 101601 [arXiv:hep-th/0107128].
- [39] A. J. Buras, B. Duling and S. Gori, JHEP **0909**, 076 (2009) [arXiv:0905.2318 [hep-ph]].
- [40] K. Agashe, G. Perez and A. Soni, Phys. Rev. D **75** (2007) 015002 [arXiv:hep-ph/0606293].
- [41] K. Agashe and R. Contino, Phys. Rev. D **80**, 075016 (2009) [arXiv:0906.1542 [hep-ph]].
- [42] B. Duling, arXiv:0912.4208 [hep-ph].
- [43] J. H. Field, Mod. Phys. Lett. A **13**, 1937 (1998) [arXiv:hep-ph/9801355].
- [44] S. Schael *et al.* [ALEPH Collaboration], Phys. Rept. **427**, 257 (2006) [arXiv:hep-ex/0509008].

- [45] A. B. Arbuzov *et al.*, Comput. Phys. Commun. **174**, 728 (2006) [arXiv:hep-ph/0507146].
- [46] A. Djouadi, G. Moreau and F. Richard, Nucl. Phys. B **773**, 43 (2007) [arXiv:hep-ph/0610173].
- [47] C. Bouchart and G. Moreau, Nucl. Phys. B **810**, 66 (2009) [arXiv:0807.4461 [hep-ph]].
- [48] The Tevatron Electroweak Working Group, arXiv:0803.1683 [hep-ex].
- [49] T. Aaltonen *et al.* [CDF Collaboration], arXiv:0805.2109 [hep-ex].
- [50] J. Carvalho *et al.* [ATLAS Collaboration], Eur. Phys. J. C **52**, 999 (2007) [arXiv:0712.1127 [hep-ex]].
- [51] G. L. Bayatian *et al.* [CMS Collaboration], J. Phys. G **34**, 995 (2007).
- [52] J. A. Aguilar-Saavedra and G. C. Branco, Phys. Lett. B **495**, 347 (2000) [arXiv:hep-ph/0004190].
- [53] M. Spira, arXiv:hep-ph/9510347 and references therein.
- [54] A. Falkowski, Phys. Rev. D **77**, 055018 (2008) [arXiv:0711.0828 [hep-ph]].
- [55] I. Low, R. Rattazzi and A. Vichi, JHEP **1004**, 126 (2010) [arXiv:0907.5413 [hep-ph]].
- [56] J. R. Ellis, M. K. Gaillard and D. V. Nanopoulos, Nucl. Phys. B **106**, 292 (1976).
- [57] M. A. Shifman, A. I. Vainshtein, M. B. Voloshin and V. I. Zakharov, Sov. J. Nucl. Phys. **30**, 711 (1979) [Yad. Fiz. **30**, 1368 (1979)].
- [58] B. A. Kniehl and M. Spira, Z. Phys. C **69**, 77 (1995) [arXiv:hep-ph/9505225].
- [59] A. Pomarol, Phys. Rev. Lett. **85**, 4004 (2000) [arXiv:hep-ph/0005293].
- [60] W. D. Goldberger and I. Z. Rothstein, Phys. Rev. Lett. **89**, 131601 (2002) [arXiv:hep-th/0204160].
- [61] K. Agashe, A. Delgado and R. Sundrum, Nucl. Phys. B **643**, 172 (2002) [arXiv:hep-ph/0206099].
- [62] W. D. Goldberger and I. Z. Rothstein, Phys. Rev. D **68**, 125011 (2003) [arXiv:hep-th/0208060].
- [63] R. Contino, P. Creminelli and E. Trincherini, JHEP **0210**, 029 (2002) [arXiv:hep-th/0208002].
- [64] K. w. Choi and I. W. Kim, Phys. Rev. D **67**, 045005 (2003) [arXiv:hep-th/0208071].
- [65] W. D. Goldberger and I. Z. Rothstein, Phys. Rev. D **68**, 125012 (2003) [arXiv:hep-ph/0303158].

- [66] F. del Aguila and J. Santiago, Phys. Lett. B **493** (2000) 175 [arXiv:hep-ph/0008143].
- [67] V. Ahrens, T. Becher, M. Neubert and L. L. Yang, Eur. Phys. J. C **62**, 333 (2009) [arXiv:0809.4283 [hep-ph]].
- [68] R. V. Harlander and W. B. Kilgore, Phys. Rev. Lett. **88**, 201801 (2002) [arXiv:hep-ph/0201206].
- [69] C. Anastasiou and K. Melnikov, Nucl. Phys. B **646**, 220 (2002) [arXiv:hep-ph/0207004].
- [70] V. Ravindran, J. Smith and W. L. van Neerven, Nucl. Phys. B **665**, 325 (2003) [arXiv:hep-ph/0302135].
- [71] S. Moch and A. Vogt, Phys. Lett. B **631**, 48 (2005) [arXiv:hep-ph/0508265].
- [72] E. Laenen and L. Magnea, Phys. Lett. B **632**, 270 (2006) [arXiv:hep-ph/0508284].
- [73] A. Idilbi, X. d. Ji, J. P. Ma and F. Yuan, Phys. Rev. D **73**, 077501 (2006) [arXiv:hep-ph/0509294].
- [74] V. Ravindran, Nucl. Phys. B **752**, 173 (2006) [arXiv:hep-ph/0603041].
- [75] A. Idilbi, X. d. Ji and F. Yuan, Nucl. Phys. B **753**, 42 (2006) [arXiv:hep-ph/0605068].
- [76] V. Ahrens, T. Becher, M. Neubert and L. L. Yang, Phys. Rev. D **79**, 033013 (2009) [arXiv:0808.3008 [hep-ph]].
- [77] A. D. Martin, W. J. Stirling, R. S. Thorne and G. Watt, Phys. Lett. B **652**, 292 (2007) [arXiv:0706.0459 [hep-ph]].
- [78] G. Aad *et al.* [The ATLAS Collaboration], arXiv:0901.0512 [hep-ex].
- [79] U. Aglietti *et al.*, arXiv:hep-ph/0612172 and <http://maltoni.home.cern.ch/maltoni/TeV4LHC/SM.html>.
- [80] G. Cacciapaglia, A. Deandrea and J. Llodra-Perez, JHEP **0906**, 054 (2009) [arXiv:0901.0927 [hep-ph]].
- [81] J. R. Espinosa, C. Grojean and M. Mühlleitner, arXiv:1003.3251 [hep-ph].
- [82] A. Djouadi and G. Moreau, Phys. Lett. B **660**, 67 (2008) [arXiv:0707.3800 [hep-ph]].
- [83] A. Djouadi, J. Kalinowski and M. Spira, Comput. Phys. Commun. **108**, 56 (1998) [arXiv:hep-ph/9704448].
- [84] T. Hahn, Comput. Phys. Commun. **140**, 418 (2001) [arXiv:hep-ph/0012260].
- [85] C. Amsler *et al.* [Particle Data Group], Phys. Lett. B **667**, 1 (2008) and updated results available at: <http://pdglive.lbl.gov/>

- [86] J. Charles *et al.* [CKMfitter Group], Eur. Phys. J. C **41**, 1 (2005) [arXiv:hep-ph/0406184] and updated results available at: <http://ckmfitter.in2p3.fr/>
- [87] A. Djouadi, Phys. Rept. **457**, 1 (2008) [arXiv:hep-ph/0503172] and references therein.